Development of Surface Plasmon Resonance Sensor for Detecting Food Preservatives

by

Md. Moznuzzaman

A thesis submitted in partial fulfillment of the requirements for the degree of Master of Science in Engineering in the department of Electrical and Electronic Engineering

Khulna University of Engineering & Technology
Khulna 920300, Bangladesh

February 2020

Declaration

This is to certify that the thesis work entitled "**Development of Surface Plasmon Resonance Sensor for Detecting Food Preservatives**" has been carried out by **Md. Moznuzzaman** in the Department of **Electrical and Electronic Engineering**, Khulna University of Engineering & Technology, Khulna, Bangladesh. The above thesis work or any part of this work has not been submitted anywhere for the award of any degree or diploma.
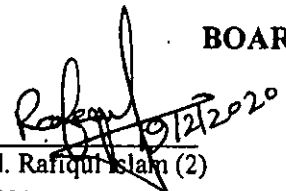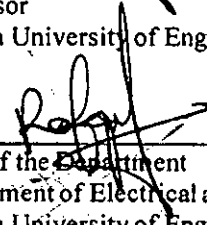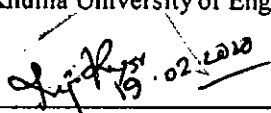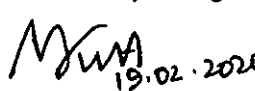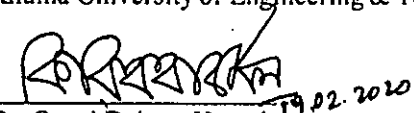
Signature of Supervisor

Signature of Candidate

Approval

This is to certify that the thesis work submitted by **Md. Moznuzzaman** entitled **"Development of Surface Plasmon Resonance Sensor for Detecting Food Preservatives"** has been approved by the board of examiners for the partial fulfillment of the requirements for the degree of M.Sc. Engineering in the Department of **Electrical and Electronic Engineering**, Khulna University of Engineering & Technology, Khulna, Bangladesh in February 2020.

BOARD OF EXAMINERS

1. _____
   Dr. Md. Rafiqul Islam (2)
   Professor
   Khulna University of Engineering & Technology

   Chairman
   (Supervisor)

2. _____
   Head of the Department
   Department of Electrical and Electronic Engineering
   Khulna University of Engineering & Technology

   Member

3. _____
   Dr. Md. Rejvi Kaysir
   Assistant Professor
   Khulna University of Engineering & Technology

   Member

4. _____
   Dr. Md. Arafat Hossain
   Assistant Professor
   Khulna University of Engineering & Technology

   Member

5. _____
   Dr. Quazi Delwar Hossain
   Professor
   Chittagong University of Engineering & Technology

   Member
   (External)

Acknowledgement

First and foremost, praises and thanks to the Almighty ALLAH, for His showers of blessings throughout my research work to complete the research successfully.

The author gratefully expresses his sincere gratitude to his thesis supervisor, **Dr. Md. Rafiqul Islam**, Professor, Dept. of Electrical and Electronic Engineering (EEE), Khulna University of Engineering & Technology (KUET), Bangladesh, for his continuous supervision, encouragements, precious guidance, advices and helps, constructive criticisms and keen interests throughout the progress of the work. The author believes that work with him is a grand opportunity and would be a never-ending memory.

I would like to thank Dr. Md. Rejvi Kaysir, Assistant professor, Dept. of Electrical and Electronic Engineering (EEE), Khulna University of Engineering & Technology (KUET), Bangladesh, who kept an eye on the progress of my work and was always available when I needed to consult with him. His helpful discussion about surface plasmon resonance makes my research easy.

Thanks to Dr. Md. Arafat Hossain, Assistant professor, Dept. of Electrical and Electronic Engineering (EEE), Khulna University of Engineering & Technology (KUET), Bangladesh, for the interesting discussions about dissertation proposal writing and for being always kind and available to help me.

I was fortunate to have Mr. Md. Biplob Hossain, Lecturer, Dept. of Electrical and Electronic Engineering (EEE), Jashore University of Science and Technology (JUST), Bangladesh, in discussing effectively my research work issues and also in writing dissertation proposal and final report.

Last but not the least, the author solemnly acknowledges his parents for giving birth to him at the first place and supporting him spiritually throughout his life.

February, 2020   Md. Moznuzzaman

Abstract

Development of Surface Plasmon Resonance Sensor for Detecting Food Preservatives

Food preservatives and adulteration is the universal concern of recent days. Particularly, developing states are the main maltreated with food contamination and it is a thoughtful problem in recent years. Formalin is a chemical compound that commonly present in food used for the preservation. Its frequent and illegal addition with food is a danger for human health and psychology. The recurrent ingesting of formalin contaminated food causes uncompromising health sicknesses. This critical issue causes fatal disease like chronic cancer. Therefore, identification of formalin in food is an extreme need, which is becoming a general problem in emerging countries.

In this dissertation, formalin is detected quantitatively by designing a Graphene-MoS_2 amalgamated 2D nano sheets with a TiO_2-SiO_2 nano-layered surface plasmon resonance (SPR) based sensor. This sensor distinguishes the presence of formalin utilizing the attenuated total reflection (ATR) approach and inspecting the reflectance vs SPR angle and transmittance vs surface plasmon resonance frequency (SPRF) attributes. Analytical approach for analyzing the sensor performance parameters has been carried out using MATLAB commercial software. The quantitative effect analysis of individual and amalgamated Graphene-MoS_2 with TiO_2-SiO_2 layers has been studied for sensitivity, detection accuracy and quality factor. In addition, optimization of Silver layer thickness is carried out for sensitivity, detection accuracy and quality factor individually.

Electric field distribution through the sensor has been investigated and analyzed by using YEE algorithm on the Lumerical FDTD solution commercial software.

An alternative composite layer sensor structure has also been designed and developed in a configuration of Graphene-PtSe$_2$-Ag-ZnO with BK7 glass prism. Formalin is detected successfully using this sensor structure by angular investigation method. The performance of this alternative sensor structure for formalin detection has been analysis analytically and it shows an outperform with very high sensitivity.

A comparative study among the performance of different composite sensor structure and the proposed sensors are also presented. Another comparison has been carried out between the existing sensor structures and the proposed sensor structures. This is the silver integrated composite sensor that shows highest performance reported by SPR technology. Finally, recommendations for additional research has been anticipated.

Dedicated

To

My Beloved Parents

&

Respected Teachers

Contents

LIST OF TABLES

LIST OF FIGURES

LIST OF ACRONYMS

HPLC	High-Pressure Liquid Chromatography
MS	Mass spectrometry
SPR	Surface Plasmon Resonance
SPs	Surface Plasmons
SPW	Surface Plasmon Wave
ATR	Attenuated Total Reflection
MoS_2	Molybdenum disulfide
SPRF	Surface Plasmon Resonance Frequency
FWHM	Full Width at Half Maximum
FDTD	Finite Difference Time Domain
TiO2	Titanium dioxide
SiO2	Silicon dioxide
DNA	Deoxyribonucleic acid
CEA	Carcinoembryonic antigen
LSPR	Localized Surface Plasmon Resonance
SPP	Surface Plasmon Polariton
RI	Refractive Index
PDEs	Partial differential equations
2D	Two dimensional
3D	Three dimensional
CAD	Computer Aided Design
IC	Integrated Circuit

DA	Detection accuracy
QF	Quality factor
SNR	Signal to Noise Ratio
PML	Perfectly Matched layer
CFL	Courant-Friedrichs-Levy

LIST OF SYMBOLS

Ag	Silver
S	Sensitivity
θ_{SPR}	Surface Plasmon Resonance angle
k_{SPW}	Wave vector of Surface Plasmon Wave
n	Refractive Index
C_0	Velocity of Light in Free Space (m/s^2)
$\Delta\theta_{0.5}$	Spectral width (deg or radian)
R_{min}	Minimum Reflectance (%)
λ_{SPR}	Surface Plasmon Resonance Wavelength (nm)
C_a	Concentration of absorbate molecule

CHAPTER I

Introduction

1.1 Background

In the past decades, portable detections of preservatives have become an emerging area of research and development for a wide range of applications including environmental, agricultural, biomedical sensing, and more particularly in the field of food security. Preservatives, known as colorless, volatile, and smelling antimicrobial agents are connotations of such ingredients that have been affixed deliberately in foodstuffs during its production or processing period. Food additives develop the defense ability against the tempering of quality as well as intensify or modify its characteristics, outlook, taste, or smell without abducting its nutritional value [1]. But the consumption of preservatives with food has a great adverse influence on human health. These impacts of ingesting preservatives may be categorized as immediate and catastrophic in the long run. The instant influence may cover headaches, energy level switching, shuffling in psychic concentration, and even physical behavior as well as an immune reaction [2]. On the other hand, long-standing effects may increase the risk of occurring cancer, cardiovascular disease, and respirational difficulties or many other health issues [2]. These health concerning issues recently have been perusing the research's attention towards food safety supremacy, as the worldwide food supply chain has been expanded day by day. The consequences of food preservatives have been outspread beyond threatening human health. Moreover, beyond 1–2% of the grown-up people and 5–8% of the children all over the world, have suffered from food additives in the recent years [3-6], moving toward a great public health concern. Repetitive and continuous monitoring has been carried out by conventional procedures for saving public lives from this crucial issue. The existing actions for detecting preservatives in food include many fundamental representatives. The detection of microbes, proteins, and small particles necessitates specialized laboratories and staff. For instance, pathogens are sensed by culturing methods followed by biochemical as well as serological detection. On the other hand, antibiotic residues are sensed using high-pressure liquid chromatography (HPLC) and mass spectrometry (MS) approaches [7-10]. Colorimetric recognition approaches such as Deniges and Eegriwes approaches have been used since the dawn of the 20th century [11]. All of these procedures require sophisticated and expensive setup, highly-trained personnel, and intricated processes for sample preparation and handling

of reagents. These reagents as well as reaction processes are sometimes hazardous to the personnel as well as the environment. Their measurements also suffer from many interferings that leads to false positions and wrong information. Another complexity with these techniques in sensing the target sample in some environmental parameters and food safety issues where sample collection and/or maintaining the quality of the collected sample is difficult [12]. All these difficult issues can confidently be overwhelmed by surface plasmon resonance (SPR) established sensor which is a potential photosensitive method to perform label-free and highly sensitive recognition [13]. It is an optical phenomenon that offers the opportunities of non-invasiveness and label-free detection ability of biomolecules [14-16]. This widespread interesting technology at first demonstrated by Liedberg and et al for chemic detecting [17]. In addition, SPR is magnificently used in plasmonic sensors [18], biomedical recognizing [19], ophthalmic solar cell [20], organic light-emitting diode [21], etc. Along with the above fascinating usages, SPR based sensors provide following versatile applications shown in **Fig. 1.1**.
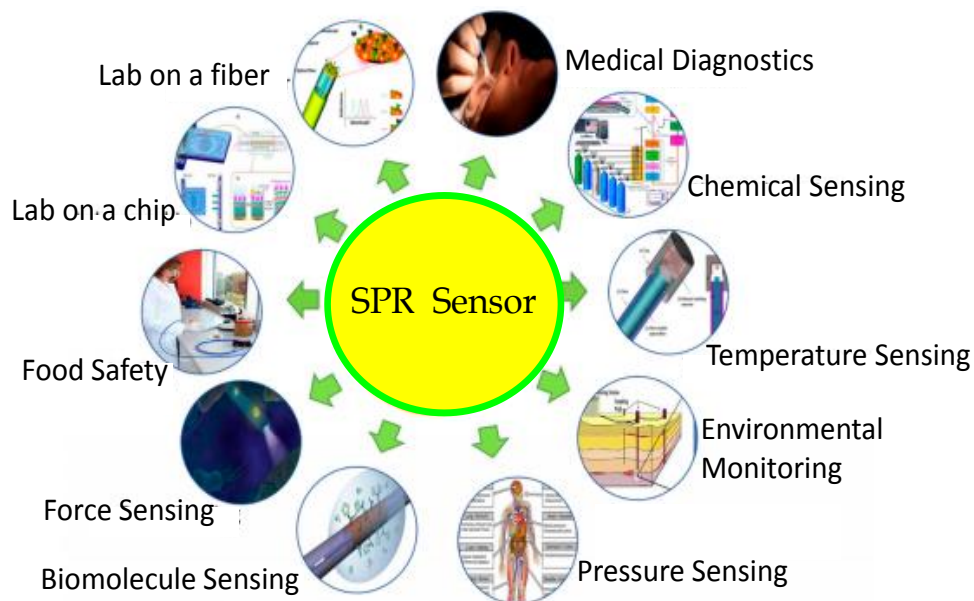
Fig. 1.1. Versatile Applications of SPR Sensors [22-25]

Generally, Surface plasmons (SPs) are united fluctuations of unbound electrons which propagate along with the interface between noble metal and dielectric material. The SPs are immensely hypersensitive to the dielectric constant of near-surface medium which is the leading functional principle of SPR sensor [26]. The incident light resonantly coupled with the SPs if the wave vector of incident light and matches with the wave vector of a surface plasmon

wave (SPW). This criteria of occurring resonance relies on the angle and wavelength of the incident light, the dielectric constant, and geometry of metal as well as sensing medium [11].
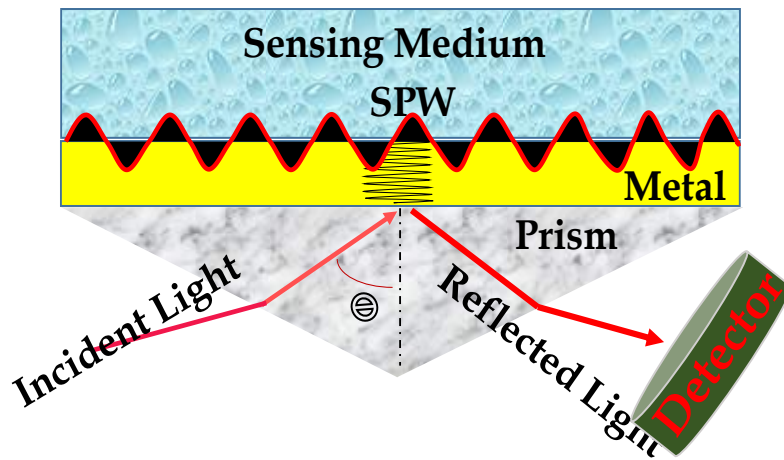
Fig. 1.2. Schematic diagram of SPR sensing set up
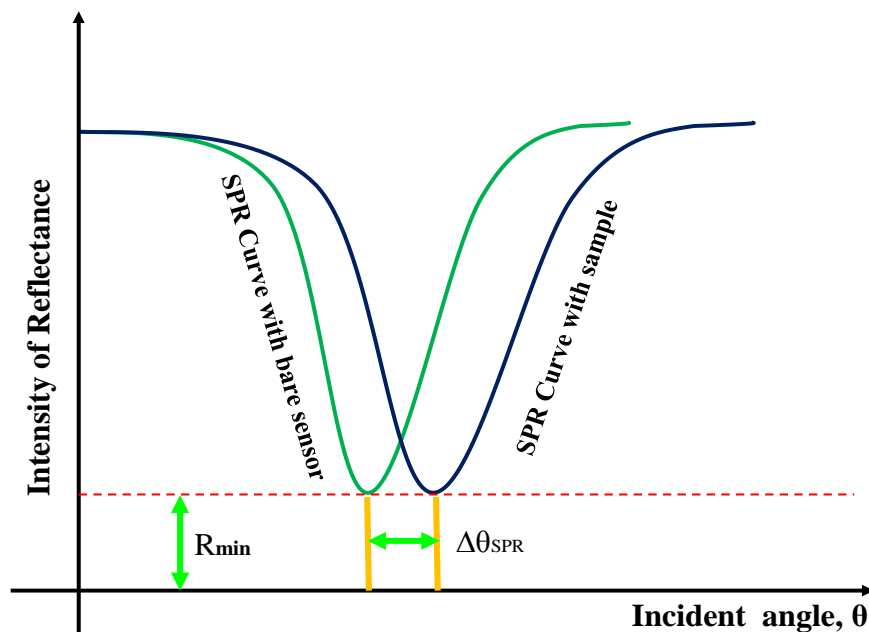
Fig. 1.3. SPR curve with and without sample

The incident angle where the absorption has the highest value for monochromatic light is called the SPR angle (θ_{SPR}) [11]. A diagram of the SPR sensor setup and its response curve is shown in **Fig. 1.2** and **Fig. 1.3** respectively for a clear understanding of the SPR phenomenon. Attenuated total internal reflection (ATR) process based SPR biosensor operates in two popular modes. First, via angular interrogation, that the imposing light wavelength is constant, and the

input angle is varying. Alternately, by wavelength interrogation, that the angle of entrance is constant and the wavelength to be changed [25]. Based on this principle numerous optical biosensors have attracted additional devotion for ensuring food security [27]. Despite the progress in devices and methods of detecting food preservatives, it still demands a detection method that offers truly field-portable and label-free with minimum efforts and cost. Expectedly, researchers are giving attention to paths of manufacturing small easily transportable devices that would offer rapid, precise, and on-site identification.

1.2 Motivation

Portable and rapid detections have become considerably important in recent researches [28, 29]. The design and development of a portable and label-free detector are largely demanded by various applications. For instance, industries for food security [30, 31], biomedical sensing and diagnosis [32, 33], and one-to-one care of agriculture, as well as environment [15, 30, 31], are using portable and label-free detector imposingly. A number of techniques recently reported aiming to serve these purposes especially for detecting food quality [30, 31, 34]. However, SPR is a better and common sensing platform, working on the binding of biorecognition elements because of their specificity, affinity, stability, and handiness which permits real-time detection with no mark [12]. Recently, SPR has become a potential photosensitive method to perform label-free and highly sensitive recognition [13]. In addition, it has been productively mass-manufactured and commercialized as a dependable stage for biomolecular action analysis [35, 36]. SP generation based sensors possess rapidness and superior responsivity to biochemical recognition [37]. Another reason for being more conducive to SPR than the fluorescence-based sensors is that it demands huge time and suffers from huge molecular fixing interruption [38].

In a conventional structure of SPR biosensor, a thin coat of a noble metal such as gold, silver, or aluminum is usually used to identify amount of molecular concentration or thickness [20, 39]. A numerous number of gold-coated SPR sensors have been designed and developed aimed at various detection purposes such as triclosan in wastewater [40], melamine detection from a sample of milk [41], amoxicillin in a chicken egg as well as human plasma [42], oxytocin in milk [43], etc. Nevertheless, gold-coated SPR sensors have a number of some downsides such as a wider SPR curve and low molecular binding ability [44]. These limitations can be mitigated by employing an immensely sensitive and cheaper silver metal instead of gold. Inspiring with these outstanding properties, a large number of research works have been

developed silver-coated SPR biosensors [45, 46]. Ag usually provides a sharper peak in SPR curve compared to Au and hence offer a better sensitivity [47]. In spite of having the capability to eradicate the difficulties connected with the use of gold, silver has an oxidation problem. [48]. However, the oxidation has diminished by combining silver with Molybdenum disulfide (MoS_2) that provides an enhanced sensitivity [49, 50] because MoS_2 has the capability of high oxidation resistance. Occasionally, MoS_2 is known as the beyond graphene transitional material as its higher bandgap energy, higher light captivation ability (5%) and more affluent work function (5.1 eV) [51]. On the other hand, graphene has become promising candidate among the researchers due to its astonishing photosensitive and electrical possessions [52]. Multiples fields of applications are covered with its employments like plasmonic filters [53, 54], attunable junction framework [55], ophthalmic modulators [56], ray splitters [57], and sensing devices [58, 59].

Another newly emerged and highly oxidation resistive 2D $PtSe_2$ material that has been commonly used on the Ag layer and this material has a strong biomolecule adsorption ability [60]. Monolayer of $PtSe_2$ can provide enhanced charge mobility and thus is of great interest for SPR sensing applications [61]. Furthermore, its less noxiousness and chemical stability have been examined on hybrid structure with monolayer of $PtSe_2$ in temperature sensing applications [62, 63]. As mono layer of $PtSe_2$ shows a similar shape in structure like graphene and phosphorene. It also possesses outstanding optical as well as electrical properties that have drawn a great fascination as a member of 2D material beyond the ancestor members [62, 64, 65].

Currently, as an excellent adhesion layer in SPR biosensor the coming out of zinc oxide (ZnO) has enhanced the sensitivity as well as detection accuracy in various sensing applications [66]. The high value of isoelectric point, outstanding chemical stability, excellent optical and electrical properties of ZnO are exhibited in glucose sensing and so on [67-70] . The admirable non-centrosymmetry characteristic between ZnO surface and metal layer intensifies the second-order susceptibility at the interface and leads to an enhanced charge transfer. Therefore, ZnO progresses the ability of light collection [71, 72]. Besides, ZnO layer is highly responsible for the significant change in SPR angle as well as sharpness of SPR curve [73].

The above studies show that each configuration of the SPR sensor bears some individual and unique difficulties that cause performance degradation. However, Nanocomposite will be the potential structure of the SPR sensor for obtaining high performance eradicating the difficulties.

1.3 Objectives

In this dissertation, two different generalized SPR based label-free detection sensors of different structures aiming to serve in food preservative sensing are designed and developed. In particular, a concentration of formalin is analyzed in liquid foods using both the proposed sensor structures. The angular interrogation method of attenuated total reflection process has been employed to analyze the optical performance of both the proposed multilayered sensors. The distinctive objectives of this thesis are completed:

i. A quantitative verification for formalin detection in liquid solution is examined for each proposed hybrid structure SPR sensors by employing an attenuated total reflection approach.

ii. Numerical study for achieving better sensitivity, quality factor, and detection accuracy have been performed by monitoring the variation of SPR angle, lowest reflectance, SPR frequency, and highest transmittance.

iii. Angular investigation technique is utilized for determining the full width at half maximum (FWHM) and its lowest value indicates the better-quality factor and detection accuracy, hence better resolution.

iv. The electric field distribution through the composite structure of the SPR sensor has been inspected using a finite difference time domain (FDTD) solution technique in the environment of Lumerical commercial software.

v. A comparative study has been carried out between these two proposed sensor structures concerning their performance parameters.

1.4 Dissertation Layout

This dissertation is primarily segmented into five chapters concentrating on the performance analysis of two different composite SPR sensor structures integrated with thin silver film in detecting food preservatives. Each of the five chapters represents the concerned potentiality of the relevant topics which are summarized as follow:

Chapter 1-Introduction provides the background of the research work including potential applications of SPR biosensors in many areas of human natural life. A reasonable state of experimental and numerical research on the SPR sensor in food preservatives detection has been conferred. Dissertation motivation and purposes are also emphasized in this chapter.

Chapter 2-Theory of SPR based Chemical Sensor pays attention to the fundamentals of SPR biosensors as probable contenders for recent and upcoming food preservatives detecting devices. Classification of SPR sensors is discussed based on designing tools, biomolecule recognition, transduction way, and investing parameters. A concise description of the performance variables and parameters of SPR sensors is presented in the last portion of this chapter. Finally, the working principle of SPR sensor in various applications are discussed.

Chapter 3- TiO$_2$ and ZnO based Structures: Modeling and Simulations presents the system designing and modeling of a composite layer sensor to quantitatively analyze performance in detecting formalin in a liquid state. The angle investigation approach is utilized to inspect light echoed from the sensor.

Chapter 4- Performance Study in Formalin Detection reveals the results of the study together with the effect of the different composite of TiO$_2$-SiO$_2$-Ag-MoS$_2$-Graphene and ZnO-Ag-PtSe2-Graphene for performance analysis. A brief FDTD analysis using Lumerical FDTD solution commercial software on electrical field distribution has been presented. Finally, for the verification of the meticulousness of this proposed sensor, the simulated results for performance have been numerically compared with other existing sensor's performance.

Chapter 5-Conclusion and Future Work concludes the outcomes of this thesis work and offers some suggestions which can serve as future problem areas for advanced research in the field of promising SPR sensors.

CHAPTER II

Theory of SPR based Chemical Sensor

2.1 Introduction

The beginning of this chapter involves a short discussion on the progression of surface plasmon resonance (SPR) sensors with their applications in the area of food preservatives recognition. A detailed classification of SPR sensors is discussed. some physical basics of surface plasmons and their ophthalmic production scheme. The finite-difference time-domain (FDTD) analysis approach is also conferred in this chapter as well as the software details. At the later most of this chapter, an ephemeral explanation of the performance variables and parameters of SPR sensors is presented.

2.2 Advancements of SPR Sensors

In 1982, Liedeberg and Nylander established the first biosensor by using SPR technology as an optical sensor [74]. Over the last three decades, this ground of research has grasped significant growth as exhibited in **Fig. 2.1**.
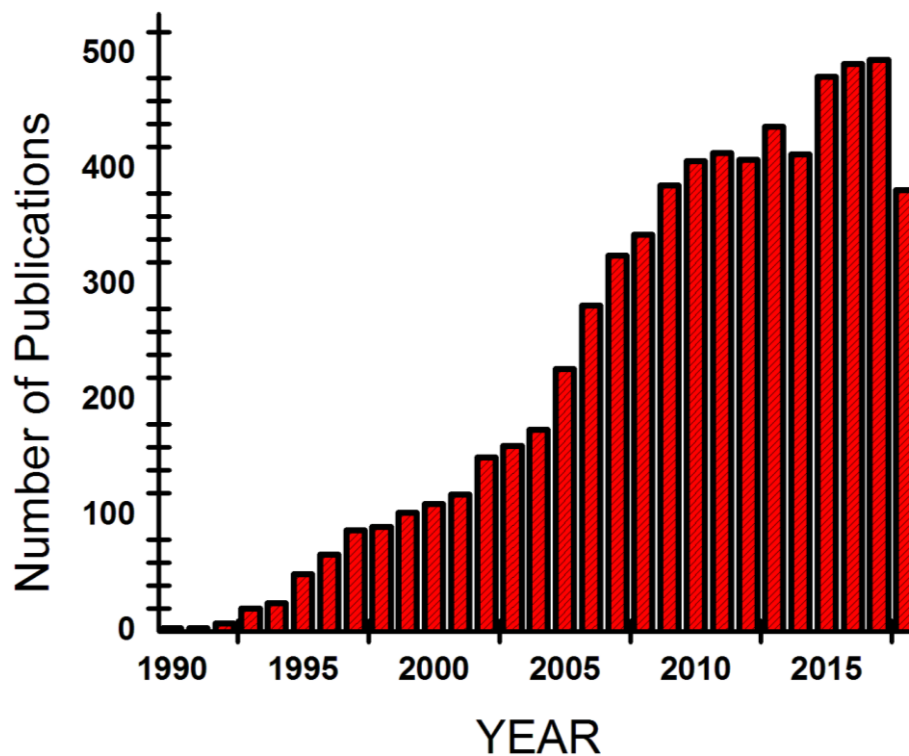
Fig. 2.1. Number of publications with the keyword "Surface Plasmon Resonance Biosensor" between 1990 to 2018. The data was retrieved in Sep 2018 from Web of Science

Recent progress in SPR sensors can be categorized into four sorts: capturing of the bio-recognition element on the sensing surface, surface alteration of the sensor, shrinking of the SPR biosensor system, and amalgamation with other delivery schemes or sensing modalities.

2.3 Area of Applications and Importance

The application areas of biosensors are structured in several sectors: clinical investigation, keeping a monitoring eye on the environment [75], public security[76], and finally sector of study of the interaction of chemicals in foods [77]. The development and commercialization of the sensor increase very rapidly by the influence of the SPR method, which has become one of the leaders of biomolecular interplay analysis. A few of the representative and impressive utilization are summarized (**Table 2.1**) here with the bio-recognition elements and the transduction approaches.

Table 2.1. Applications of Biosensors

Analyte	Bio-recognition element	Sample medium	Transduction modality	Reference
Prostate-specific	Prostate-specific	Prostate-specific	Prostate-specific	[78]
	DNA Amtaper	Buffer	Chemiluminescent	[79]
Pancreatic cancer	Antibody	Buffer	SPR	[80]
Colorectal cancer marker carcinoembryonic antigen (CEA)	Antibody	Buffer	SPR & Electrochemical	[81]
	Antibody	Buffer	Electrochemical	[81, 82]
Hepatitis B virus	Antibody	Serum	SPR	[32]
	Antibody	Buffer, blood serum and plasma	LSPR	[83]
Dengue virus	Antibody	Buffer	Electrochemical	[84]
Formalin	Buffer	Chitosan	SPR	[85]

2.4 Categorization of Sensors

Based on the various features and methods, biosensors can be classified in many different aspects. The most significant and immensely representative way of categorization of sensors are listed below:

a) Affinity or catalytic detection
b) Labeled or label-free detection
c) Bio receptor type
d) Transduction methods.
e) Designing Instruments
f) Investigation parameters

2.4.1 Affinity or Catalytic Detection

The functionalization of catalyst enzyme is denoted as catalytic detection. The identification is accomplished employing several techniques:

a) the analyte gets converted to a detectable object by the enzyme
b) the inhibition or activation of the enzyme by the analyte
c) regulating the change of enzyme properties for the consequence of interluding with the analyte

On the other side, the straightforward evaluation of capturing between two species is referred to as affinity detection. Normally, it is specified as chitosan-formalin, antigen-antibody, biotin-avidin, or complementary DNA strands interactions. In the rough, this interplay is overseen by a variation in mass, magnetic field, refractive index, or other chemical-physical alteration.

2.4.2 Label-free or Labeled Detection

The sensors can be categorized as labeled or label-free, according to the use of a mark or label on the sample to be detected. At first, a label is marked to the molecules to be detected and the tie-up of bioreceptor- biomolecule is detected. For labeling, fluorophores or fluorochromes are normally used, which contains the elements having the capability of binding biomolecule and can generate fluorescent light at the condition of illuminating with a certain wavelength. Furthermore, many other types of labels such as enzymes, radiolabels, metal nanoparticles, or magnetic nanoparticles are used for labeling the sample. Howsoever, the labeling of the sample

produces a series of complications: high expense, production of large contaminant or noxious waste, squashing phenomena, probable degradation or change of the biomolecule itself, and its interludes with the bioreceptor are the most occurring cases.

By the same token, a label-free sensor can identify the molecule-receptor fixing without adhering exogenetic components to a biomolecule. It is paramount to flourish a greater extent of sensitive sensors such as SPR biosensor where the existence of biomolecules in the sensing environment leads to a modification of optical properties [86].

2.4.3 Bioreceptor based Detection

In addition, biosensors are also categorized based on engaged receptors. The common bioreceptor sensors are enzymatic, immunosensors, and DNA sensors and are discussed below:

The enzymatic biosensors utilize enzyme having the ability to stimulate reactions, driving to the presence of a product or exodus of a substrate. Many substrate molecules convert to product repeatedly by a single enzyme catalyst and this action of the enzyme is called amplification action. This action permits the detection ability of enzymes in an absolutely low degree of concentration.

The antigen-antibody interlude detection is known as immunosensor. Either antigen or antibody can be a bioreceptor in this type of sensor. Generally, indirect assay refers to the case of antibody detection. On the other hand, the detection of antigens is celebrated as a direct assay.

Eventually, the sensors with high specificity are DNA sensors. They work immobilizing the single-stranded DNA probes on the surface to identify its complementary DNA object sequence by hybridization.

2.4.4 Sensors based on Transduction Method

Sensors are also categorized by the transduction method which is described below:

➢ Electrochemical Sensors: the stimulating action of an oxidoreductase enzyme is utilized to attach its substrate leading a redox reaction. The electrons of this redox reaction can be calculated by an electrical transducer, either amperometric, potentiometric or impedimetric [87, 88]. The calculation of frequency response can be carried out by this method too [89].

- Magnetic Sensors: in these sensors, magnetic nanoparticles are used in order to detect a shift in the magnetic field [90].
- Optical Sensors: It is possible to distinguish between label sensors such as fluoro immunoassay and enzyme immunoassay and label-free optical sensors e.g. SPR, optical resonators.

2.4.5 SPR Instrumental Design

Based on the arrangement of designing tools SPR sensors are categorized into four key types that are utilized in the individual device. The proper SPR apparatus can be selected by the urge of applications and investigation requirements. An ephemeral elucidation of each class is discussed in the following sections. couple

2.4.5.1 Prism based Sensors

Prism combined sensors are classified into three configurations based on the placement of prism in the sensor. The first arrangement is shown in **Fig. 2.2** is known as Otto arrangement [91]. In this formation, there is a gap between the metal and light-reflecting surface. A lower RI medium is to incorporate between metal and reflecting medium. The use of this configuration frequently noticed in SPR studies.

The second configuration is Kretschmann and its difference from the Otto configuration is that the metal sheet is on the prism avoiding the gap between them. More efficient plasmon generation can be achieved in this configuration.
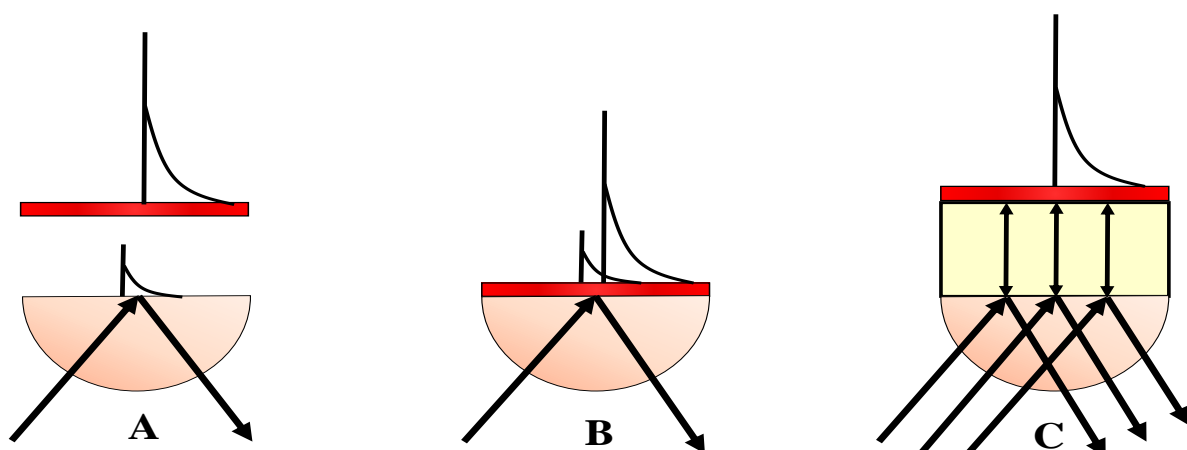
Fig. 2.2. Prism tied sensors: A) Otto arrangement B) Kretschmann arrangement C) Frustrated Total Internal reflection arrangement

Finally, the third one is known as frustrated total internal reflection arrangement alike to the Otto configuration but a distinct layer is inserted between two media. **Fig. 2.2** displays the schematic explanation of these three classes of sensors.

2.4.5.2 Optical Fiber-based Sensors

Sensors fitted with optical fiber are classified as extrinsic and intrinsic sensors [92]. The fiber acts as a transmission means to receive light to and from the object sample. In general, it is applied as the end part of the fiber where the immobilizing receptor is localized combinedly with a membrane. The sensing lamella plays the role of a transduction system which generates the change of optical property when interacts with the analyte. The interplay generates a variation of fluorescence discharge and optical absorption.

The transduction operation is performed by the optical fiber itself because of its physical property's changes. By bringing to light the evanescent field on the sample analyte at the surface of fiber the sensing is accomplished. The field exposure can be occurred by removal or reduction of the cladding of an optical fiber.

2.4.5.3 Grating Attached Sensors

The grating paired sensors were first employed for applications in 1983 [93]. The operation of this type of sensor is as that of a diffraction grating. The resonance wavelength is determined by calculating the span and peak of the grating. A binding curve is formed by altering the incident angle and determining the intensity of reflected. The excitation mode of GC sensors is classified into two kinds. One is input grating coupler and the other is output grating coupler.

2.4.5.4 Optical Waveguide Sensors

Based on instrumental design requirements optical waveguide is the former most SPR sensor shape. These kinds of sensors work on the variation of the incident angle. Light propagates evanescently when it passes through the areas of gating and a thin layer of metal. At the opposite end of waveguides, the transmitted light is sensed by photodiodes [94]. The simplicity of governing the ophthalmic bath, the small size along with rigidity are the main advantages of these sensors.

2.4.6   Investigation Parameter based SPR Sensors

The categorization on investigating parameters, SPR sensors are classified into the following four types:

2.4.6.1 Angular Investigation based SPR Sensors

In order to excite surface SPPs a light beam having a single wavelength is utilized in the angular investigation based SPR sensors (**Fig. 2.3**). The pairing intensity between the wavevector of incident light and the SPP shifts are evaluated by calculating the reflected light intensity at various angles of light incidence. For example, the graphical representation shown in **Fig. 2.3** reveals the angle shift due to the change of RI of the sample solution.
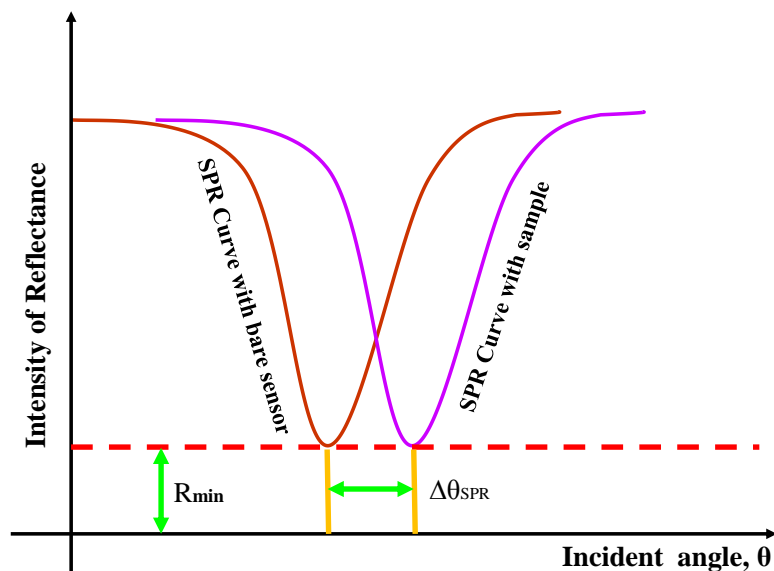
Fig. 2.3. Reflected light intensity in the act as an action of incident angle for different refractive indices

2.4.6.2 Wavelength Investigation based SPR Sensors

In the wavelength investigation approach, a light beam of multicolor is utilized on a metal lamella under a single incident angle (**Fig. 2.4**). By taking a measurement of reflected light intensity for multicolor wavelengths and calculating the wavelength that is responsible for the strongest pairing of light wave vector and SPW wave vector. The propagation constant and its variation to RI change can be evaluated. Optical fiber-based SPR sensors work using a wavelength investigation approach for taking the value of detecting attributes.
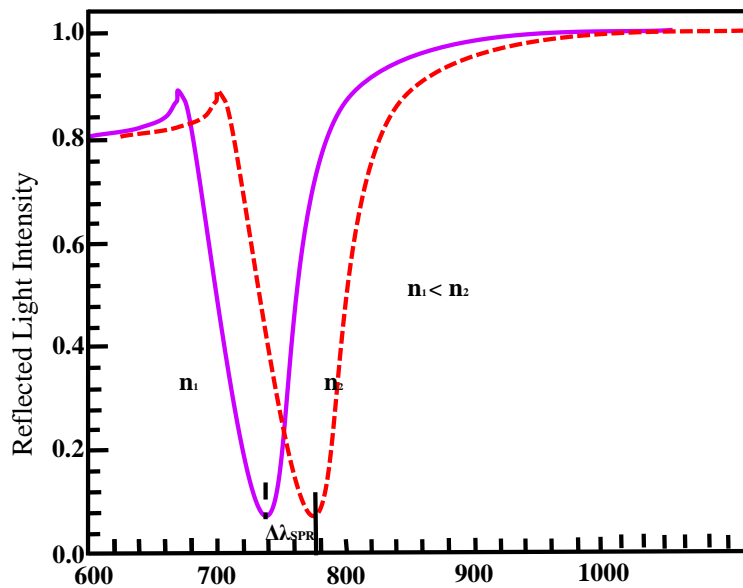
Fig. 2.4. Reflected light intensity in the act as an action of wavelength for different refractive indices

2.4.6.3 Intensity Investigation based SPR Sensors

The intensity investigation approach uses a single-color light beam to be hit on the metal lamella keeping both its incident angle and wavelength constant. In this approach, the variation of light intensity is calculated with the variation of the RI of the target medium.

2.4.6.4 Phase Investigation based SPR Sensors

The change of phase features for differently polarized light are calculated due to the variation of RI of the surrounding medium keeping incident angle and wavelength constant.

2.5 Surface Plasmons Excitation by Light

In apropos to the excitement of SPR with the light treatment a condition of phase matching must be contented which enunciates that it is only possible to excite the SPR when the propagation constant of the SPs coequals the propagation constant of the electromagnetic field of the light vector [95]. For a wavelength after the fashion on dispersion relation [96], the light waves have the smaller wavevector than the wavevector SPs propagating at the surface with the same frequency. For this reason, the excitement of SPs is quite impossible by the direct incident of shining light on an even metal surface. The light wavevector can easily be regulated to coequal of the SPs wavevector launching it care of the metal from a higher RI medium than the RI of the medium at the flashpoint where the excitement of SP is going to happen. The

typical ways of the excitement of SPs are to pair light through a waveguide [51], a prism [25], and a grating [97]. Howsoever, prism paired is one of the primary and maiden tested configurations of SPR which is considered to be described in the following section.

2.6 SPR Designing Tools

In order to design and investigate different structured SPR sensors, various software is used. The commonly used software for the simulation of optical multilayered systems is MATLAB, COMSOL, CST studio, Lumerical FDTD, etc. In this thesis work, MATLAB 17b and Lumerical FDTD solution Multiphysics v10.1.0 software are used. In this section, firstly, the basic theory to apply the finite difference time domain (FDTD) technique has been discussed. Secondly, the information about the software is also discussed.

2.6.1 Finite Difference Time Domain (FDTD) Method

Partial differential equations (PDEs) are usually used as the potential and prominent tools for solving most of the time and space-dependent laws and problems of physics. Its analytical solution is very simple and comfortable. But for complex structure and multisegmented system modeling and analytically response analysis is very difficult and problematic with the PDEs approach. For this reason, mathematicians modeled a discretization model for solving Maxwell's electromagnetic field equations as well as many other complicated mathematical expressions. The solution of this discretization approximation yields the same result getting by numerical simulation of PDEs. FDTD technique is built on this fundamental concept. This quantitative approach for finding estimated results to boundary value problems of PDEs. This technique gives the benefits of structural uniformity through the propagation way with a consideration of the 2D computational field which needs less computational resources and time.

2.6.2 Lumerical FDTD Solution Multiphysics Software

Lumerical FDTD software works employing the FDTD method-based package. In general, it is used in numerous problems associated with physics and engineering applications. It was first intended for designing phonic devices. It is also a Multiphysics suite software. The device suite encourages engineers in precisely modeling of different components where the complex and critical optical activities, electronic and thermal phenomena affect the performance. Material

modeling for a wide range of wavelengths with this suite is very precise as it utilizes the multi-coefficient models. The advantageous features are as follows:

i. Precisely characterize physical materials over a wide range of wavelength
ii. Automatic model production from an existing example model is a user-friendly feature for beginner
iii. Data and user define-function designing is a handy feature for self
iv. The progressive conformal mesh is well-matched with dispersive and high RI difference materials, with extreme accuracy for the coarse mesh

2.6.2.1 3D CAD Environment

The 3D CAD Environment as well as more parameter attributable simulation items permit a speedy model reiteration. The employment of this simulation objects also allows importing customized geometry from typical CAD and IC formats. A graphical representation of the 3D CAD environment is shown in **Fig. 2.5**.
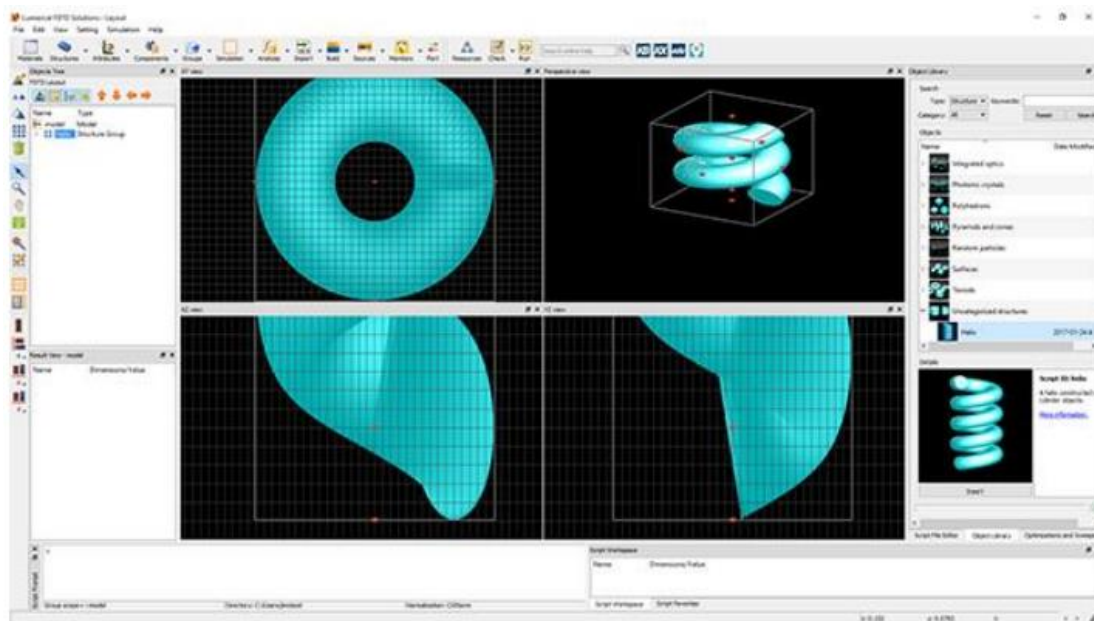
Fig. 2.5. 3D design environment of Lumerical FDTD solution Multiphysics

2.6.2.2 Nonlinearity and Anisotropy

The devices, fabricated with nonlinear and spatially varying anisotropy materials can be simulated by following the steps:

✓ Select an extensive array from nonlinear, negative index and gain models

✓ Express models of new material by the plugging-in flexible material

2.7 SPR Performance Variables

The terms including performance variables of SPR sensor are SPR Angle, SPR Frequency, Minimum Reflectance, Maximum Transmittance, SPR Wavelength are specified with their mathematical existence. Afterward, the performance of the SPR sensor is discussed which are most importantly evaluated based on the parameters- sensitivity (S), detection accuracy (DA), and the quality factor (QF).

2.7.1 Surface Plasmon Wave (SPW)

A molecular concentration variation of sensing dielectric medium will make a slight change in the refractive index. This fluctuation of the RI will eventually alter the surface plasmon wave vector (k_{SPW}) shown in **Fig.2.6**. It is defined by Equation (2.1), where n_{Au} denotes the RI of gold and n_g denotes the RI of graphene [98]:

$$K_{SPW} = \frac{2\pi}{\lambda_{633}} \sqrt{\frac{n_{Au}^2 n_g}{n_{Au}^2 + n_g}} \qquad (2.1)$$
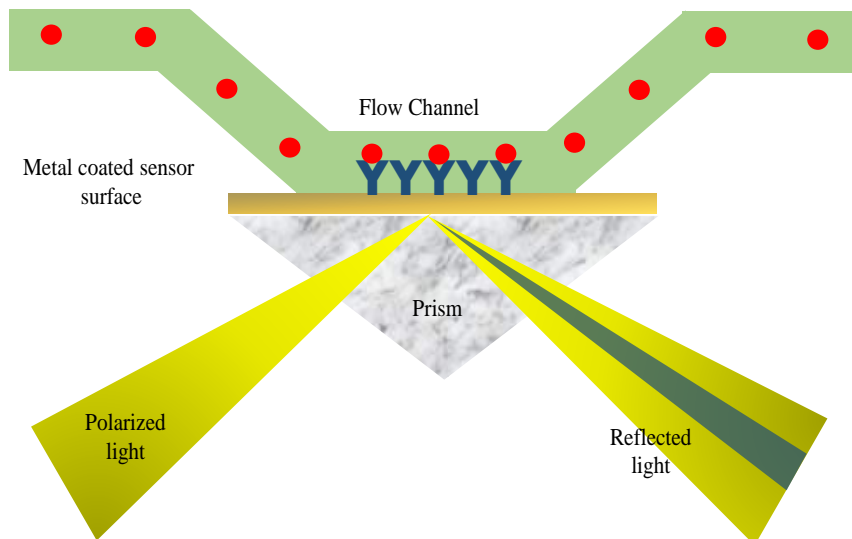
Fig 2.6. Schematic model diagram of a single-layer surface plasmon resonance sensor

The wave vector matching of both incident light and SPW is the main condition of occurring resonance oscillation of excited electrons and it results an angle shift of incident light [99].

2.7.2 Surface Plasmon Resonance Angle (θSPR)

The incident angle at which SPR happens is named the SPR angle. At this SPR angle, both the wave vector of incident light and SPW become numerically the same. At this condition, the generation of plasmon is maximum and the reflectance of light is minimum that is attenuated total reflection is lowest [99]. This SPR angle of being expressed by equation (2.2) [100]:

$$\theta_{SPR} = \sin^{-1} \sqrt{\frac{n_{Au}^2 n_s}{n_p^2 (n_{Au}^2 + n_s)}} \tag{2.2}$$
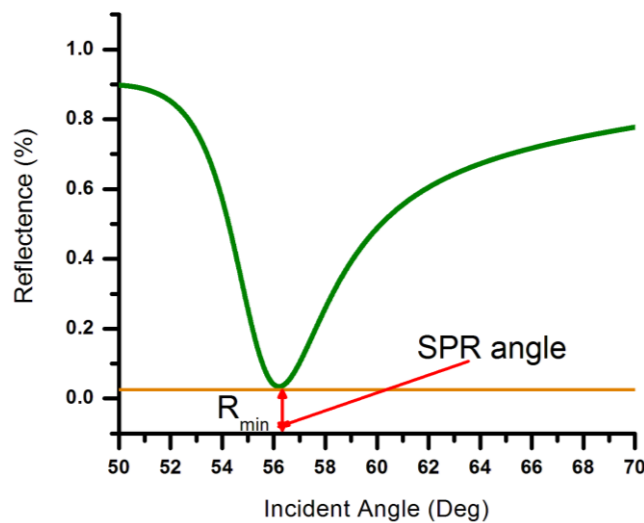
Fig. 2.7. Typical SPR Curve of a conventional sensor

Fig. 2.7 shows a typical SPR curve. In this figure, the minimum reflectance 0.027 is achieved at 56.48°. Therefore, the value of the SPR angle for the above SPR curve is 56.48° for the bare sensor. The SPR curve has been achieved by Matlab-16a, simulating using He-Ne light at 633 nm wavelength.
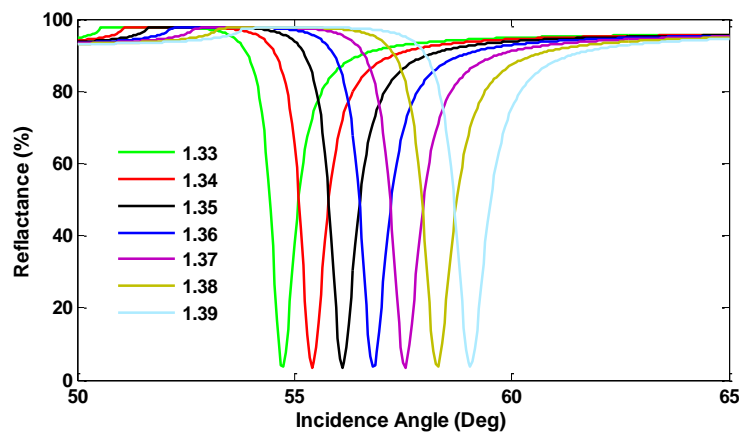
Fig. 2.8. The reflection intensity spectra for different RI sample

The RI change of the sensing medium causes a change in the SPR angle. The angle shifts rightward with RI increment of the sensing medium and its graphical representation is shown in **Fig 2.8**.

The change of RI of the detecting target solution affects significantly the reflectance and the SPR angle [100]. The SPR angle plays an active role in deciding on successful interaction either sample is detected or not as shown in **Table 2.2**.

Table 2.2. Four Possible Criteria for Making Decision regarding Effective Interaction using $\Delta\theta_{SPR}$ and R_{min} as sensing attributor

Criteria for using & R_{min} as sensing attributor	Decision
$\Delta R_{min}^{P-T} \geq (\Delta R_{min}^{P-T})_{min}$ && $\Delta\theta_{sp}^{P-T} \geq (\Delta\theta_{sp}^{P-T})_{min}$	Sample is detected
$\Delta R_{min}^{P-T} \geq (\Delta R_{min}^{P-T})_{min}$ && $\Delta\theta_{sp}^{P-T} \leq (\Delta\theta_{sp}^{P-T})_{min}$	Re-evaluate
$\Delta R_{min}^{P-T} \leq (\Delta R_{min}^{P-T})_{min}$ && $\Delta\theta_{sp}^{P-T} \geq (\Delta\theta_{sp}^{P-T})_{min}$	Re-evaluate
$\Delta R_{min}^{P-T} \leq (\Delta R_{min}^{P-T})_{min}$ && $\Delta\theta_{sp}^{P-T} \leq (\Delta\theta_{sp}^{P-T})_{min}$	Free Probe

The criteria mentioned in Table 2.2 provides four possible situations that may occur in any sensing operation. The initial criterion indicates the expected one where the second and third criteria need cautious recheck for achieving the anticipated situation and finally, the fourth criterion authorizes that the probe of the sensor is still free of the target molecule.

2.7.3 Minimum Reflectance

The incident light causes a production of waves that propagates evanescently at the moment of passing through a prism as well as its reflection from the vicinity of the prism-gold interface. The reflected light intensity for a p-polarized light wave is stated by equation (2.3) [101]:

$$R = \frac{A + \dfrac{B}{Z_f} - Z_i\left(C + \dfrac{D}{Z_f}\right)}{A + \dfrac{B}{Z_f} + Z_i\left(C + \dfrac{D}{Z_f}\right)} \tag{2.3}$$

The reflectance at the SPR angle is called Minimum Reflectance (R_{min}) [102]. The SPR curve is shown in the above **Fig. 2.2**. The value of Minimum Reflectance (R_{min}) is 0.027 %. The R_{min}

also plays an active role in deciding on successful interaction either sample is detected or not as shown in **Table 3.1** [102].

2.7.4 Surface Plasmon Resonance Frequency

The point at which the optical wave vector is the same as the SPW vector known as SPR point [101]. Equation (2.4) indicates that the SPR angle depends on the RI of detecting medium. The frequency at SPR point is known as SPR frequency (SPRF) and it is expressed by equation (2.4).

$$SPRF = \frac{c_0}{n_{geo}} \frac{k_{SPW}}{2\pi} \qquad (2.4)$$

Equation (2.4) indicates that SPR angle is a reliant on RI of detecting medium, the propagation velocity of SPW that is perpendicularly confined evanescent electromagnetic wave [101], n_{geo} is the geometric mean of RI gold and sensing medium ($n_{geo}=\sqrt{(n_{Au}n_s n_{prism})}$), neglecting imaginary part and it is crucial in real-world design [100]). Here it works on a real surface but its imaginary portion comes into action for sensor designing as surface Plasmon wave propagates along with the interface between metal and sensing dielectric medium.
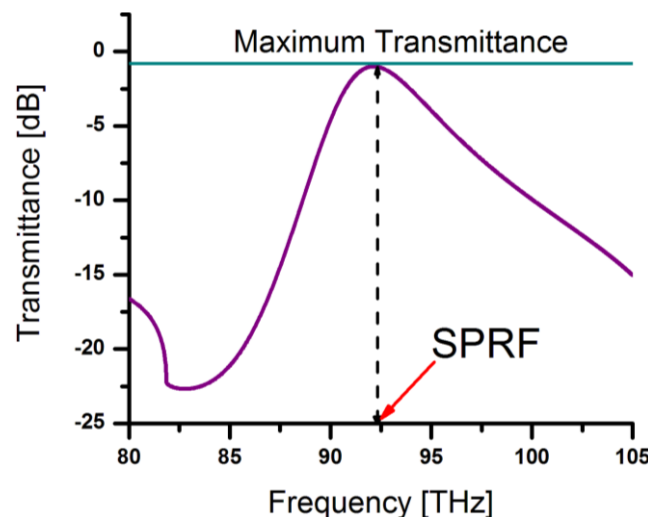
Fig. 2.9. SPR Transmittance vs Frequency Curve

The SRF is shown in **Fig. 2.9**. The value of SPR frequency for the above SPR curve is 92.82 THz. The SRF curve has been achieved by MATLAB -16a, simulating at 633 nm wavelength light. The SRF also plays an active role in deciding on successful interaction either sample is detected or not as shown in **Table 2.3**.

Table 2.3. Decision Table with Four Probable Conditions Concerning Successful Interaction using ΔSRF and T_{max} as detecting attributor

Conditions for using ΔSRF & T_{max} as detecting attributor	Decision
$\Delta T_{max}^{p-t} \geq (\Delta T_{max}^{p-t})_{min}$ && $\Delta SRF_{p-t} \geq (\Delta SRF_{p-t})_{min}$	Sample is detected
$\Delta T_{max}^{p-t} \geq (\Delta T_{max}^{p-t})_{min}$ && $\Delta SRF_{p-t} \leq (\Delta SRF_{p-t})_{min}$	Re-evaluate
$\Delta T_{max}^{p-t} \leq (\Delta T_{max}^{p-t})_{min}$ && $\Delta SRF_{p-t} \geq (\Delta SRF_{p-t})_{min}$	Re-evaluate
$\Delta T_{max}^{p-t} \leq (\Delta T_{max}^{p-t})_{min}$ && $\Delta SRF_{p-t} \leq (\Delta SRF_{p-t})_{min}$	Free Probe

The quantitative value indicates successful or unsuccessful molecular interactions. The first criterion in **Table 2.3** indicates the expected situation, whereas second and third criteria necessitate cautious recheck for achieving the wanted condition, the fourth criterion ensures that the probe is still target molecule free.

2.7.5 Maximum Transmittance (T_{max})

The transmitted light can be determined by [103] equation (2.5):

$$T = \frac{2\cos\theta_i}{A + \dfrac{B}{Z_f} + Z_i\left(C + \dfrac{D}{Z_f}\right)\cos\theta_f} \qquad (2.5)$$

The transmittance at SPRP is called Maximum Transmittance (T_{max}) [103]. For resonance conditions the maximum transmittance is necessary. The result is expressed in decibel (dB). The SPR curve is shown in the above **Fig. 2.10**. The value of Maximum Transmittance (T_{max}) is 0.8 dB. The T_{max} also plays an active role in deciding on successful interaction either sampled is detected or not as shown in **Table 2.3**.

2.7.6 Surface Plasmon Spectral Width

Spectral width ($\Delta\theta_{0.5}$) is related to both of SPR angle and reflection. It is a very important variable for determining sensor signal to noise ratio (SNR) and Quality Factor (QF). It is inversely proportional to noise ratio (SNR) and Quality Factor (QF). The spectral width of the SPR curve ($\Delta\theta_{0.5}$) is the shift of SPR angle ($\Delta\theta_{SPR}$) corresponding to 50% reflection [103]. The mathematical identity of Spectral width is given in equation (2.6)

$$\Delta\theta_{0.5} = [\Delta\theta_{SPR}]_{R_{0.5}} = 50\% \, R \qquad (2.6)$$
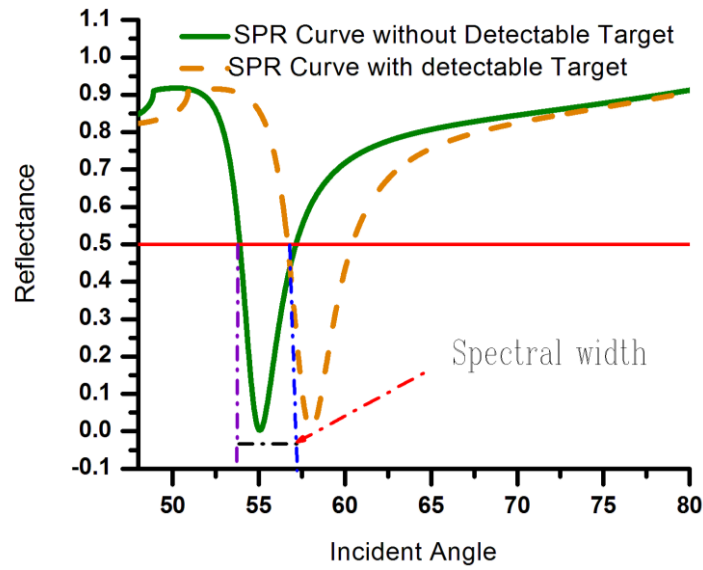
Fig. 2.10. SPR Curve for with and without Detectable sample

Fig. 2.10, shows the calculation process of spectral width. At 50% reflection, the SPR angle with no detectable sample is 53.88° and the SPR angle with detectable sample solution is 56.85°. The change of SPR angle at 50% reflection is 2.97°. According to equation (2.6), the spectral width is 2.97°.

2.7.7 SPR Wavelength

SPR wavelength is subjected to vary when the angle of incident light is constant. For example, an incident angle (θ)= 55°, the variation of reflectance is shown in **Fig. 2.11** with respect to wavelength.
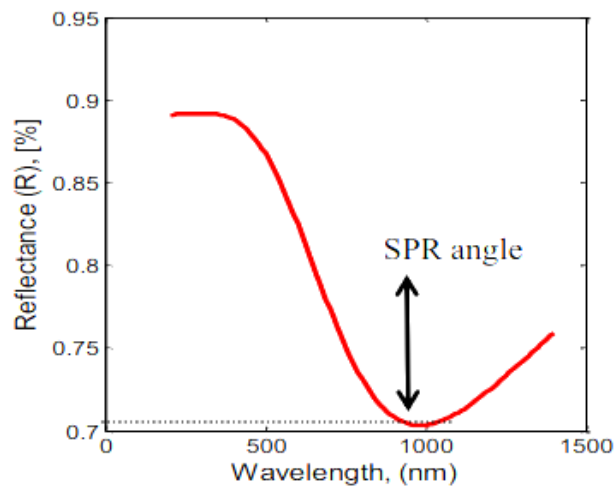
Fig. 2.11. SPR Wavelength (λ_{SPR}) without the Graphene layer

The wavelength at which Minimum Reflectance (R_{min}) has occurred is called SPR wavelength for a given incident angle. From **Fig. 2.11**, it is apparently clear that the value of the SPR wavelength is 880 nm.

The excitation of surface plasmon polariton (SPP) at resonant state is acknowledged as attenuated total reflectance. The wavelength of incidence light at which ATR minimum is obtained that can be defined by the following equation (2.7) [99]:

$$\lambda_{SPR} = \frac{2\pi}{k_{SPW}} n_p \sin\theta_{SPR} \qquad (2.7)$$
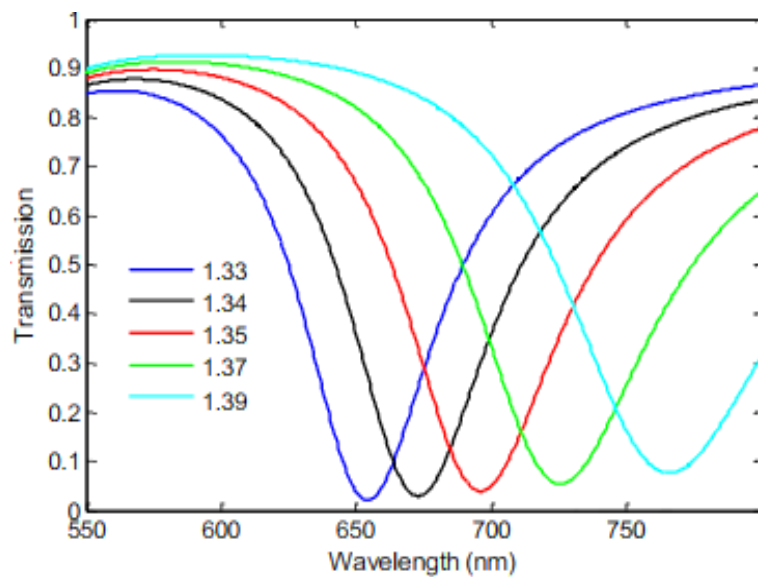
Fig. 2.12. The reflection intensity spectra and SPR wavelength are varied with the varied RI

The SPR curve has been achieved by Matlab-16a. In **Fig. 2.12** the picture of variation of SPR wavelength with the change of refractive index changes is shown clearly.

The RI of the sensing medium has a significant effect on the reflected light and the SPR wavelength [99]. The sensitivity (S), detection accuracy (DA), and the quality factor (QF) are directly proportional to the shift in the SPR wavelength ($\Delta\lambda_{SPR}$). The SPR wavelength plays an active role in making a decision about successful interaction either sample is detected or not as shown in **Table 2.4**.

Table 2.4 shows the conditions by which successful and unsuccessful interaction of the target molecule with the probe molecule can easily be declared.

Table 2.4. Decision Table with Four Probable Conditions Concerning Successful Interaction using $\Delta\lambda_{SPR}$ and R_{min} as detecting attributor

Conditions	Decision
$\Delta T_{min}^{p-t} \geq (\Delta T_{min}^{p-t})_{min}$ && $\Delta\lambda_{SPR}^{p-t} \geq \left(\Delta\lambda_{SPR}^{p-t}\right)_{min}$	Sample is detected
$\Delta T_{min}^{p-t} \geq (\Delta T_{min}^{p-t})_{min}$ && $\Delta\lambda_{SPR}^{p-t} \leq \left(\Delta\lambda_{SPR}^{p-t}\right)_{min}$	Re-evaluate
$\Delta T_{min}^{p-t} \leq (\Delta T_{min}^{p-t})_{min}$ && $\Delta\lambda_{SPR}^{p-t} \geq \left(\Delta\lambda_{SPR}^{p-t}\right)_{min}$	Re-evaluate
$\Delta T_{min}^{p-t} \leq (\Delta T_{min}^{p-t})_{min}$ && $\Delta\lambda_{SPR}^{p-t} \leq \left(\Delta\lambda_{SPR}^{p-t}\right)_{min}$	Free Probe

2.7.8 SPR Detection Appraisal

The detection idea launches with analyzing the reflectance-incident angle characteristic curve (R~Ө) at a bare sensor. The dependency of reflectance versus incident angle is measured by the SPR device within the PBS solution. Here, RI changes to changes in molar concentration, and this relationship can be expressed as the equation (2.8) [104]:

$$n_s^2 = n_s^1 + C_a \frac{dn}{dc}$$

(2.8)

Here, n_s^1 is RI of the sensing dielectric without adsorbing the probe molecules. When a target molecule is absent within the sample solution, the value of n_s^1 is equal to the RI value of PBS saline. It is called then a bare sensor. C_a indicates the concentration value of adsorbed biomolecules. The RI of sensing medium after adsorbing the target molecule is n_s^2.

2.8 SPR Performance Parameters

In order to compare among different sensor topologies, it is provocative to present some measures which are usually used to exactly describe their performance. Although there are many parameters found in literature, five are the most significant performance parameters and are described below. The fundamental parameters for an SPR sensor performance analysis are considered basically focusing on its sensitivity, detection accuracy, quality factor, specificity, and linear range. All of which should be as high value as conceivable for a good sensor [104].

2.8.1 Sensitivity

Sensitivity analysis of SPR based sensors has been widely studied [9, 100, 104, 105]. In angle investigation approach the sensitivity of SPR RI sensors changes is in with falling operating wavelength [104]. On the contrary, the sensitivity of SPR RI sensors using wavelength investigation and signal strength measurement approach intensifies with the increase of operating wavelength [106].

The sensitivity is defined as the change of the transduction magnitude as a function of the concentration of target analyte. In optical sensors, this magnitude is commonly the angular or spectral position of resonance as it is illustrated in **Fig. 2.13**. The sensitivity depends indeed on the physical magnitude which is being investigated. Therefore, this magnitude has to be chosen with great care for each typology of the sensor.
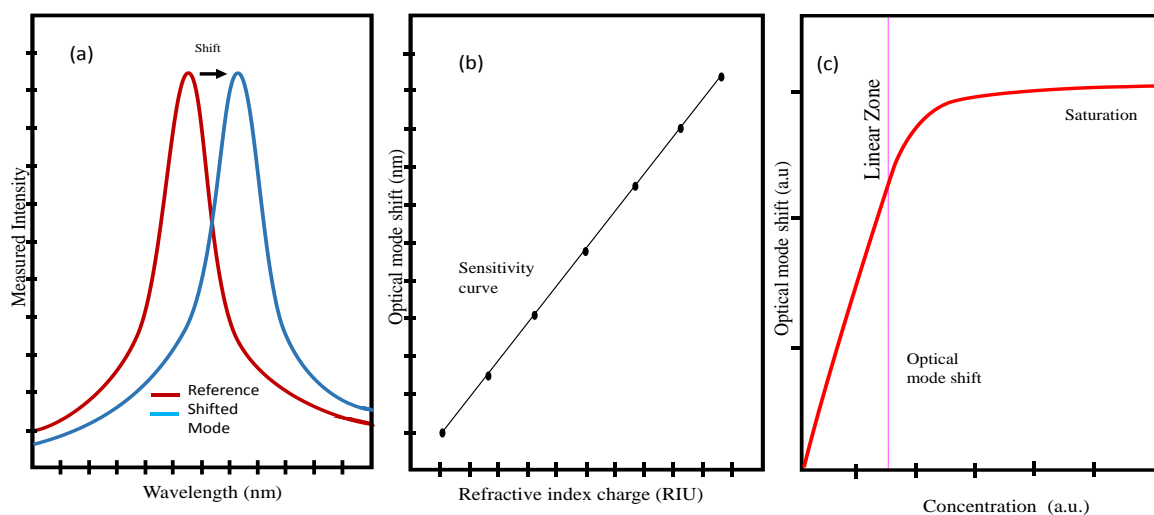
Fig. 2.13. (a) Wavelength change of sensor (b) Spectral change with respect to RI (c) Standard response curve of a biosensor. Adapted from (Casquel 2013)

Accordingly, it can be explained the optical or refractive index (RI) sensitivity as the resonance shifting as a function of the RIU shift in the surface of the sensor following equation (2.9).

$$RI\ Sensitivity = \frac{\Delta\ resonance}{\Delta n} \qquad (2.9)$$

These basic parameters for analyzing the performance of the SPR sensor should be a high value as conceivable for a better sensor. The sensitivity of SPR sensor can be well-defined as the

ratio of the shifting of output parameters (i.e. change of SPRF, θ_{SPR}) to the shifting in the concentration of biomolecules, Δca (sensor input) as given below:

$$Sensitivity = \frac{\Delta\theta_{SPR}}{\Delta C_a} \qquad (2.10)$$

or

$$Sensitivity = \frac{\Delta SPRF}{\Delta C_a} \qquad (2.11)$$

Alternatively, in angular interrogation, it is defined as the alteration in resonance angle for a unit alteration in the RI of the sensing medium [104]:

$$Sensitivity, \ S = \frac{\Delta\theta_{SPR}}{\Delta n_s} ; \ \text{deg/RIU} \qquad (2.12)$$

In the case of wavelength interrogation, the sensitivity parameter is defined as the change in the resonance wavelength for a unit change in the RI of the target medium [106]:

$$S = \frac{\Delta\lambda_{SPR}}{\Delta n_s} \qquad (2.13)$$

When detectable molecules are augmented into the target medium, the RI changes, and therefore the shift of resonance angle $\Delta\theta_{SPR}$ or wavelength ($\Delta\lambda_{SPR}$) causes. The larger the shift of resonant wavelength/ resonant angle for the same amount of RI shift leads to a higher sensitive sensor [106].

2.8.2 Signal to Noise Ratio (SNR)

The signal-to-noise ratio, also known as the detection accuracy (DA). DA for wavelength interrogation technique can be determined by inspecting the SPR curve and is given as:

$$DA = \frac{\Delta\lambda_{SPR}}{\Delta\lambda_{0.5}} \qquad (2.14)$$

Alternatively, in angular interrogation, detection accuracy can be subjected to a measure of the spectral width of 50% reflectivity of SPR curve and is given by [106],

$$SNR = \frac{\Delta\theta_{SPR}}{\Delta\theta_{0.5}} ; \ \text{dimensionless} \qquad (2.15)$$

DA is a dimensionless parameter. Where $\Delta\theta_{0.5}$ is denoted as the spectral width of the SPR curve for 50% reflectivity. The greater the shift of resonant wavelength/ resonant angle for the same amount of RI change, broaden the SNR value of biosensor [106] and lower the value of spectral width, the higher will be the value of SNR. A favorable sensor should possess a higher DA value.

2.8.3 Quality Factor (QF)

The Quality Factor, also known as the figure of merit (FOM). The QF for wavelength interrogation technique can be determined by inspecting the SPR curve and by equation 2.16:

$$QF = \frac{Sensitivity, S}{\Delta\lambda_{0.5}}; \quad (RIU)^{-1} \tag{2.16}$$

Alternatively, in angular interrogation, QF can subject to the spectral width of 50% reflectivity. The QF of the SPR sensor is dependent on the sensitivity as well as on the spectral width of the SPR curve, that is expressed by [106]:

$$Q.F = \frac{\Delta\theta_{SPR}}{\Delta n_S \Delta\theta_{0.5}}; \text{RIU}^{-1} \tag{2.17}$$

A good sensor should provide a high-quality factor.

2.8.4 Specificity

This parameter announces about the capability of the sensor to confirm the correct recognition of a particular analyte, and therefore, the response achieved is not provoked by another undesired connection. Rough specificity means a higher option of finding a 'false positive' results. As specificity depends on the analyte numbers, it is very hard to measure. Higher the number of analytes, the higher the possibility of misleading to undesired interaction of molecules or cross-reaction between them.

2.8.5 Linear Range

It is the range of concentration values of a target analyte in which the detection results are to be effective. In this range, the sensing attribute and concentration are almost linear. Besides, the threshold, the value of concentration from which the linear range starts. An example can be

seen in Figure 3.8(c), where the linear range is located between concentration values C_0 and C_1, being C_0 the threshold concentration of the sensing response.

2.9 Applications of Surface Plasmon Resonance Biosensor

The working principle of affinity biosensors depends on the surface plasmon spectroscopy, the immobilizing bio-recognition elements that can recognize and arrest target analyte molecules in a presented liquid solution. This capturing of analyte results in a rise in the RI at the sensing surface. The increase in RI leads to a rise in the value of propagation constant of the sensing surface and it is commonly determined by measuring the change of optical characteristic that is caused by interacting with surface plasmon. In the recent literature, an extraordinary advancement has been witnessed in the literature of affinity design and their area of applications such as monitoring of various environmental parameters, clinical diagnostics, food safety, drug screening. The elementary applications of SPR involved absorbance measurements [107], biokinetic [108] and biosensing techniques [109], gas detection [110], process analytics [111], SPR microscopy [48], refractive index measurements [112], and thin-film characterization [107]. Recently, the improvement of SPR has been directed toward food security techniques. However, SPR has not been confined to this field, for it has been implemented extensively in electrical engineering, chemistry, theoretical physics, and experimental optics.

2.9.1 DNA Hybridization Detection

In DNA hybridization sensing sensor recognize the right positioning and alignment of the nucleotide connection between guanine (G) to cytosine (C) and thymine (T) to adenine (A). Now a days, the efficient diagnosis of genetic diseases and many other complex mortal diseases like cancer and hepatitis B succesfully utilized the DNA hybridization detection sensors [113]. SPR principle based sensor works by identifying and determining the effective RI change of the detecting medium utilizing the attenuated total reflection (ATR) on an angular investigation mode [114]. When the phase matching of incident TM-polarized light and wave vector of SPW achieved, the resonance occurred at particular wavelength [51].

A double strand complementary DNA forms by binding two single-strand DNA and between these two single strand DNA one is target DNA and another is probe DNA. In SPR biosensor the probe DNAs coated on the sensor surface and the target DNAs are kept in target sample.

The bindings between probe and target DNAs changes the concentration of detecting solution that results a change in RI of sensing medium. The detecting principle of the SPR sensor works on the change of effective RI sensing solution after complementary DNA formation. The change of RI makes a change in propagation constant of SPW resulting an SPR angle shift which is a detecting attribute.

2.9.2 Formalin Detection

In a formalin detecting sensor, initially biorecognition element, chitosan has to immobilize on the sensor surface. When formaldehyde immobilized onto the chitosan surface, the alteration in RI value of the sample medium has been inspected with respect to the effects of response time, pH range, scan rate, and formaldehyde concentration on the hydrolysis of formaldehyde. For example, with the change of formaldehyde concentration in sensing solution, the refractive index of the medium changes. This change in RI of the sensing medium causes an SPR angle shift. The shift of SPR angle indicates the concentration or existence of formalin in the detecting solution. Since, formalin has the most attractive and significant property of chitosan is its high selectivity to formalin. Ping et al, have reported that chitosan makes a significant bond or adsorption with formalin. On the other hand, this probe cannot make a significant bond with the coexisting intrusive compounds together with some common aldehyde compounds and many other probably concomitant chemical species in real food samples (such as Fe^{3+}, Ca^{2+}, NO_3^-, Mg^{2+}, Cl^-, L-cysteine, L-arginine, N-acetyl-cysteine, N-acetyl glycine, sodium pyruvate, chloral and acetaldehyde) [115]. This investigation report clearly demonstrates the quite good selectivity of the chitosan as probe for formalin detection. Besides, chitosan (CHIT) has been utilized on the sensor surface to effective immobilization of formalin molecules and it also improves the chemical stability [116].

In summary, the main idea on which the use of SPR for sensing applications is based on the fact that the analyte (formalin), interacting with a selective center attached at the interface, increases the refractive index of the medium in the area of the penetrating wave thereby varying the resonance conditions. By following the changes of the resonance conditions from the variation of a quantity, such as the SPR angle on the angular dependence, it is possible to monitor directly the amount of the analyte attached to the receptor.

2.9.3 Virus Detection

The E-protein of dengue virus carries a significant amount of ability to attract antibody. This structural protein is formed a coating surrounded to the host virus itself. Thus, it is sufficient to develop appropriate immune response by creating identifiable antibodies for diagnosis in patient's body [117, 118]. The RI change of dielectric medium close to the sensing layer can be effectively detected by SPR sensor [119]. In this virus detection approach, an antibody coating has to be provided on the sensor surface which can effectively and selectively immobilized the virus to be detected. When a sample of virus is to provide on the sensing surface the antibody coating immobilized the virus on its surface that makes the medium's refractive index change. This change in refractive index causes a SPR angle to match the wave vector. The change of SPR angle is and effective detection attribute. For example, Nur et al. reported an study to detect dengue virus using SPR biosensor[120]. In this report, an IgM antibody had been coated on the gold surface. The E-spike protein of dengue virus are the attractive protein for the IgM antibody coating. When a sample of E- protein of dengue virus is provided on the sensing surface the IgM specific antibody of dengue virus immobilizes the E-protein and it leads to a refractive index change of the sensing medium. By angular investigation method this existence of dengue virus can effectively and easily be identified as the refractive index change of the sensing medium makes an SPR angle shift.

2.10 Chapter Summary

This chapter first focuses on the theoretical review of SPR sensors that basically covers its classification with working principles, applications, and importance. In the last part of this chapter, the description of performance variables and parameters of SPR biosensor has been explicated. The term relating performance variables of SPR sensor such as SPR Angle, SPR Frequency, Minimum Reflectance, Maximum Transmittance, SPR Wavelength are defined with their mathematical identity. After then the performance parameters of the SPR sensor are mainly evaluated based on its sensitivity (S), detection accuracy (DA), and the quality factor (QF), specificity, linear range are described. The working principles of different SPR sensor in various applications are discussed with explanation.

CHAPTER III

TiO₂ and ZnO Based Structures: Modeling and Simulations

3.1 Introduction

This chapter makes a clear concept about the mathematical modeling and designing of SPR sensor. At first, the design consideration with optimized geometries have been stated for two different surface plasmon resonance sensor structures. Then the reflection and transmittance intensity of incident light in the proposed sensor has been conferred. Finally, FDTD analysis model using YEE algorithm in Lumerical solution environment has been reported.

3.2 Design of TiO₂-SiO₂ and MoS₂-Graphene Composite layer Based Sensor

The proposed SPR sensor consists of seven lamellas and the compositional structure is represented through **Fig. 3.1**. The transverse magnetically polarized incident light is the most significant requirement for the Surface plasmon excitation as this p- polarized light is the only responsible for exciting the SPR [121]. In order to enliven the TM polarized light wave, in the path of incidence a polarizer is set up. The propagation constant of surface plasmon waves (SPW) is always higher than that of optical wave propagation in the dielectric and thus the SPW cannot be excited directly by a normal incident light at a planar metal dielectric interface [122].Therefore, the wave vector mismatch between free space and SPW has been compensated by increasing the momentum of the incident optical wave. This momentum change is commonly achieved using attenuated total reflection (ATR) in prism couplers [122]. In order to provide additional momentum to the incident light, it is essential to install a high wave vector photonic crystal [123]. Therefore, in the urge to meeting this requirement, a high RI glass prism as a foundation infrastructure is recommended for the proposed sensor. The specified high refractive index SF11 glass prism for the proposed sensor with refractive index n_p=1.7786 which mentioned with detail information in **Table 3.1**.

The optical nonlinearity improved with higher operating frequency as well as overall performance improved with smallest Kerr effect at low operating frequency [124]. Therefore, the operating light wavelength is chosen as λ=633nm and all the refractive index [RI] values of each materials are considered at λ=633nm. Fresnel optical design system with an association of Kretschmann structure is employed to design the recommended sensor for the angular

investigation scheme whose detail discussion was presented in the previous report [49, 104, 121, 125, 126].
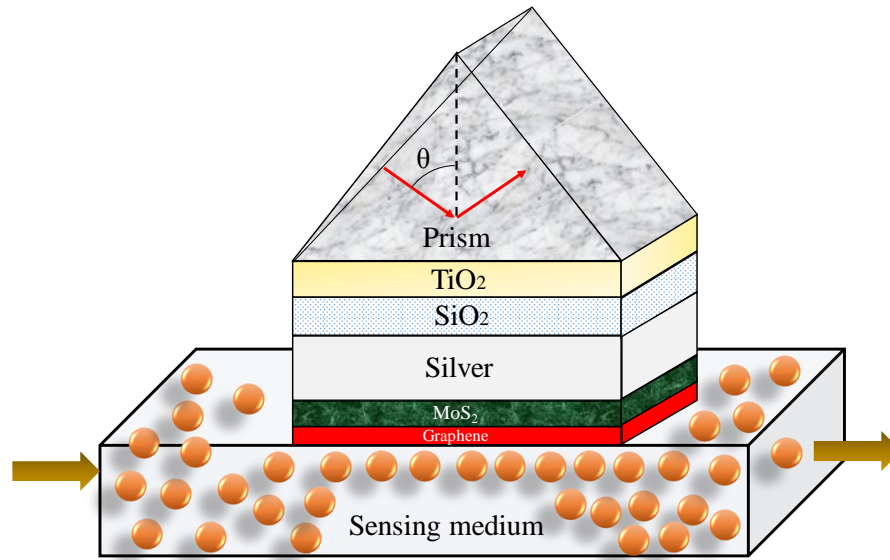
Fig.3.1. Schematic diagram of TiO₂- SiO₂ and MoS₂-graphene composite SPR sensor

Table 3.1. Sensor Constructional Details with Optimized Geometries

Layer Position	Materials	Refractive Index (RIU)	Optimized Thickness (nm)	Reference
Layer1	SF11 glass prism	1.7786	N/A	[102, 103]
Layer2	TiO₂	2.5837	37	[102, 127]
Layer3	SiO₂	1.4570	20	[102, 127]
Layer4	Silver (Ag)	0.1726 +i 3.421	45	[102, 121]
Layer5	MoS₂	5.9+i0.8	0.65	[102, 128]
Layer6	Graphene	$3.0+j1.1487$	0.34	[112, 129, 130]
Layer7	PBS Solution	1.34	N/A	[107, 131]

The refractive index of TiO2 and SiO2 is purely real and therefore, their used as adherence layer on prism of SPR sensor is appreciating. The RI of TiO2 is higher than the SiO2 for a certain wavelength. Therefore, a combination of TiO2 and SiO2 as the low RI layer over the high RI is possible. The composite layer of TiO2 and SiO2 performs as adherence layer better than the performance while they acted individually in the SPR sensor [132, 133]. The reason is that the reaction of plasma generation occurs at the close to the TiO2–SiO2 interface [134]

and also for this reason the trapping of light is efficiently improved [135]. This impressive light trapping produces more surface plasmons (SPs) which lead to enhanced SPR angle and frequency. This increase of SPR angle and frequency causes the improved performance of the SPR sensor [136]. The RI of TiO_2 and SiO_2 are tabulated in **Table 3.1**.

Commonly the silver and gold films are treated as the ideal contenders in visible region [137]. Usually, the sharpness of SPR curve is obtained better by using Ag layer instead of Ag layer and therefore it is utilized in order to improve biosensor performance [47]. In this report, silver is employed as the plasmonic metal. Usually, a coating of silver (Ag) in the SPR sensor serves greater sensitivity, detection accuracy as well as quality factor with appreciable narrowness in spectral width which than the SPR sensor with gold (Au) coating. However, the SPR sensor only based on Ag prohibits useful charge transfer because of its poor impedance to oxidation and corrosion in various situations [138]. Accordingly, the selection of silver would be a better metal for improving the performance of the SPR sensors if the surface of silver lamella can be possible to make chemically inactive to oxidation [139]. To provide a strong impedance to oxidation and corrosion, better stability in a chemical reaction, and superior optical performances [49, 121], insertion of a monolayer MoS_2 [140], a 2D material can be successfully employed. The sensitivity of the quantum-imprisonment acquired direct bandgap [141] in single-layer MoS_2 makes capable of highly sensitive identification of bio-objects [142]. It also possesses greater optical absorption efficiency [8, 140], large fluorescence quenching capability [142] and a distinct affinity toward biomolecules.

Graphene has the properties of high analyte adsorption ability and optical features. It is one of the most broadly employed 2D nanomaterial since its early period of discovery by K.S. Novoselov et. al. [143]. It is the leanest, vigorous, translucent, self -polarization consequence, very low phase falsification, relatively large nonlinearity, tunable semiconductor, nice thermal conductivity, and great optical absorption [144]. The choice goes on the favor of graphene-skinned SPR sensors because of its wide surface to volume ratio which is advisable for creating the bond with analytes [145]. Additionally, another argument is that the surface of graphene can carefully identify scented compounds through the pi-stacking force [146].

Finally, a layer of phosphate buffer saline (PBS) medium is imposed as a bare detecting medium that allows better adsorption of molecules [107, 131]. A comprehensive theoretical structure of the proposed sensor with different materials of optimum geometries has been listed up in **Table 3.1.**

After the confirmation of the simulation arrangement, a TM polarized He-Ne ray of 633 nm is imposed and it goes across the prism and some share of incident light strike to the composite layer interface. Resonant stimulation of photon-electron coupling occurs when the wavevector of the incident light is the same as the wavevector od SPW and remains overcrowded at the interface and collapses exponentially in the crosswise directions [106, 147]. This momentarily varied exponential SPR tail is very responsive to the complex RI change of a metal layer, nearby dielectric medium, and also their geometries [106, 121], that results a high sensitivity [121].

3.3 Design of ZnO and PtSe2-Graphene Composite layer Based Sensor

The proposed SPR sensor consists of six lamellas and the compositional structure is represented through **Fig. 3.2**. The transverse magnetically polarized incident light is the most significant requirement for the Surface plasmon excitation as this p- polarized light is the only responsible for exciting the SPR [121]. In order to enliven the TM polarized light wave, in the path of incidence a polarizer is set up. The propagation constant of surface plasmon waves (SPW) is always higher than that of optical wave propagation in the dielectric and thus the SPW cannot be excited directly by a normal incident light at a planar metal dielectric interface [122].Therefore, the wave vector mismatch between free space and SPW has been compensated by increasing the momentum of the incident optical wave. This momentum change is commonly achieved using attenuated total reflection (ATR) in prism couplers [122]. In order to provide additional momentum to the incident light, it is essential to install a high wave vector photonic crystal [123]. Therefore, in the urge to meeting this requirement, a high RI glass prism as a foundation infrastructure is recommended for the proposed sensor. The specified high refractive index BAF 10 glass prism for the proposed sensor with refractive index n_p=1.6671[148].

The optical nonlinearity improved with higher operating frequency as well as overall performance improved with smallest Kerr effect at low operating frequency [124]. Therefore, the operating light wavelength is chosen as λ=633nm and all the refractive index [RI] values of each materials are considered at λ=633nm. Fresnel optical design system with an association of Kretschmann structure is employed to design the recommended sensor for the angular investigation scheme whose detail discussion was presented in the previous report [49, 104, 121, 125, 126].
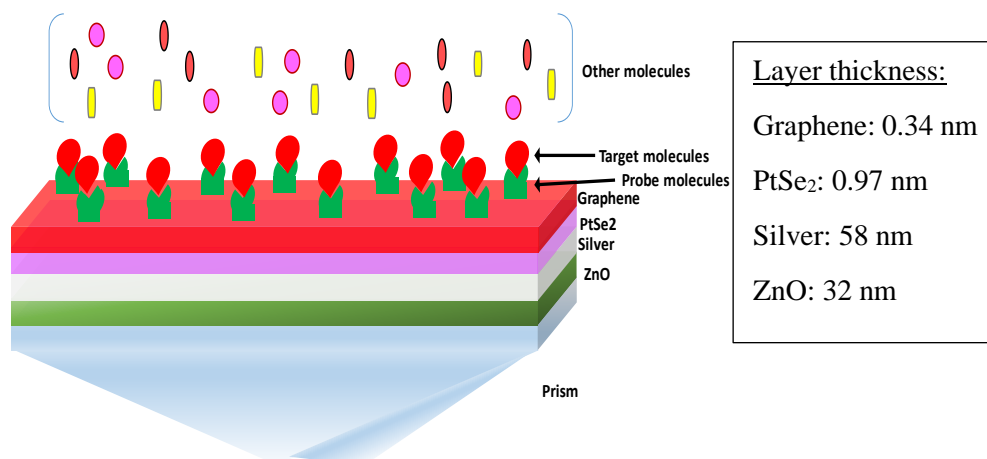
Fig.3.2. Proposed ZnO and PtSe2-graphene composite sensor structure

On the prism base a nano layer of Zinc oxide has been considered to deposit. Recently, as adhesion layer in SPR sensor Zinc oxide (ZnO) has been used and it improves the sensor performance [66]. The high value of isoelectric point, outstanding chemical stability, excellent optical and electrical properties of ZnO are exhibited in glucose sensing and so on [67-70]. The admirable non-centrosymmetry characteristic between ZnO surface and metal layer intensifies the second-order susceptibility at the interface and leads to an enhanced charge transfer. Therefore, ZnO progresses the ability of light collection [71, 72]. Besides, ZnO layer is highly responsible for the significant change in SPR angle as well as sharpness of SPR curve [73].

Generally silver and gold are considered the potential candidates as plasmonic metal in SPR sensor [137]. Usually, the sharpness of SPR curve is obtained better by using Ag layer instead of Au layer and therefore it is utilized in order to improve biosensor performance [47]. In this design, silver is employed as the plasmonic metal. Usually, a coating of silver (Ag) in the SPR sensor serves greater sensitivity, detection accuracy as well as quality factor with appreciable narrowness in spectral width which than the SPR sensor with gold (Au) coating. However, the SPR sensor only based on Ag prohibits useful charge transfer because of its poor impedance to oxidation and corrosion in various situations [138]. Accordingly, the selection of silver would be a better metal for improving the performance of the SPR sensors if the surface of silver lamella can be possible to make chemically inactive to oxidation [139]. Therefore, to mitigate this problem a highly resistive 2D material PtSe2 has been used on the Ag layer and this material has a strong biomolecule adsorption ability [60]. Monolayer PtSe2 can provide an enhanced charge mobility and thus is of great interest for SPR sensing applications [61]. Furthermore, less toxicity and chemical stability has been examined of PtSe2 in various sensing

applications [62, 63]. The mono layer PtSe2 shows the similar shape of structure as graphene and phosphorene. It also possesses outstanding optical as well as electrical properties which have engrossed great attention as a member of 2D material beyond the ancestor members [62, 64, 65].

The most biocompatible graphene layer has been considered to deposit on PtSe2. Since graphene has the properties of high analyte adsorption ability and optical features. It is one of the most broadly employed 2D nanomaterial since its early period of discovery by K.S. Novoselov et. al. [143]. It is the leanest, vigorous, translucent, self -polarization consequence, very low phase falsification, relatively large nonlinearity, tunable semiconductor, nice thermal conductivity, and great optical absorption [144]. The choice goes on the favor of graphene-skinned SPR sensors because of its wide surface to volume ratio which is advisable for creating the bond with analytes [145]. Additionally, another argument is that the surface of graphene can carefully identify scented compounds through the pi-stacking force [146].

Finally, a layer of phosphate buffer saline (PBS) medium is imposed as a bare detecting medium that allows better adsorption of molecules [107, 131].

After the confirmation of the simulation arrangement, a TM polarized He-Ne ray of 633 nm is imposed and it goes across the prism and some share of incident light strike to the composite layer interface. Resonant stimulation of photon-electron coupling occurs when the wavevector of the incident light is the same as the wavevector od SPW and remains overcrowded at the interface and collapses exponentially in the crosswise directions [106, 147]. This momentarily varied exponential SPR tail is very responsive to the complex RI change of a metal layer, nearby dielectric medium, and also their geometries [106, 121], that results a high sensitivity [121].

In this formation, the most practiced constituent is prism (BAF10 glass) with a RI of 1.6671[148]. The subsequent section on the prism is a ZnO layer with RI of 1.98 [73]. The succeeding is the silver layer with a complex RI of 0.1726+j3.421[48]. The next two layers are PtSe2 and graphene with RI of 4.7954+j1.2405 [149] and 3.0+j1.1487 [150], respectively. The thickness of each layer is also shown in **Fig. 3.2**.

3.4 Modeling of Proposed Sensor

An evanescent wave formed, known as SPW when the energy of an incident light excites the electron of composite lamella interface. The value of propagation constant of SPW can be adjusted so that it becomes same with the value of incident light wave propagation constant. This point of same propagation constant is called SPR point [103]. At this resonant point, minimum reflection comes back on the detector. In the following section mathematical modeling of the proposed SPR based sensor for food preservatives detection is mentioned with a detail explanation.

3.4.1 Mathematical Modeling of Reflectivity

As we know that transfer matrix method needs no approximation [145], this method has been employed in order to calculate the reflected light back from the prism and an N-layer. T_k denotes the layer thickness of each nanocomposite layers and it is painstaking along the z-axis. In some respects, n_k and ε_k denotes k^{th} layer RI and permittivity respectively. The tangential component of the fields at the first periphery is continuous to the last periphery [124].

$$\begin{bmatrix} U_1 \\ V_1 \end{bmatrix} = M \begin{bmatrix} U_{N-1} \\ V_{N-1} \end{bmatrix} \tag{3.1}$$

In some respects, U_1 conveys the tangential components of the electric field and V_1 bears the extraneous magnetic field components at the edge of the first layer. Also, U_{N-1} and V_{N-1} are presented for the corresponding fields at the border of the Nth layer. The characteristics matrix for corresponding composite sensor structure is represented by M_{ij}. Similarly, for transverse magnetically polarized light the corresponding characteristic matrix can be formed by the equation (3.2)-(3.5) [49].

$$M_{ij} = \left(\prod_{k=2}^{N-1} M_k \right)_{ij} = \begin{pmatrix} M_{11} & M_{12} \\ M_{21} & M_{22} \end{pmatrix} \tag{3.2}$$

With, $$M_{ij} = \begin{pmatrix} \cos \beta_k & -(i \sin \beta_k)/q_k \\ -(i q_k \sin \beta_k) & \cos \beta_k \end{pmatrix} \tag{3.3}$$

where,

$$q_k = \left(\frac{\mu_k}{\varepsilon_k}\right)^{\frac{1}{2}} \cos\theta_k = \frac{\left(\varepsilon_k - n_1^2 \sin^2\theta_1\right)^{\frac{1}{2}}}{\varepsilon_k} \tag{3.4}$$

$$\text{and } \beta_k = \frac{2\pi}{\lambda} n_k \cos\theta_k (Z_k - Z_{k-1}) = \frac{2\pi T_k}{\lambda}\left(\varepsilon_k - n_1^2 \sin^2\theta_1\right)^{\frac{1}{2}} \tag{3.5}$$

After some simple mathematical calculations, one can easily make the relationship represented by equation (3.6) of the reflection coefficient for p-polarized light.

$$r_p = \frac{(M_{11} + M_{12}q_N)q_1 - (M_{21} + M_{22}q_N)}{(M_{11} + M_{12}q_N)q_1 + (M_{21} + M_{22}q_N)} \tag{3.6}$$

The reflectivity, R_p of the composite multilayer sensing device is revealed by equation (3.7).

$$R_p = |r_p|^2 \tag{3.7}$$

3.4.2 Mathematical Modeling of Refractive Index

The alteration in the refractive index (RI) of the sensing medium occurs because of the submersing of probe chitosan of the sensing medium. The shifted RI $\left(n_S^a\right)$ of target medium after the adsorption of formalin molecules is mathematically modeled by equation (3.8) as [125, 151]:

$$n_S^a = n_S + c_a \frac{dn}{dc} \tag{3.8}$$

Where, c_a represents the concentration of molecules subject to be detected, n_S represents the RI of the detecting medium before adsorption of formalin molecules and dn/dc indicates the RI increment of the adsorbate. The change of RI is denoted by dn/dc cm^3/gm [151] when standard buffer solution is used. The presence of formalin molecules alters the SPR angle to right shift because of the inclusion of probe which alters the RI of the detecting dielectric. The incorporation of formalin molecules enriches the number of carriers which alters the carrier concentration on the graphene layer leading to a change in propagation constant. Consequently, this proposed SPR sensor with high performance is employed to identify the formalin governed by the SP angle changes.

3.4.3 Modeling of Performance Parameters

The characterization of SPR based sensor's performance parameters basically depends upon the sensitivity, the quality factor and also on the detection accuracy. Intended for reaching a good act of an SPR sensor, all performance indicating parameters should own the capability of having a high value as conceivable [48]. The reflectance and SPR angle changes for the change of RI of target sample. The sensitivity S, is defined by the percentage change in θ_{SPR} of fallen light with the RI change, Δn_a, which can mathematically be represented by equation (3.9) and it is expressed by the unit of deg/RIU [150, 152].

$$S = \frac{\Delta\theta_{SPR}}{\Delta n_a} \qquad (3.9)$$

Secondly, the most excellent parameter, known as signal to noise ratio (SNR) and it is usually familiar as detection accuracy. The value of this parameter can be figured out inspecting the SPR curve with the help of equation (3.10) and this parameter's value is expressed without dimension [49].

$$SNR = \frac{\Delta\theta_{SPR}}{\Delta\theta_{0.5}} \text{ ; dimensionless} \qquad (3.10)$$

Where $\Delta\theta_{0.5}$ portrayed the wider size of SPR curve for the 50% reflection. And the third parameter but carrying the lion's share significance of sensor performance is the quality factor that vigilant to both on $\Delta\theta_{0.5}$ and the sensitivity and it can be reported by equation (3.11) [49]:

$$Q.F = \frac{\Delta\theta_{SPR}}{\Delta n_S \Delta\theta_{0.5}} \text{ ; RIU}^{-1} \qquad (3.11)$$

The properties of high detection accuracy, larger sensitivity and enhanced quality factor are indicated as better sensors [153].

3.5 SPR Sensor Designing for FDTD Solution using Lumerical Multiphysics

Initially, a study of four sub cell layered stack that terminated into a perfectly matched layer (PML) has been carried out (**Fig. 3.3**). Sub cell FDTD is used to model parallel dielectric layers and regular FDTD is used to design model for comparison as uniform mesh. Each layer is separated by 75 μm in the x-direction from another one.
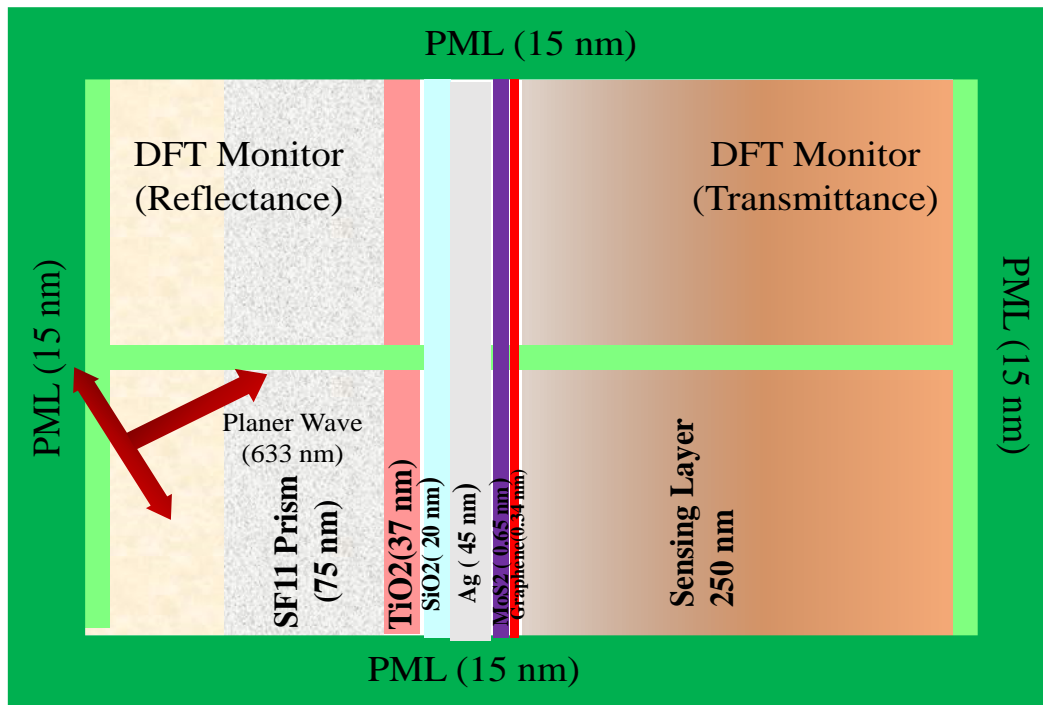
Fig. 3.3. 2D Computational Domain for the electric field distribution along the x-direction

Initially, a study of four sub cell layered stack that terminated into a perfectly matched layer (PML) has been carried out (**Fig. 3.4**). Sub cell FDTD is used to model parallel dielectric layers and regular FDTD is used to design model for comparison as uniform mesh. Each layer is separated by 75 μm in the x-direction from another one.

The sensor structure is concluded by PML sub cell in the z-direction, and this structure is simulated in FDTD mode solution to study. Correspondingly, the time step size and spatial mesh size for FDTD are set to $\Delta t = \Delta / 4C_0$ and $\Delta = \lambda / 10$, to satisfy the CFL stability criterion, where $\lambda = 633$ nm. Here, $\Delta x = \Delta y = \Delta z = \Delta = 63.3$ nm. At last, the computational space is concluded by a 15 nm PML sub cells. In order to reach the steady state of field components, the simulation time step size is chosen 50,000 times [154].
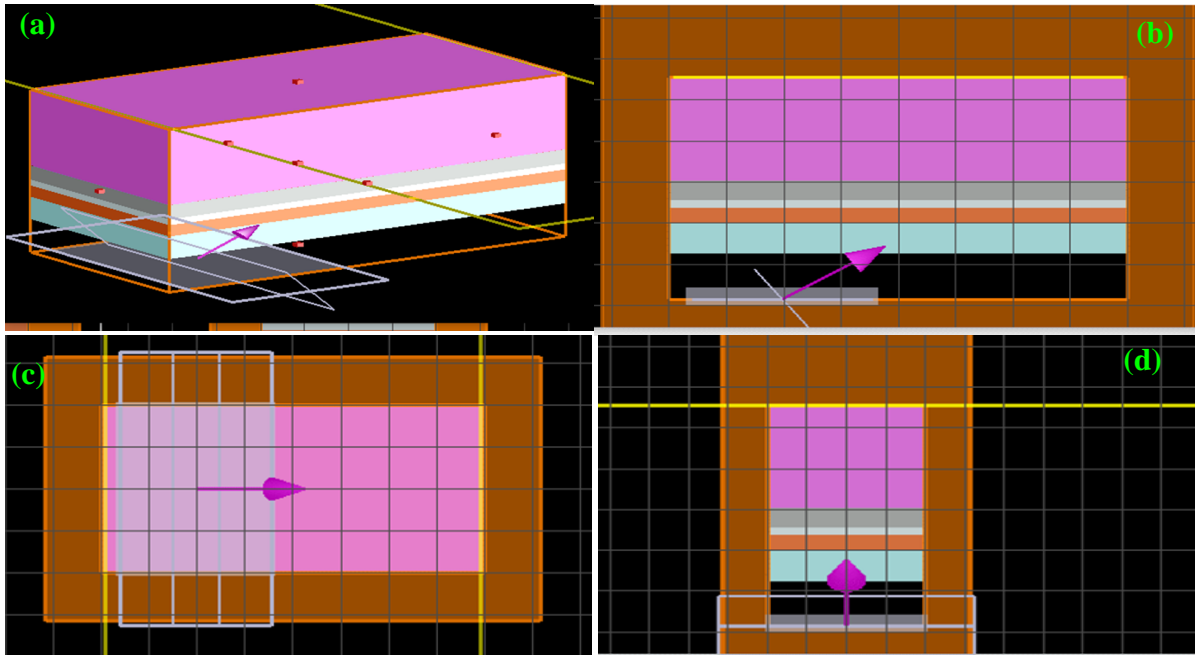
Fig 3.4. Software simulation diagram for designing SPR sensor: (a) 3D perspective view, (b) grid view of XZ plane, (c) grid view of XY plane (d) grid view of YZ plane

3.6 Chapter Summary

In this chapter, the designing of two different sensor structures as well as modeling of minimum reflected light intensity, maximum transmittance light intensity, SPR angle, SPR frequency, spectral width is presented. The mathematical models of sensitivity, quality factor and detection accuracy are depicted briefly for multilayered sensor structures. A schematic modeling of proposed composite sensor is described using Lumerical solution commercial software.

CHAPTER IV

Performance Study in Formalin Detection

4.1 Introduction

The surface plasmon resonance sensor is an influential device for detecting and monitoring food security issues. However, the SPR sensor necessitates to be more sensitive as well as high quality expedient. In this research, two different composite structure Ag coated SPR sensor has been studied: one is TiO2-SiO2-Ag-MoS2-graphene and the another is ZnO-Ag-PtSe2-graphene. To analyze the overall performance of this sensor, sensitivity, detection accuracy, and quality factor have been investigated. All the performance is analyzed individually for both the different composite sensor structures and a comparison has made regarding their performance in formalin detection. In order to make a clear understand about the electric field distribution through the sensor structure FDTD analysis has been carried out. A comparative study between two different sensors is carried out and finally, another comparison between the two different proposed sensors' performance and the existing sensors' performance also presented in this chapter.

4.2 Optimization

In this work two different sensor structure but the plasmonic metal of them are the noble silver has been proposed. Initially, the optimization of silver layer has been carried out for each sensor structure focusing on their better performance parameters. First the silver layer thickness optimization of TiO2-SiO2 and MoS2-graphene composite based silver coated structure has been carried out and then ZnO and PtSe2 composite based silver coated structure has been accomplished. The details of optimization approach are described in the following section of this chapter.

4.2.1 Optimum Silver Layer Thickness Selection for TiO2-SiO2 based structure

A laser of 633 nm wavelength was chosen as the light source for the sensor. The initial RI of the sensing medium is assigned as 1.33 RIU and the increment Δn_s of RI is considered to 0.01 RIU. In addition, the initial thickness of TiO2 and SiO2 layer are set to 37 nm and 20 nm respectively. To optimize the thickness of silver layer, we set its initial thickness at 20 nm and

took the values of performance parameters by varying the thickness up to 70 nm with an incremental rate of 5 nm.

The variation of minimum reflectance curve of proposed sensor of different thickness of silver layer where the minimum reflectance value for the RI of the sensing medium is presented in **Fig. 4.1**. This curve shows that the minimum reflectance is higher at the initial thickness and it gradually decreases from 25nm and the lowest level of minimum reflectance obtained at 45 nm of silver thickness. After 45 nm the minimum reflectance value further goes through an increasing trend. Anther curve of minimum reflectance for different silver layer thickness is present in **Fig.4.2** keeping the sensing medium RI fixed at 1.41. From this figure it is transparent that the most significant point of minimum reflectance is at 45 nm thickness.
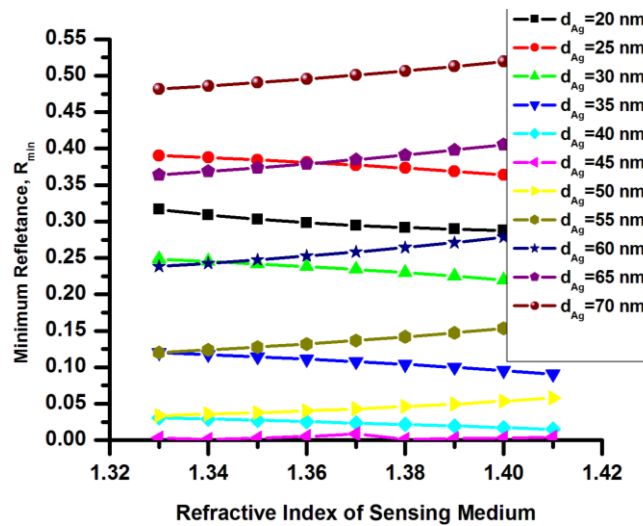
Fig. 4.1. Minimum Reflectance vs RI curve of Proposed Sensor for varying Ag thickness
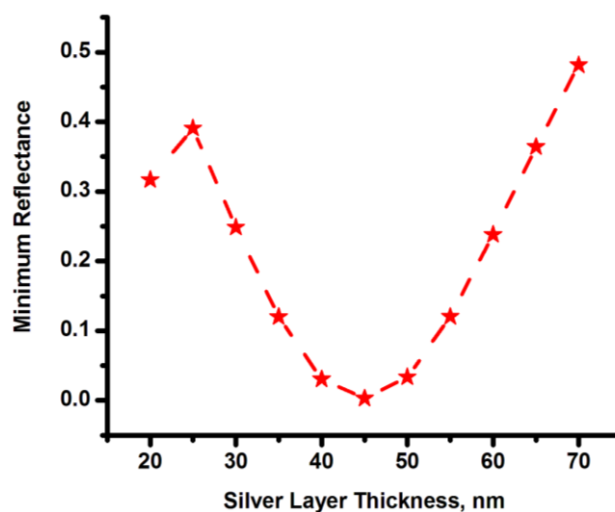
Fig. 4.2. Minimum Reflectance vs Silver Layer Thickness Curve

In **Fig. 4.3**, the sensitivity of this proposed structure with different concentrations of sensing medium for various thickness of Ag layer is presented. For the thickness of 45 nm of the Ag layer, the sensor shows highest sensitivity for the RI range of 1.33 to 1.41.
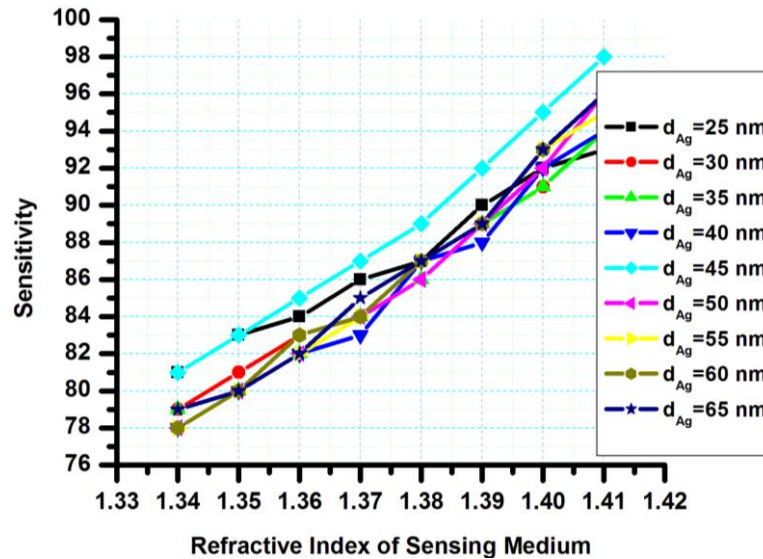
Fig. 4.3. Sensitivity vs RI of Sensing Medium curve for different Ag Layer Thickness

Fig. 4.4 shows the sensitivity of the proposed hybrid structure sensor with a uniform variation of the Ag layer thickness. The sensitivity increases up to the thickness 45 nm and then starts to decreases with the increase of silver thickness. At the thickness of 45 nm, the sensor shows the highest sensitivity. Below and above of the 45 nm thickness, the sensor shows lower sensitivity.
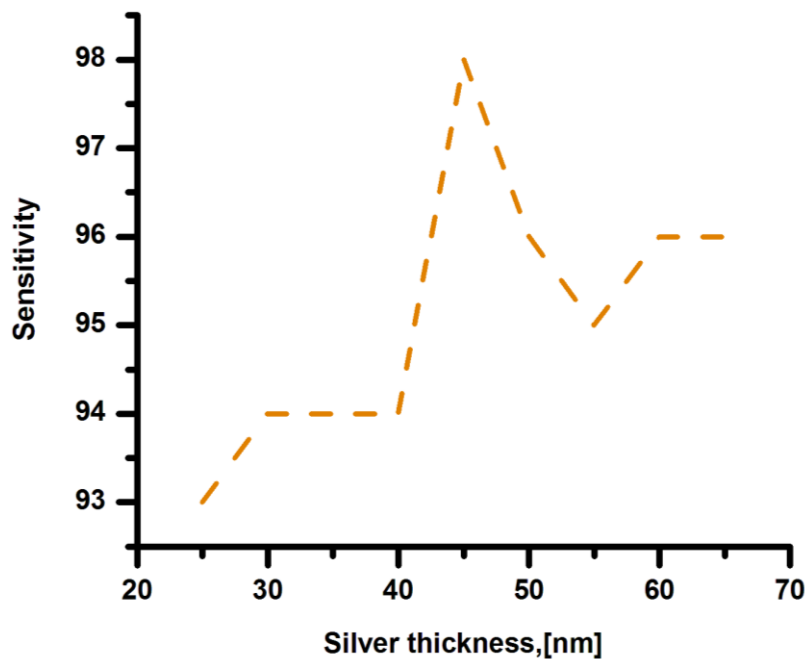
Fig. 4.4. Sensitivity vs Ag Layer Thickness

Fig. 4.5 exhibits the detection accuracy of the proposed hybrid sensor varying the Ag layer thickness. The detection accuracy decreases to a minimum value at 40 nm thickness of silver layer and above the 40 nm it starts to an increasing trend. The effective choice of silver thickness should be above the 40 nm.
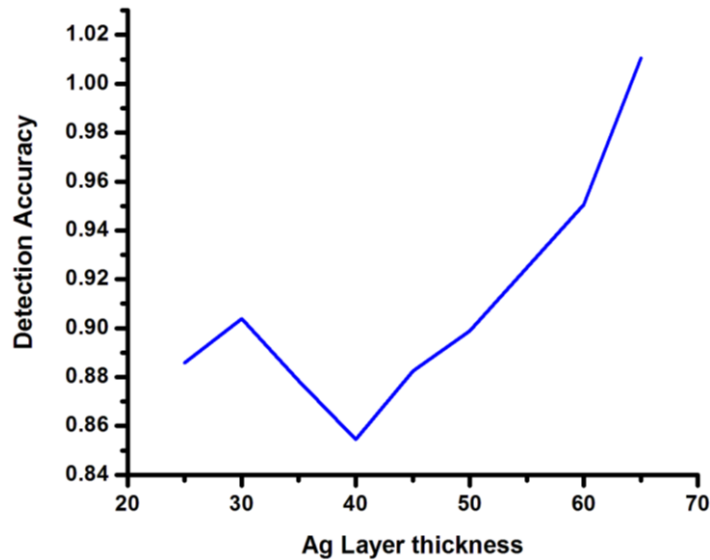
Fig. 4.5. Detection Accuracy vs Ag Layer Thickness Curve

The quality factor of this proposed sensor with the variation of silver layer thickness is obtained and represented by the curve shown in **Fig. 4.6**. Similar to detection accuracy vs silver thickness curve, quality factor vs silver thickness curve shows the similar trend. The quality factor is lowest at 40 nm of the Ag layer thickness. Above the 40 nm thickness, the sensor shows an increasing trend with the silver thickness. From the above study it is transparently evident that the choice of silver thickness should be above 40 nm.
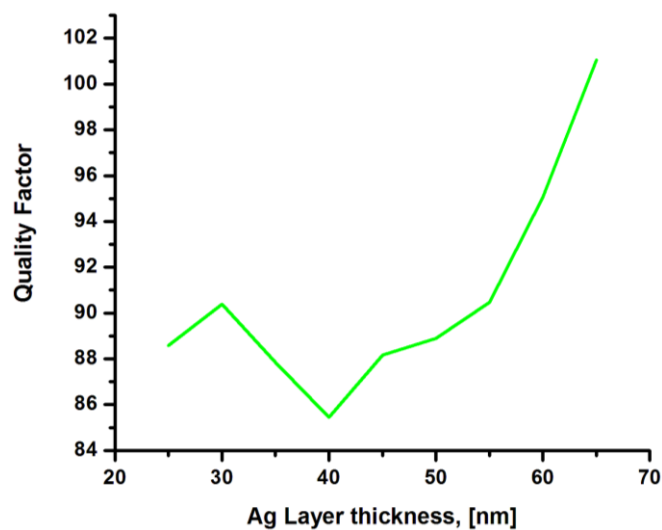
Fig. 4.6. Quality Factor vs Ag Layer Thickness Curve

From the above discussion, it is certain that signal-to-noise (SNR) and quality factor (Q.F) are increasing gradually just above 40 nm thickness of silver layer for this proposed structure of SPR sensor. On the other hand, the sensitivity of the sensor gradually decreases by the increased thickness of the Ag layer beyond the 45 nm thickness. Therefore, the optimal thickness of the Ag layer that secures the highest sensitivity and ensures enhanced SNR and QF of this proposed structure that has been quantitatively evaluated. The thickness of the silver layer has been varied from 25 nm to 65 nm.
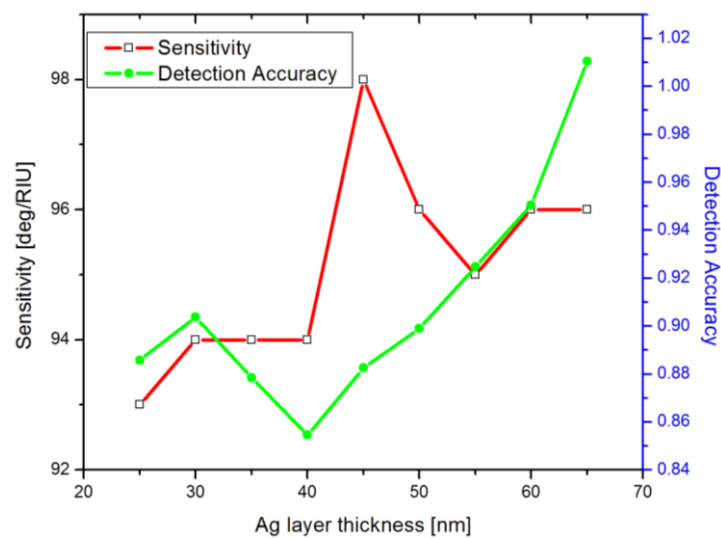
Fig. 4.7. Change of sensitivity and Detection Accuracy for varying Ag thickness
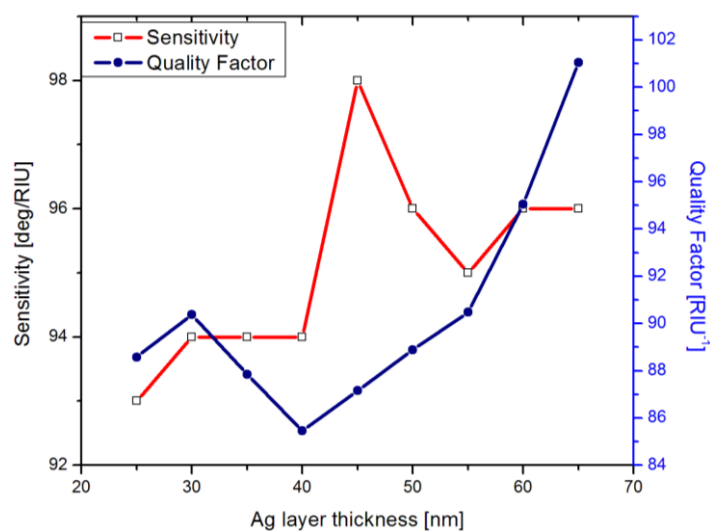
Fig. 4.8. Variation of the sensitivity and Quality Factor as the function of the thickness of Ag layer

As shown in **Fig. 4.7** and **Fig. 4.8**, the highest sensitivity is at the thickness of 45 nm whereas the DA is increased appreciable for the SPR sensor. However, at the 45 nm thickness of silver

layer, highly enhanced both sensitivity and quality factor, minimum reflectance, as well as satisfactory detection accuracy have been obtained which is the key feature of a good sensor. Therefore, we choose the optimum layer thickness be 45 nm.

4.2.2 Optimization for ZnO based Structure

The optimization of sensor geometries for better performance of this proposed structure can be discussed dividing in two parts. In one part, the silver layer thickness optimization for better performance and the second one is to find optimum glass prism for best performance. Both these to optimization details are discussed below.

4.2.2.1 Silver Layer Thickness Selection

A laser of 633 nm wavelength was chosen as the light source for the sensor. The initial RI of the sensing medium is assigned as 1.33 RIU and the increment Δn_s of RI is considered to 0.05 RIU. In addition, the initial thickness of ZnO layer is set to 32 nm. To optimize the thickness of silver layer, we set its initial thickness at 26 nm and took the values of performance parameters and FWHM by varying the thickness up to 58 nm with an incremental rate of 2 nm. **Fig. 4.9** shows the variation of sensitivity and quality factor with shift of Ag layer thickness. This curve shows an increasing trend of sensitivity with the increase of silver thickness and quality factor first decreases up to 44 nm and then starts to increase with the increase of silver thickness.
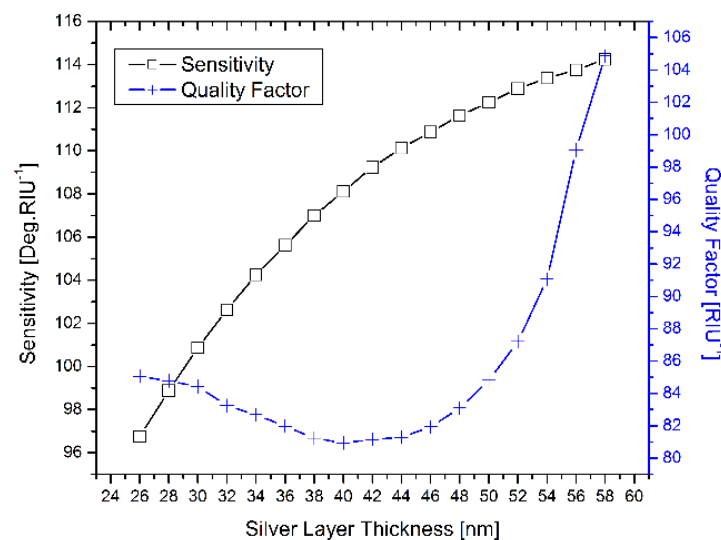
Fig. 4.9. Variation of sensitivity and quality factor with respect to silver layer thickness

The variation of sensitivity and detection accuracy is plotted in **Fig. 4.10** with the variation of Ag layer thickness. Though the sensitivity increases with the increase of Ag layer thickness,

the detection accuracy decreases initially up to the thickness at 44 nm and then it starts to increase again.
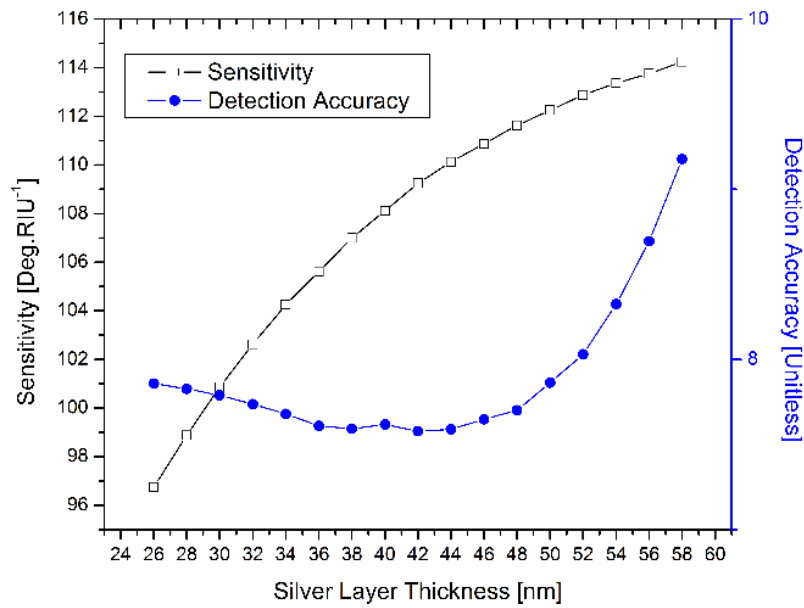
Fig. 4.10. Variation of sensitivity and detection accuracy with respect to silver layer thickness

In addition, the sensitivity is potted against FWHM in **Fig. 4.11** with respect to the thickness of silver layer. The sensitivity rises with the rise of silver layer thickness. Similarly, the FWHM increases with the increase of silver layer's thickness up to 45 nm and then started to decrease gradually. Previous study found that at thickness of 55 nm, silver showed high quality factor with lower FWHM comparing with the gold film for SPR-based sensor application [155].
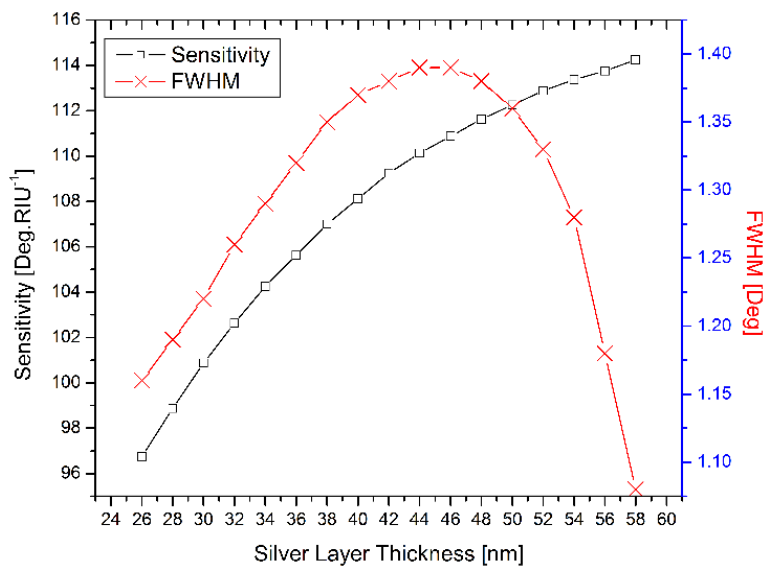
Fig. 4.11. Variation of sensitivity and FWHM with respect to silver layer thickness

However, in this study 58 nm is found to be the best thickness for silver with respect to the sensitivity, quality factor, and detection accuracy of the proposed sensor. Beyond this thickness, the quality factor and detection accuracy were found to be unchanged. Thus, the thickness of silver film was chosen as 58 nm for this proposed sensor structure, along with different material layers. In addition, silver in multi-layered structure was found to have enhanced quality factor than the single layer [156].

4.2.2.2 Glass Prism Selection

In terms of prism selection, sensitivity, quality factor, and detection accuracy were taken into account and the results are illustrated in **Fig. 4.12** as a function of the RI of the prism. The highest sensitivity, quality factor, and detection accuracy were found at the RI of 1.56671 and it is BAF10 prism. Thus, the BAF10 prism was chosen for this proposed sensor. Due to these characteristics of BAF10 prism, this prism was used in many previous studies such as [148, 157].
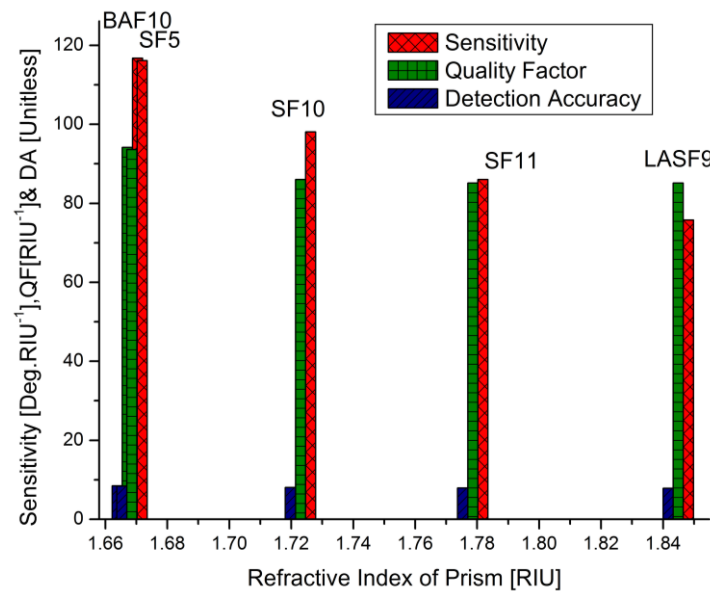
Fig. 4.12. Performance of different glass prism

4.3 Performance Analysis of Proposed Structure

The performance of both the two proposed sensor structures has been analyzed by checking its layer by layer response on a solution of certain refractive index. The detail discussion for each sensor structure is individually arranged in the following sections.

4.3.1 Performance Analysis of TiO2-SiO2 based Proposed Structure

The TiO2-SiO2 and MoS2-graphene composite based SPR sensor has been put into account for analyzing sensitivity, quality factor, detection accuracy and electric field distribution. The detail analysis focusing on different performance parameters are discussed in the following sections.

4.3.1.1 Effect of Different Layers on Angle Variation

At first, the effect of introducing different layers into the proposed multilayered sensor is analyzed, which alters the RI of the overall dielectric medium that is explained by the equation (4.1), leading to the formalin molecules increasing the SPR angle.

The number of layers have noteworthy factors in the enhanced performance and ameliorate the sensitivity for the proposed SPR sensing device. Therefore, the fluctuation of the refractive index for different layers has been shown in **Fig. 4.13**. According to **Fig. 4.13**, the resonance angle rises with the attachment of new layers [48]. So, the SPR optical biosensor's sensitivity increases with the proposed hybrid structure.

$$\Delta n_{sens} = n_{sens}^{d} - n_{sens} = \left(n_{sens} + C_a \frac{dn}{dc} \right) - n_{sens} = C_a \frac{dn}{dc} \tag{4.1}$$
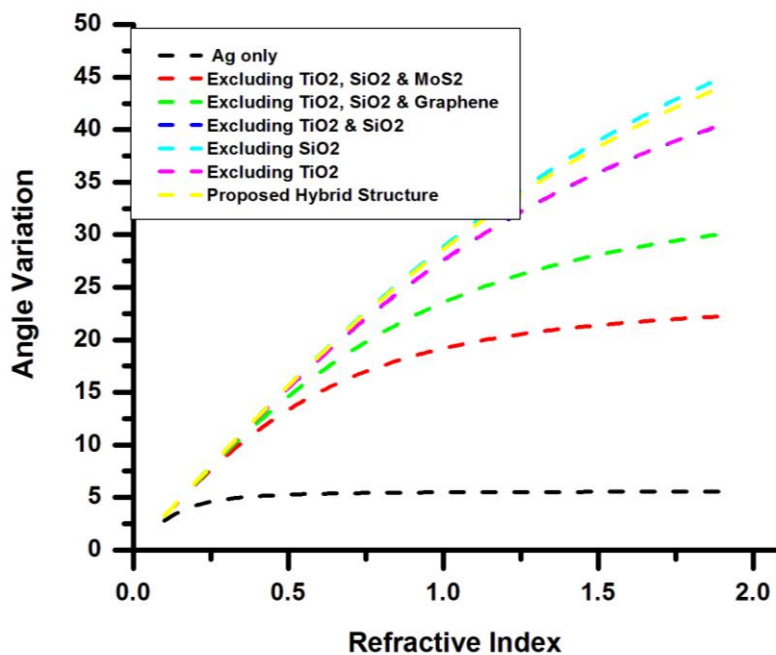
Fig. 4.13. SPR angle vs. Refractive Index Curve for the different structure

The number of carrier changes with the insertion of target molecules in the graphene surface that leads to an change of wavevector [158], lastly a change in the SPR angle is occurred as depicted by the equation (4.1).

4.3.1.2 Effect of Different Material on Sensitivity

The sensor's performance is estimated in terms of sensitivity (S) which is expressed by equation (4.2) [111, 141]:

$$S = \frac{\Delta\theta_{SPR}}{\Delta n_{sens}} = \frac{\Delta\theta_{SPR}}{C_a} \frac{1}{\frac{dn}{dc}} \tag{4.2}$$

Here, $\Delta\theta_{SPR}$ is the alteration of θ_{SPR} for the existence of target molecules and Δn_{sens} is the alteration of RI of the detecting dielectric medium after getting adsorbed target molecules, designated by equation (4.2). The θ_{SPR} makes a shift in rightward with the rise of the RI according to equation (4.3).

$$\theta_{SPR} = \sin^{-1} \frac{\left(n_{eff} n_{sens}\right)}{n_{prism}\sqrt{\left(n_{eff}^2 + n_{sens}^2\right)}} \tag{4.3}$$
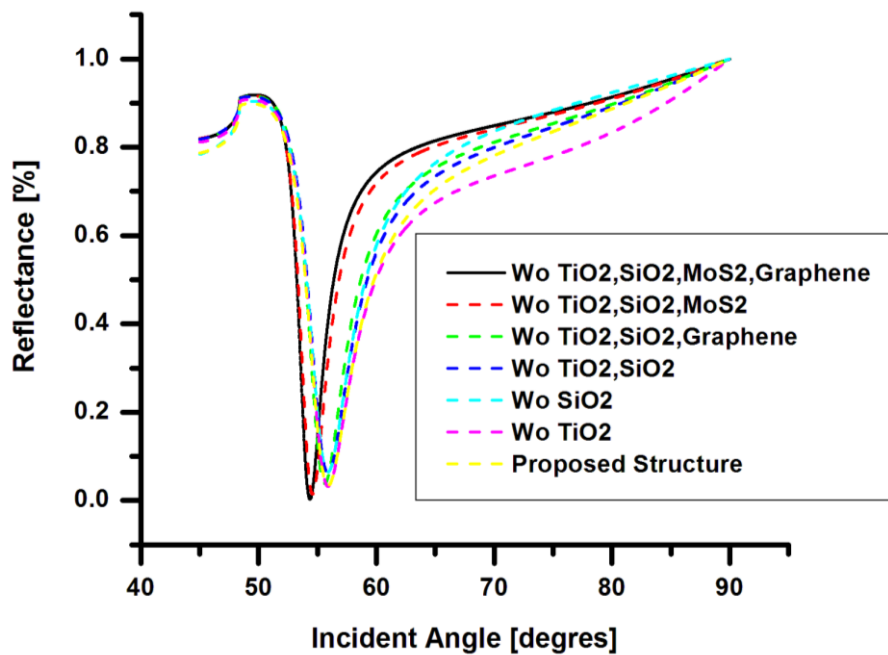
Fig.4.14. SPR curve for several composite structure at 633 nm wavelength
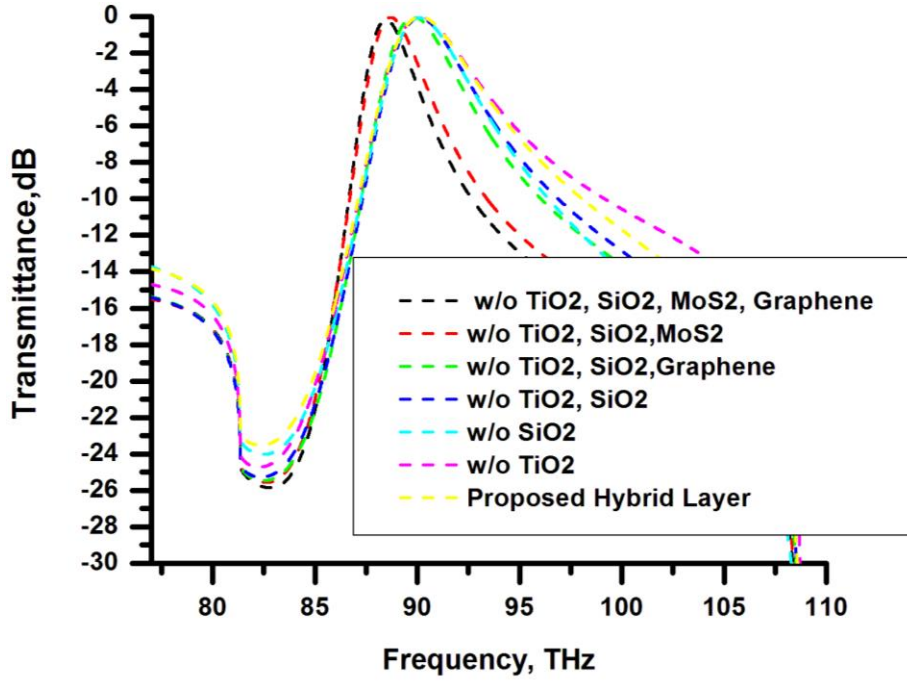
Fig. 4.15. SPR curve, Transmittance vs Frequency for Conventional SPR sensor and for several different composite structure at an operating wavelength of 633 nm

The propagation constant of incident light wave must be numerically equal to the propagation constant of SPW at SPR condition which is denoted by equation (4.4) and equation (4.5). SP propagation constant is altered bestowing to the alteration of RI of detecting target medium. Lastly, it is detected that the θ_{SPR} varying features are responsible for the modification of RI of the detecting medium.

$$K_{SPW} = \frac{2\pi}{\lambda} n_{prism} \sin\theta_{SPR} \qquad (4.4)$$

$$F_{SPR} = \frac{K_{SPW}}{2\pi} \frac{C_0}{n_{eff}} \qquad (4.5)$$

Initially, in this section, the effect on the identifying attributes for introducing different layers such as the alteration of θ_{SPR} and F_{SPR} in the sensor arrangement has been discussed. **Fig. 4.14** and **Fig. 4.15** show the minimum reflectance (Rmin) vs SPR angle (Θ_{SPR}) and maximum transmittance (Tmax) vs F_{SPR} graphs for dissimilar structures together with the conventional as well as the proposed structure at RI $n_{sens} = 1.34$ RIU (sample free sensor). **Fig. 4.14** and **Fig. 4.15** displays that the θ_{SPR} and F_{SPR} for conventional layer sensors are 54.36° and 94.1547 THz respectively. Yet again, **Fig. 4.14** and **Fig. 4.15** illustrate that the value of θ_{SPR} and F_{SPR} shift

to 54.57° and 94.4015 THz for the composition of graphene and silver sensor structure respectively. In such manner, it can confidently be said that the alteration of θ_{SPR} and F_{SPR} for the conventional configuration is very weak. Considering this, the sensitivity for a composite configuration with graphene is dependably better than the only silver structure. Due to this reason, the electron drops of graphene, which is associated with the imaginary part of permittivity. This augmented shift of SPR angle will cause an improvement in sensitivity of the sensor since sensitivity is directly proportional to the change of SPR angle which is conferred [125, 127, 159] according to equation (4.6).

$$ Z_f = \frac{k_s n_j \cos\theta}{\omega \varepsilon_j^2} \qquad (4.6) $$

Moreover, **Fig. 4.15** displays that the θ_{SPR} and F_{SPR} without TiO_2, SiO_2, and graphene but attaching with MoS_2 layer are 55.60° and 95.5935 THz respectively. This is because of MoS_2's higher bandgap [49, 105, 141], advanced optical absorption efficiency [48, 105, 147] and greater work function (5.1 eV) than the graphene [49].

After more, if only the graphene-MoS_2 composite used with Ag, **Fig. 4.14** and **Fig.4.15** displays the shift of θ_{SPR} and F_{SPR} to 55.86° and 96.2495 THz respectively. These values are greater than that for the previous structure due to the presence of contribution for both graphene and MoS_2. Furthermore, if TiO_2-SiO_2 combinedly employed with the Graphene-MoS_2 as well as Ag, the θ_{SPR} and F_{SPR} are changes to 55.90° and 96.9236 THz respectively. The RI value of TiO_2 and SiO_2 is real and hence, can be utilized in place of an adherence layer just above the prism base. The performance of TiO_2 and SiO_2 is better while they act combinedly than the individual case [7, 111, 141]. The reason is the occurrence of rich plasmon at the interface of TiO_2-SiO_2 [141]. In addition, this plasmon improves light trapping successfully. By cause of this added SPs, enhancement of SPR angle occurs. This rise of SPR angle increases the sensitivity. Lastly, the simulation for θ_{SPR} and F_{SPR} on the proposed SPR configuration have been carried out, and the result is 56.26 degrees and 97.968 THz respectively which is the uppermost value among all the values obtained for previous structures. The adding of probe molecules makes a right shift of θ_{SPR} because of RI changing of detecting sample medium. By the immobilization of ions, the surface become electron-rich which alters the concentration and lead to a variation in the propagation constant.
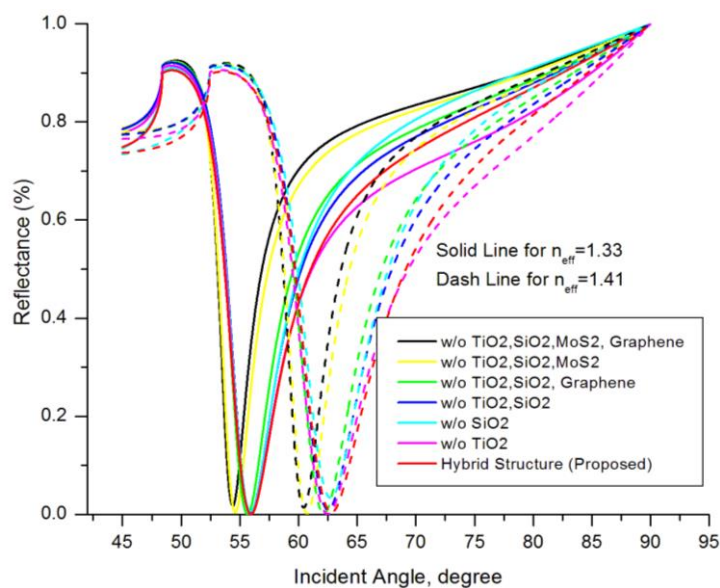
Fig. 4.16. Change of Reflection vs Incidence Angle for different Composite Sensor
Structures

Secondly, the alteration of SPR angle for alteration of RI is presented in **Fig. 4.16**. In **Fig. 4.16**, it is revealed that the shift of SPR angle for the shift of RI in case of conventional shape and different proposed composite configurations. This shift of SPR angle ($\Delta\theta_{SPR}$) for conventional sensor is very weak, that ensures inferior sensitivity because this performance parameter depends on the change of $\Delta\theta_{SPR}$ proportionally. And for the proposed hybrid biosensor is maximum which ensures the maximum sensitivity. The equation (3.2) expresses, how the SPR angle alters as a result of the alteration of molarity of the sample medium and its RI. By measuring the SPR angle, it can easily be measured the RI of the target medium. A plotting is drawn based on the change of reflected light intensity for every change of the incidence angle and is shown in **Fig. 4.16**. The SPR curves for detecting medium of 1.34 RIU (target molecule free sensor) and 1.41 RIU (existing of formalin) are represented by solid and dashed appearances of dissimilar colors correspondingly.

The proposed assembly of SPR sensor is compared with some other configuration of sensors in respect to their sensitivity. The other six structures include firstly only the Ag layer on prism, secondly graphene with Ag structure, thirdly MoS_2 and Ag, fourthly MoS_2-graphene with Ag, fifthly Ag-MoS_2-graphene layer composition with SiO_2 and finally Ag-MoS_2-graphene layer composition with TiO_2. The resonance angle (θ_{SPR}) for the medium of 1.34 RIU and 1.41 RIU are computed and using these values the sensitivity is measured. An effortless observation can be made inspecting the **Fig. 4.17**, that the sensitivity rises progressively with the addition of

layers and this value become supreme for hybrid configuration of sensor structure (proposed structure).
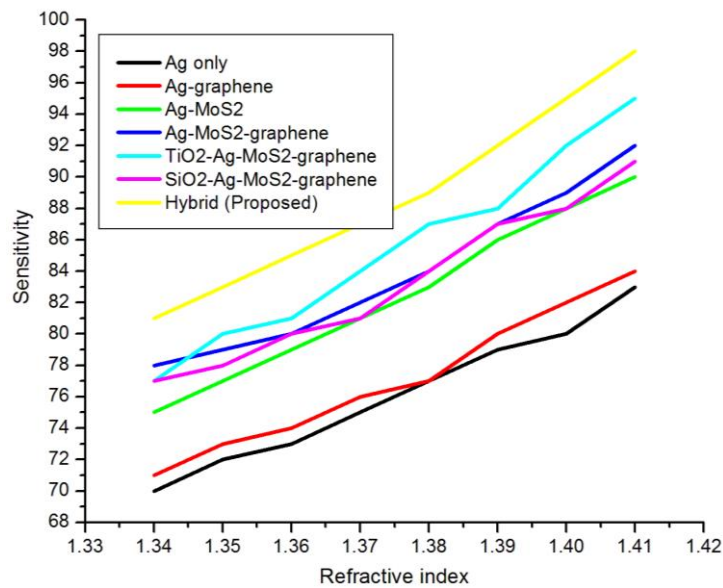
Fig. 4.17. Advancement of sensitivity with RI variation for different composite structure of sensor

Thirdly, in this segment, the shifting of SPR angle with the augmentation of RI for a step size of $\delta C_n = 0.01$ is counted and also the corresponding increase of the sensitivity is calculated for proposed sensor and graphically revealed in **Fig. 4.17**.

The first observation is that the sensitivity for the conventional configuration is very weak ranging from 70 % to 83 % for the RI variation range of $n_{sens}^d = 1.34$ to $n_{sens}^d = 1.41$ respectively. After then the sensitivity of conventional with graphene keeping TiO$_2$-SiO$_2$ and MoS$_2$ away from the structure is investigated and it has been found that the range of sensitivity is 71 % to 84% which is relatively better than the conventional sensors. Further, the sensitivity of Ag with only MoS$_2$ but without TiO$_2$-SiO$_2$ and graphene covers a range from 75 % to 90 %. Again, if both graphene-MoS$_2$ are used with Ag but TiO$_2$-SiO$_2$ are not used then sensitivity improves than the previous structures which cover from 78% to 92 %. Now, if the SiO$_2$ and TiO$_2$ used individually with Ag- MoS2-Graphene, the sensitivity has been developed to a range of 77% to 91% and 95% respectively. Therefore, using all the layers at a time, the sensitivity is achieved the highest value among all the previous discussed structures. It covers the range from 81% to 98%. Lastly, in this section, the sensitivity for the different structure is summarized in **Table 4.1**.

Table 4.1. The Sensitivity for Different Sensor Structures with a Sample of RI 1.34 to 1.41

Structural Configuration	Sensitivity (s) [degRIU^{-1}]							
	n_s^2 =1.34	n_s^2 =1.35	n_s^2 =1.36	n_s^2 =1.37	n_s^2 =1.38	n_s^2 =1.39	n_s^2 =1.40	n_s^2 =1.41
Only Silver	70	72	73	75	77	79	80	83
Ag with Graphene	71	73	74	76	77	80	82	84
Ag with MoS$_2$	75	77	79	81	83	86	88	90
Ag- MoS$_2$- Graphene	78	79	80	82	84	87	89	92
TiO$_2$-Ag- MoS$_2$- Graphene	77	80	81	84	87	88	92	95
SiO$_2$- Ag- MoS$_2$- Graphene	77	78	80	81	84	87	88	91
Hybrid	**81**	**83**	**85**	**87**	**89**	**92**	**95**	**98**

4.3.1.3 Effect of Different Layers on Quality Factor

Here it is observed that the quality parameter of the proposed SPR biosensor with a multilayer sensor structure is much higher than the conventional SPR biosensor composed with only a silver layer. The comparisons with respect to the quality factor are shown in **Fig. 4.18**. The numerical values of the quality factor for different structures are also shown in **Table 4.2**. Thus, it is observed that the graphene-based multilayered hybrid SPR sensor is better than the conventional SPR sensor in terms of the quality parameter.
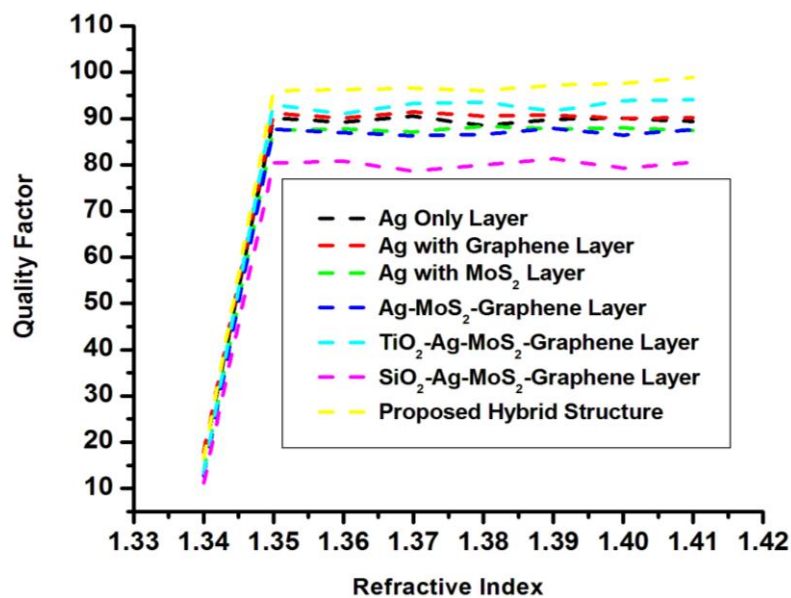
Fig. 4.18. Quality Factor vs RI Curve for various dissimilar sensor structures

In **Fig. 4.18**, the quality factor increases with the addition of the graphene layer whereas the quality factor decreases with the addition of a single MoS$_2$ layer. Again, the TiO$_2$ contributes

much whereas SiO_2 contributes in reducing the quality factor of the proposed sensor that can be effortlessly perceived by the inspection of **Fig. 4.18** and **Table 4.2**. Thus, it should be emphasized on the TiO_2 for the improvement of the quality factor of the proposed sensor.

Table 4.2. The Quality Factor of Different Structures of Sensor

Structural Configuration	QF [/RIU]							
	n_s^2 =1.34	n_s^2 =1.35	n_s^2 =1.36	n_s^2 =1.37	n_s^2 =1.38	n_s^2 =1.39	n_s^2 =1.40	n_s^2 =1.41
Only Silver	16.51163	90.12346	89.15663	90.47619	88.50575	89.88764	90.10989	89.3617
Ag with Graphene	17.7665	91.13924	90.12346	91.46341	90.58824	90.8046	90.05525	90.21739
Ag with MoS_2	13.46499	87.50000	87.77778	87.09677	88.29787	87.7551	88.00000	87.37864
Ag- MoS_2- Graphene	12.66667	87.77778	86.95652	86.31579	86.59794	87.87879	86.40777	87.61905
TiO_2-Ag- MoS_2-Graphene	13.11755	93.02326	91.01124	93.33333	93.54839	91.66667	93.87755	94.05941
SiO_2- Ag- MoS_2-Graphene	11.14327	80.41237	80.80808	78.64078	80.00000	81.30841	79.27928	80.53097
Hybrid	**16.53846**	**96.02151**	**96.31579**	**96.59794**	**96.00000**	**97.2549**	**97.61905**	**98.88889**

4.3.1.4 Effect of Different Layers on SNR
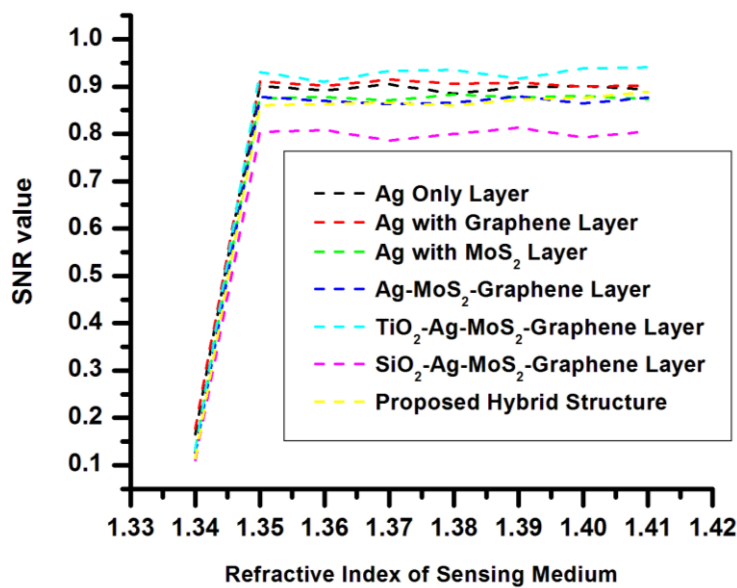
Fig. 4.19. SNR vs RI Curve for various dissimilar sensor structures

One can make an effortless observation from **Fig. 4.19**, that the detection accuracy or signal to noise ratio increases when silver with graphene layer structure than the silver only structure but with the MoS_2 layer it falls down. Similarly, the Ag-MoS_2-graphene structure with TiO_2 the SNR value rises much whereas with SiO_2 the SNR value falls down. Finally, the proposed structure with both TiO_2 and SiO_2 provides an SNR value of moderate range that can be easily comprehended from **Fig. 4.19**.

Table 4.3. The Detection Accuracy of Different Structures of Sensor

Structural Configuration	DA or SNR [Unit Less]							
	n_s^2 =1.34	n_s^2 =1.35	n_s^2 =1.36	n_s^2 =1.37	n_s^2 =1.38	n_s^2 =1.39	n_s^2 =1.40	n_s^2 =1.41
Only Silver	0.1651	0.9012	0.8916	0.9048	0.8851	0.8989	0.9011	0.8936
Ag with Graphene	0.1777	0.9114	0.9012	0.9146	0.9059	0.9080	0.9006	0.9022
Ag with MoS_2	0.1347	0.8750	0.8778	0.8710	0.8830	0.8776	0.8800	0.8738
Ag- MoS_2- Graphene	0.1267	0.8778	0.8696	0.8632	0.8660	0.8788	0.864	0.8762
TiO_2-Ag- MoS_2- Graphene	0.1312	0.9302	0.9101	0.9333	0.9355	0.9167	0.9388	0.9406
SiO_2- Ag- MoS_2- Graphene	0.1114	0.8041	0.8081	0.7864	0.8000	0.8131	0.7928	0.8053
Hybrid	0.1154	0.8602	0.8632	0.8660	0.8600	0.8726	0.8762	0.8889

Additionally, in this segment, the shifting of SPR angle with the augmentation of RI for a step size of δC_n= 0.01 is determined and also the corresponding change of SNR value for the proposed biosensor is determined and tabular representation is shown in **Table 4.3**.

4.3.1.5 Electric Field Distribution Analysis

Finally, in this segment of study, electric field distribution is analyzed by integrating the finite difference time domain (FDTD) technique using commercial Lumerical FDTD solution software. Electric field dispersal is investigated along the normal to the interface. To simulate the sensor configuration, we consider all the required design parameter according to the **Table 3.1**. This influential FDTD method for solving Maxwell's equations in a nano sheet by using the YEE-algorithms. The simulation was carried out using the Gaussian-modulated continuous wave at 633 nm as the center wavelength. SP excitation is made using angular interrogation practice. The perfectly matched layer (PML) boundary condition was used in such a manner that waves enter into the layers with producing minimum reflections (R_{min}) and Reflected intensity was reported using DFT reflectance and transmission Monitor at 250 nm away from the graphene-sensing interface. In **Fig. 4.20**, it is observed that the maximum field is stimulated

at the MoS$_2$–graphene interface because most of the plasmonic effect rises close to the interface that turns into the rise of sensitivity for the proposed structure. Moreover, Ag layer expands the field gradually till to Ag–MoS$_2$ interface which signifies the excitation of SPs at this interface. The field intensity falls abruptly in the SiO$_2$ and then nonstop to lessening at a gradual rate.
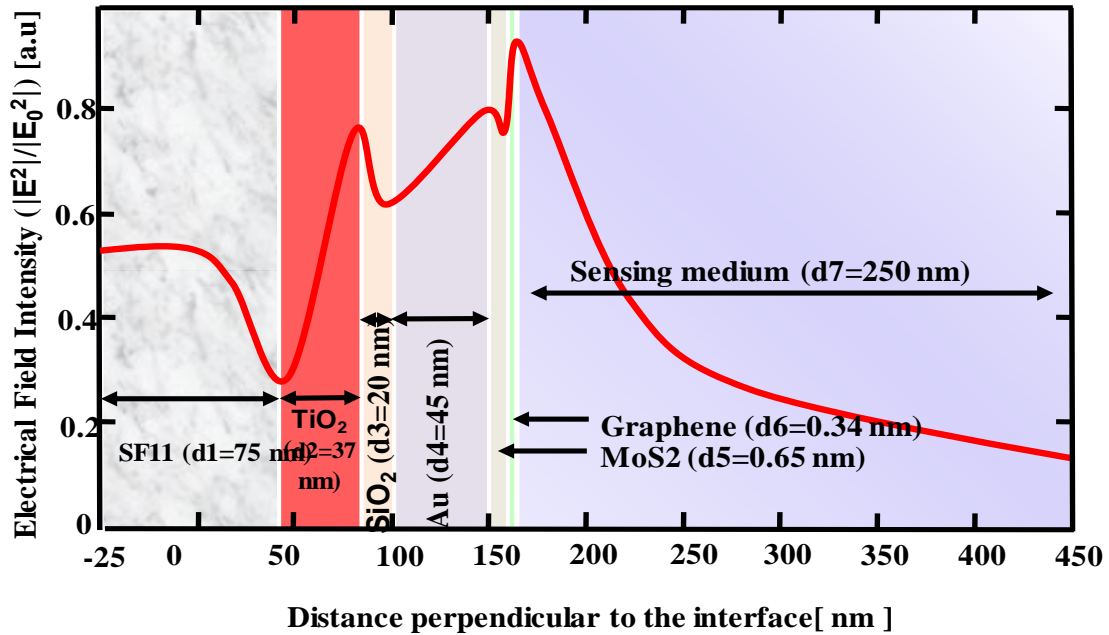
Fig. 4.20. The distribution of electric field through the proposed sensor at different interfaces formalin as sample

4.3.2 Performance Analysis of ZnO based Proposed Structure

The ZnO and PtSe$_2$-graphene composite based SPR sensor has been put into account for analyzing sensitivity, quality factor, and detection accuracy. The detail analysis focusing on different performance parameters are discussed below.

The performance of the proposed sensor was compared with different layers of material to check sensor's sensitivity. The refractive index of the sensing medium is given as $n_a = n_s + \Delta n_s$, where Δn_s represents the variation of RI of target solution medium. As exhibited in **Fig. 4.21**, the reflectance of silver only SPR sensors structure is presented with the variation of incident angle, in this computation, the change in the RI of sensing solution is considered Δn_s=0.10 RIU and has been found a corresponding SPR angle shift of 10.88°.
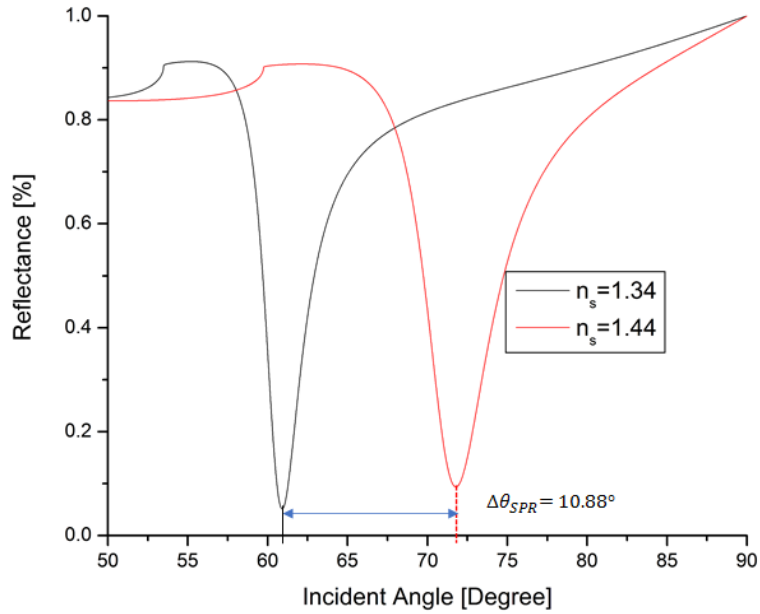
Fig. 4.21. Variation of reflectance for silver only sensor structure: $\Delta\theta_{SPR} = 10.88^0$

The reflectance with the incident angle variation of silver-graphene sensor structure is exhibited in **Fig. 4.22.** In this computation, the change of SPR ang has been found 11.10° for the 0.10 RIU change of sensing dielectric medium.
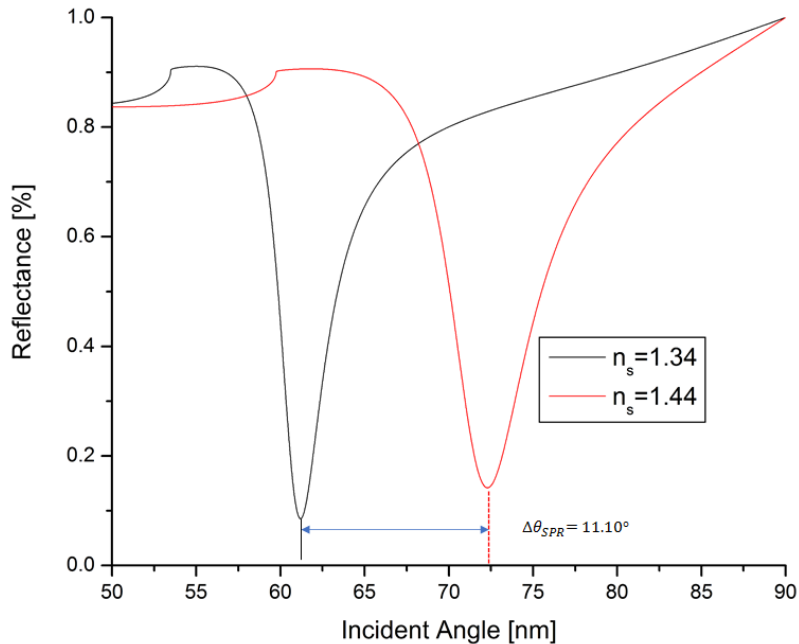
Fig. 4.22. Variation of reflectance for silver-graphene sensor structure: $\Delta\theta_{SPR} = 11.10^0$

The reflectance with the incident angle variation of silver-PtSe2 sensor structure is exhibited in **Fig. 4.23.** In this computation, the change of SPR angle has been found 12.24° for the 0.10 RIU change of sensing dielectric medium.
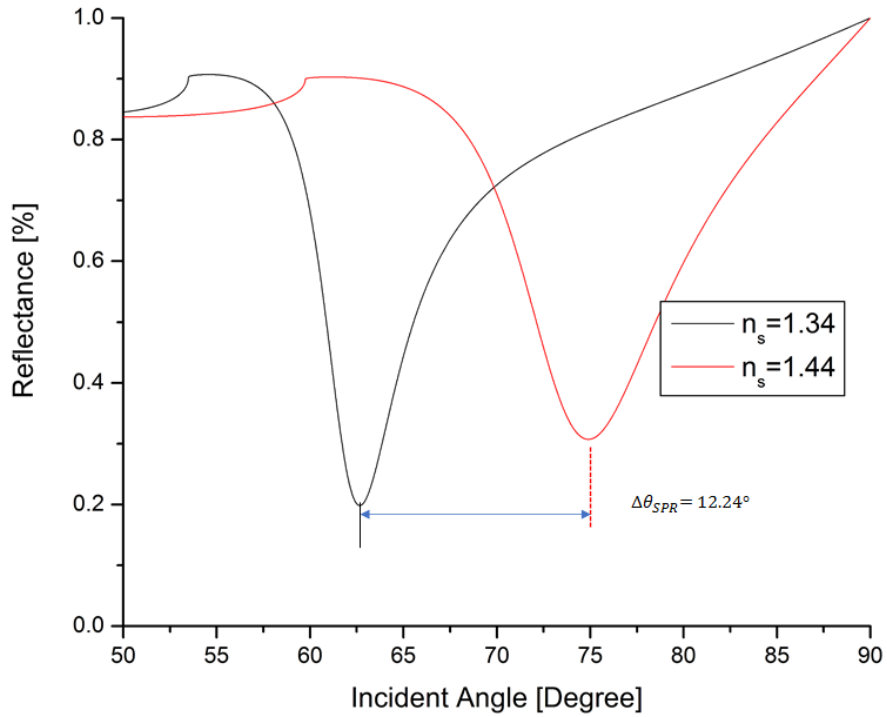
Fig. 4.23. Variation of reflectance for silver-graphene sensor structure: $\Delta\theta_{SPR} = 12.24^0$

The variation of reflected light intensity with the incident angle variation for silver-PtSe$_2$-graphene sensor structure is presented in **Fig. 4.24.** The shift of SPR angle has been found 12.47^0 for the 0.10 RIU change of the sensing dielectric medium.
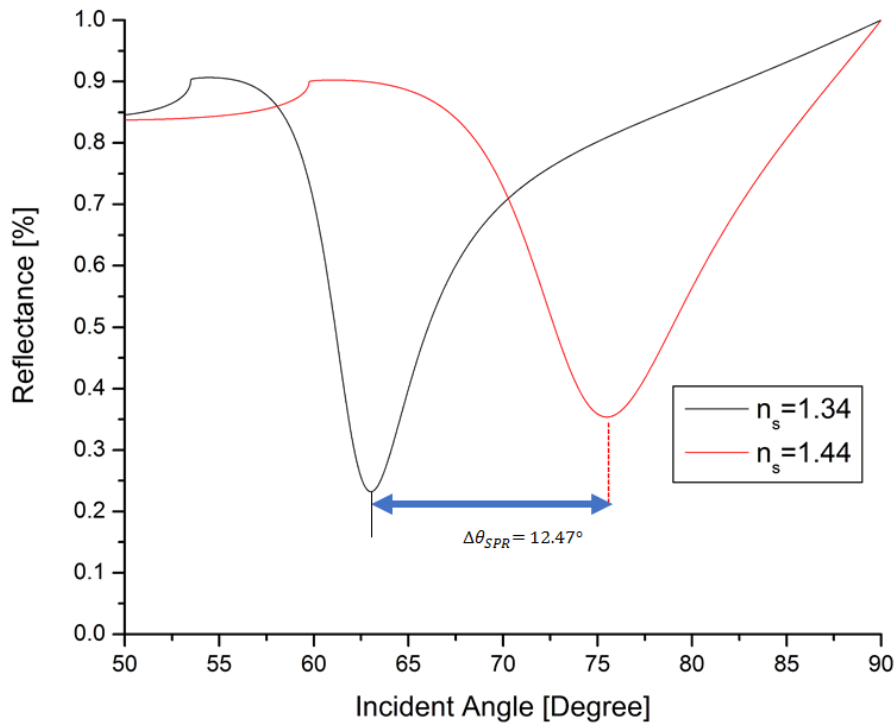
Fig. 4.24. Variation of reflectance for silver-PtSe$_2$-graphene sensor structure: $\Delta\theta_{SPR} = 12.47^0$

The variation of reflected light intensity with the incident angle variation for ZnO-silver-PtSe$_2$-graphene sensor structure is presented in **Fig. 4.25.** The shift of SPR angle has been found 12.65^0 for the 0.10 RIU change of the sensing dielectric medium.
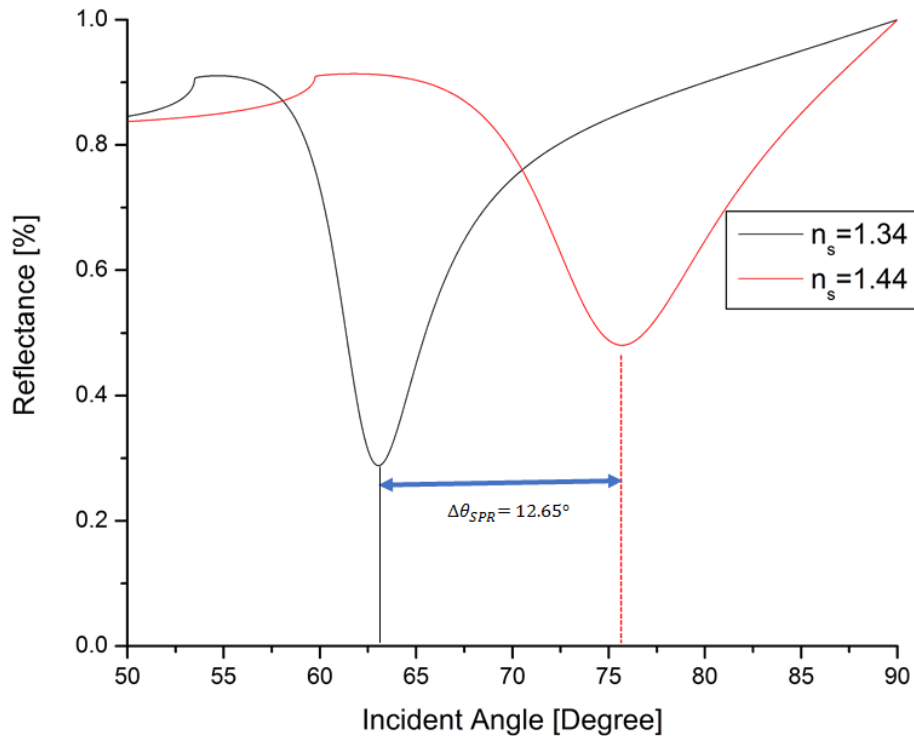
Fig. 4.25. Variation of reflectance for ZnO-silver-PtSe$_2$-graphene sensor structure: $\Delta\theta_{SPR} = 12.65^0$

From the above results and discussions, it is clear that the highest shift of SPR angle has been achieved with the introduction of ZnO layer with the Ag-PtSe$_2$-Graphene hybrid structure, which is   12.65° [see **Fig. 4.25**]. On the other hand, the lowest shift [10.88°] is observed for the silver only structure [see **Fig. 4.21**]. The highest shift of SPR angle induced for the case of PtSe2 layer introduction into this proposed sensor structure which is 12.5% greater than the conventional silver only structure.

4.4 Detection of Formalin

In this work, a chitosan probe is used to detect formalin in aqueous solution. Formalin is efficiently adsorbed by the polymeric amino group of chitosan [160]. Chitosan has been used as probe for detecting formalin which has been reported in many research papers [99, 159, 161, 162]. This is a non-toxic, biocompatible and biodegradable natural polymer [160]. In addition, the most attractive and significant property of chitosan is its high selectivity to formalin. Ping et al, have reported that chitosan makes a significant bond or adsorption with formalin. On the

other hand, this probe cannot make a significant bond with the contemporaneous intrusive compounds together with some common aldehyde compounds and many other probably contemporaneous chemical species in real world food samples (such as $Fe3+$, $Mg2+$, $Cl-$, $Ca2+$, $NO3-$, , L-cysteine, L-arginine, N-acetyl-cysteine, N-acetyl glycine, sodium pyruvate, chloral and acetaldehyde) [115]. This investigation report clearly demonstrates the quite good selectivity of the chitosan as probe for formalin detection.

The immobilization of formalin on the chitosan increases the RI of sensing layer and this increased RI leads to a right shift of SPR angle. By investigating this angular shift using attenuated total reflection (ATR) it can easily be determined the existence of formalin in the target sample.

4.4.1 Performance of TiO2-SiO2 based Proposed Structure
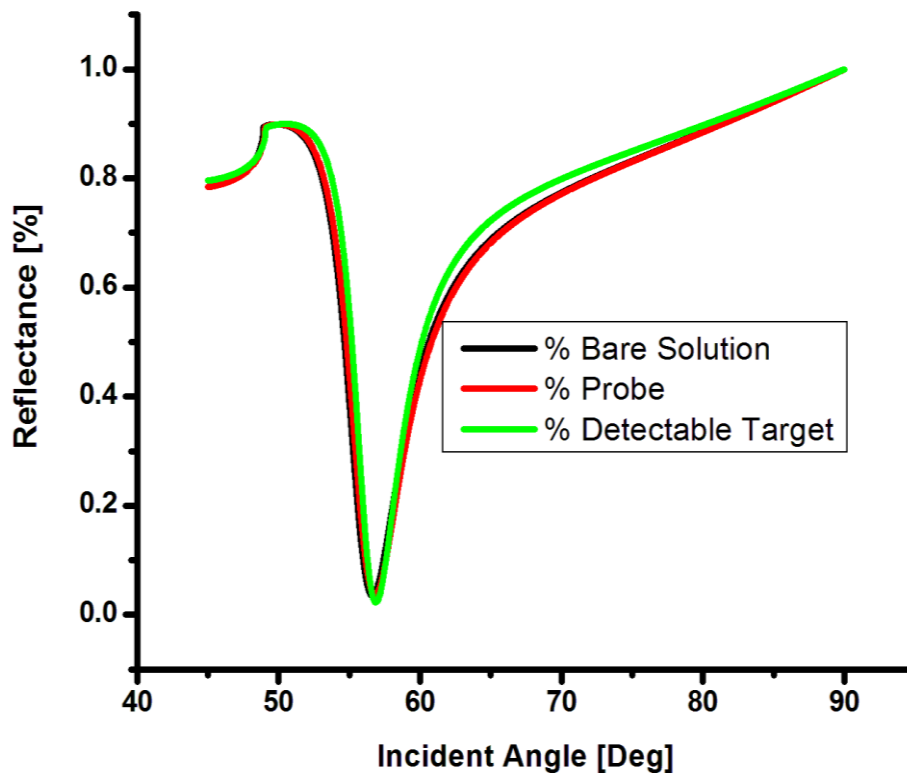
Fig. 4.26. Reflectance vs incident angle curve for empty sensor, chitosan and formalin

The revelation of recognition concepts shown in **Fig. 4.26** and **Fig. 4.27**, demonstrating the reflectance with the change of the incident angle that specifies the elementary characteristics of SPR based sensing devices.
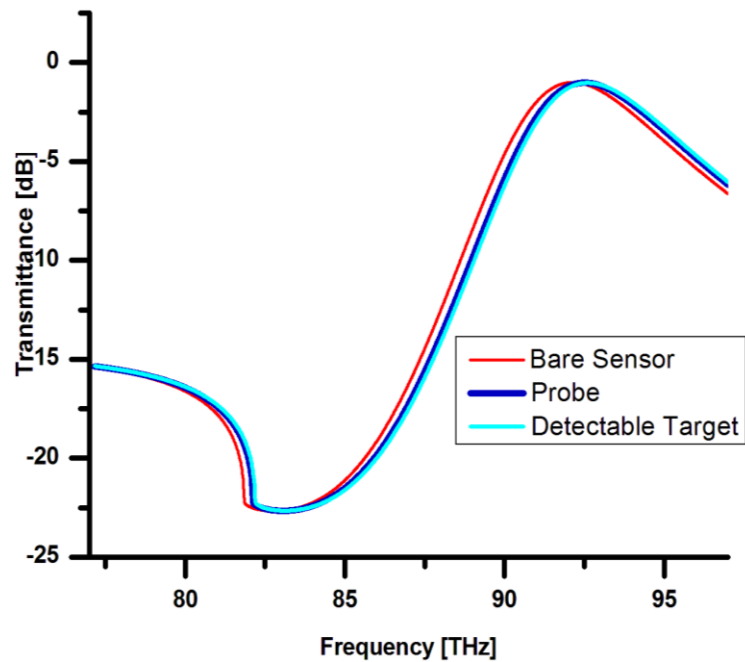
Fig. 4.27. Transmittance vs frequency curve for empty sensor, with chitosan and formalin

Firstly, the agreement of reflectance on incident light angle is determined considering the only chitosan solution. In this account, equation (4.1) shows the relationship between the change of RI with the variations concentration (Δn_{sens}) and it is verified. When formalin is passing into chitosan, the RI of sensing medium alters for happening chemical interaction between chitosan and formaldehyde [103, 126, 151, 163]. For illustration, a solution of 1000 nM formalin and $\dfrac{dn}{dc}$ represents the increment factor of RI. The RI increment factor for formalin solution is 0.181 cm3/gm [102, 103, 127, 164].

Formalin is recognized by combining biochemical molecules with Chitosan components. Thus, when a chemical bond is made with the probe that is adhered to the object ingredient, it makes an additional bonding that exhibits specific phenomena. From the response of this phenomena, it can effortlessly be figured out that whether the test sample contains the molecules of formalin or not. For the different values of concentration of sample solution, the minimum reflectance and SPR angle as well as the SPR frequency and maximum transmittance that helps in the successful detection of formalin. A detailed argument has described in the manner how the proposed sensor contradistinguishes the existence of formalin in the sample solution.

Since the RI of detecting medium alters with the adscription of formalin molecules, the SPR angle makes a rightward shift. Having electron affluency formalin molecule alters the carrier concentration in the MoS$_2$-graphene interface that causes to vary the wave vector. In this

means, this proposed SPR sensor with high performance is employed to identify the formalin governed by the SP angle variation.

For the hard and fast check of the proposed SPR sensing device, quantitative analysis has been started and by marking out the variation of SPR angle and the minimum reflectance as well as the variation of surface resonance frequency and maximum transmittance. These attributes are graphically represented in **Fig. 4.26** and **Fig. 4.27** respectively. Correspondingly, the SPR angle and the SPR frequency are $56.15°$ and 91.4858 THz when the sensor is analyte free. In addition, the SPR angle and the SPR frequency have been growing up to 56.21^0 and 92.1658 THz respectively after employing a probe of 1000 nM chitosan. Inspecting these results, it can effortlessly be stated that there is no indicative variation in these attributes ($0.06°$ and 0.68 THz respectively). The cause is that the nonexistence of formalin indicates no functioning bonding between the target and probe molecules.
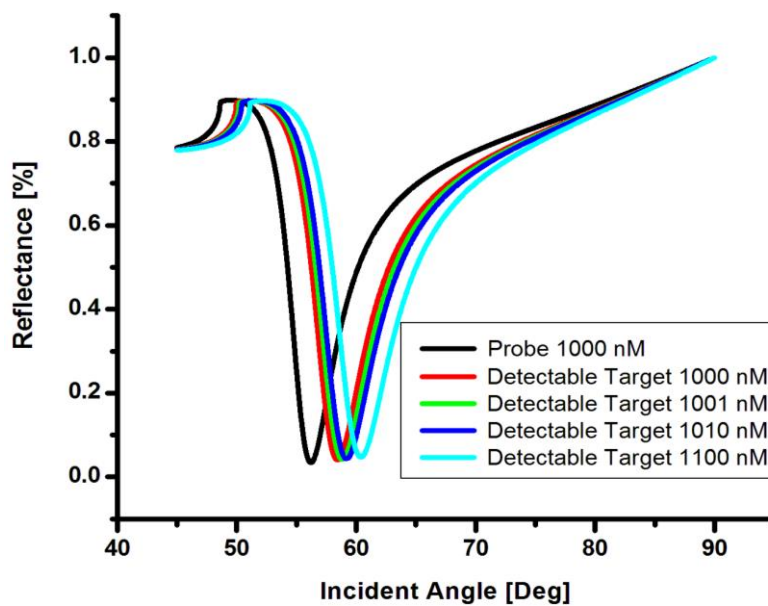
Fig. 4.28. Reflectance vs incident angle curve for varying detectable formalin concentration

The definitive conception regarding the recognition approach in SPR sensor will be translucent by going through the **Fig. 4.28** and **Fig. 4.29**. Change of the attributor (θ & R_{min}) and (ΔSPRF & T_{max}) with a concentration of 1000 nM formalin is drowning in the exploration. Quantitatively the variation in θ_{SPR} and F_{SPR} is altered to 58.43^0 and 94.1584 THz respectively that advises a reliable alteration for identifying formalin. Another representation in **Table 4.4,** that displays the frontward further change of above two attributes with a rise of 1 nM formalin to 100 nM and the curvature depiction is revealed in **Fig. 4.28** and **Fig. 4.29**.
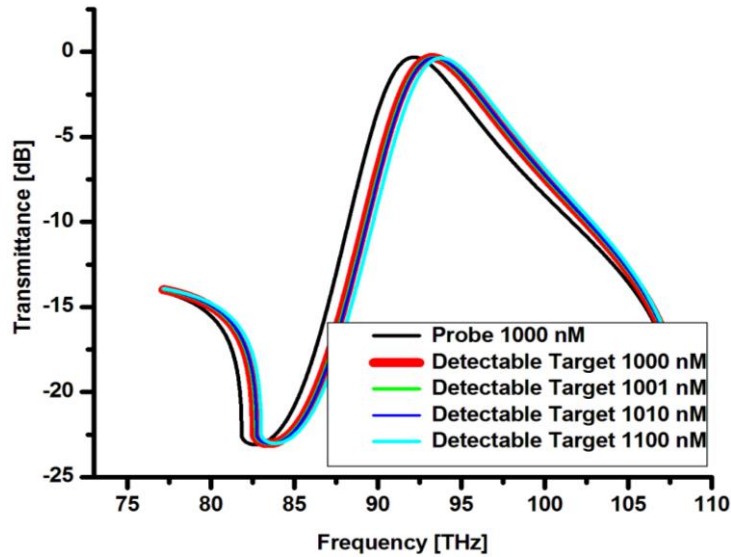
Fig. 4.29. Transmittance vs frequency curve for varying detectable formalin concentration

Table 4.4. Rmin, θ_{SP}, Tmax, and SPRF for Different Formalin Concentrations

Concentration (Ca)	R_{min} [%]	θ_{SPR} (Deg)	T_{max} (dB)	SPRF (THz)
Bare sensor	0.0022	56.15°	0.9676	91.4858
1000 (Probe)	0.0034	56.21	0.9695	92.1658
1000 (Target)	0.0041	58.43	0.9666	94.1584
1001 (Target)	0.0042	58.85	0.9666	94.3030
1010 (Target)	0.0044	59.33	0.9666	94.4226
1100 (Target)	0.0048	60.39	0.9666	95.1404

It is pointedly detected that admirable rising of θ_{SPR} and SPRF is a sign of forming a bond between probe and target, shown in **Table 4.4**. Thus, this reflection can detect the presence of formalin in the sample, as well as the absent of formalin, construct a redundant and repeating connection that expose incredible interaction.

For the thought of taking a statement about detection, firstly, figuring out the values of ΔR_{min}^{P-T} and $\Delta \theta_{sp}^{P-T}$ which are tabulated in **Table 4.5** and corresponding matching with margin indicating values $(\Delta R_{min}^{P-T})_{min}$ and $(\Delta \theta_{sp}^{P-T})_{min}$ have been carried out. The presence of formalin in the detecting solution will be translucently stated only when the calculated magnitude of

reflection and angle are greater than the margin indicating values. By this means, this data provides a translucent clue regarding the presence and absence of formalin. The values of marginal constraints are implied by the equations (4.7) and (4.8):

$$\left(\Delta R_{\min}^{P-T}\right)_{\min} = \left|R_{\min}^{\mathrm{Probe}} - R_{\min}^{T\arg et}\right| = 0.0012 \qquad (4.7)$$

$$\left(\Delta \theta_{sp}^{P-T}\right)_{\min} = \left|\theta_{sp}^{\mathrm{Probe}} - \theta_{sp}^{T\arg et}\right| = 0.06 \qquad (4.8)$$

The marginal parameter $(\Delta R_{min}^{P-T})_{\min}$ indicates the value that is required for least alteration of reflectance. On the other hand, $(\Delta \theta_{sp}^{P-T})_{\min}$ signifies the level of marginal value for least modification of SPR angle. The tiny reflectance of test legend and the perceptible target are signified by R_{min}^{Probe} and R_{min}^{Target} respectively.

Table 4.5. Estimated Values of $(\Delta R_{\min}^{P-T})_{\min}$, $(\Delta \theta_{SPR}^{P-T})_{\min}$, $(\Delta T_{\max}^{P-T})_{\min}$, and $(\Delta SRF_{P-T})_{\min}$ for Different Level of Target Solution Concentrations

Concentration (Ca)	$\Delta R_{\min}^{P-T}[\%] = $ $\left\|R_{\min}^{\mathrm{Probe}} - R_{\min}^{T\arg et}\right\|$	$\Delta \theta_{\min}^{P-T}[deg]$ $\left\|\theta_{SPR}^{\mathrm{Probe}} - \theta_{SPR}^{T\arg et}\right\|$	$\Delta T_{\max}^{P-T}[dB] = $ $\left\|T_{\max}^{P} - T_{\max}^{T}\right\|$	$\Delta SRF_{P-T}[THz] = $ $\left\|SRF_{P} - SRF_{T}\right\|$
1000 (Immobilizer Probe)	$(\Delta R_{\min}^{P-T})_{\min}$	$(\Delta \theta_{SPR}^{P-T})_{\min}$	$(\Delta T_{\max}^{P-T})_{\min}$	$(\Delta SRF_{P-T})_{\min}$
1000 (Detectionable Object)	0.0001	0.16	0.0098	0.6766
1001 (Detectionable Object)	0.0017	2.20	0.0306	1.9927
1010 (Detectionable Object)	0.0021	2.61	0.0330	2.1372
1100 (Detectionable Object)	0.0025	2.95	0.0349	2.2569
1110 (Detectionable Object)	0.0037	3.95	0.0448	2.8345
1200 (Detectionable Object)	0.0039	4.15	0.0472	2.9744

Similarly, the tiny change of SPR angle of test medium and detectable target are signified by θ_{sp}^{Probe} and θ_{sp}^{Target} respectively. The same calculation has been carried out for SRF frequency and also listed in the same table by stating $\Delta SPRF_{p-t}$ and ΔT_{max}^{p-t} as borderline attributes. In order to calculate the attributes equation (4.9) and (4.10) are utilized:

$$\left(\Delta T_{\max}^{p-t}\right)_{\min} = \left|T_{\max}^{p} - T_{\max}^{t=1000nM}\right| = 0.0019 \qquad (4.9)$$

$$\left(\Delta SPF_{p-t}\right)_{\min} = \left|SRF_{p} - SRF_{t=1000nM}\right| = 0.68 \qquad (4.10)$$

These captured data legitimately make a condition regarding the existence of formalin target solution. By inspecting and matching the collected data with **Table 4.6** unquestionably, a decision can be stated whether the sample holds a substantial quantity of formalin or not. The fulfilment of the principal criterion in **Table 4.6** directs the presence of formalin. On the other hand, the two middle conditions of **Table 4.6** are fulfilled that indicates additional check. The fourth and last criterion exposes the nonexistence of a formaldehyde.

Table 4.5. Reasonable Conditions for Giving Judgement about the Presence of Formalin

Conditions for using $\Delta\theta$ & $R_{\min}$ as detecting attributor	Conditions for using ΔSRF & $T_{\max}$ as detecting attributor	Decision
$\Delta R_{\min}^{P-T} \geq (\Delta R_{\min}^{P-T})_{\min}$ **&&** $\Delta\theta_{SPR}^{P-T} \geq (\Delta\theta_{SPR}^{P-T})_{\min}$	$\Delta T_{\max}^{P-T} \geq (\Delta T_{\max}^{P-T})_{\min}$ **&&** $\Delta T_{\max}^{P-T} \geq (\Delta T_{\max}^{P-T})_{\min}$	**Formalin is Present**
$\Delta R_{\min}^{P-T} \geq (\Delta R_{\min}^{P-T})_{\min}$ **&&** $\Delta\theta_{SPR}^{P-T} \leq (\Delta\theta_{SPR}^{P-T})_{\min}$	$\Delta T_{\max}^{P-T} \geq (\Delta T_{\max}^{P-T})_{\min}$ **&&** $\Delta T_{\max}^{P-T} \leq (\Delta T_{\max}^{P-T})_{\min}$	**Further Check Required**
$\Delta R_{\min}^{P-T} \leq (\Delta R_{\min}^{P-T})_{\min}$ **&&** $\Delta\theta_{SPR}^{P-T} \geq (\Delta\theta_{SPR}^{P-T})_{\min}$	$\Delta T_{\max}^{P-T} \leq (\Delta T_{\max}^{P-T})_{\min}$ **&&** $\Delta T_{\max}^{P-T} \geq (\Delta T_{\max}^{P-T})_{\min}$	**Further Check Required**
$\Delta R_{\min}^{P-T} \leq (\Delta R_{\min}^{P-T})_{\min}$ **&&** $\Delta\theta_{SPR}^{P-T} \leq (\Delta\theta_{SPR}^{P-T})_{\min}$	$\Delta T_{\max}^{P-T} \leq (\Delta T_{\max}^{P-T})_{\min}$ **&&** $\Delta T_{\max}^{P-T} \leq (\Delta T_{\max}^{P-T})_{\min}$	**Empty Probe**

4.4.2 Performance of ZnO based Proposed Structure

The immobilization of formalin on the chitosan increases the RI of sensing layer and this increased RI leads to a right shift of SPR angle. By investigating this angular shift using attenuated total reflection (ATR) it can easily be determined the existence of formalin in the target sample.
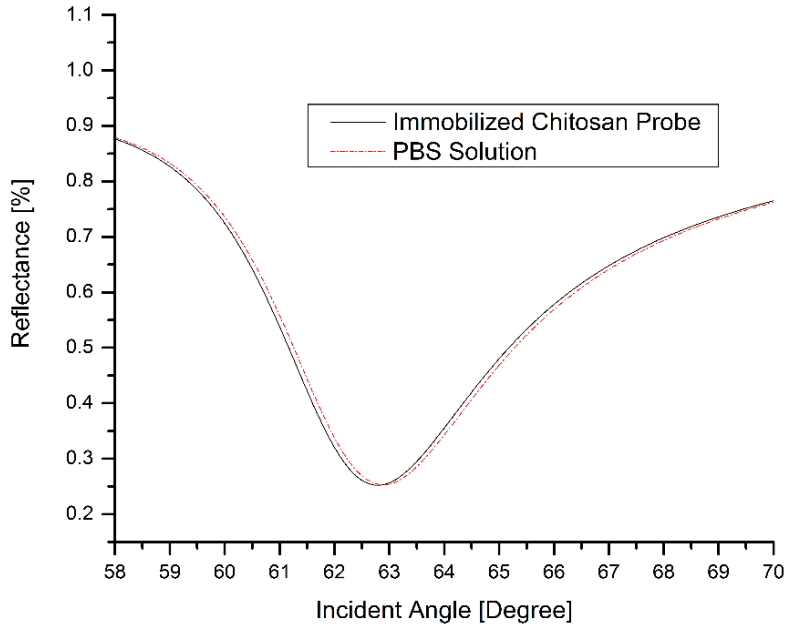
Fig. 4.30. Surface Plasmon Resonance Curve for Immobilized Chitosan Coating and for PBS Solution

Fig. 4.30 shows the reflectance versus incident angle curves. The resonance angle of chitosan coating on graphene layer is 62.79° whereas the resonance angle with the PBS solution is 62.89°.

In this technique, the collected SPR angle shift makes available conditions regarding either the presence of formalin or not. The borderline criterion is signified by equation (4.11):

$$\left(\Delta\theta_{SPR}^{Probe-target}\right)_{min} = \left|\theta_{SPR}^{Chitosan} - \theta_{SPR}^{Formalin}\right| = 0.10° \qquad (4.11)$$

Where, $\left(\Delta\theta_{SPR}^{Probe-formalin}\right)_{min}$ directs the borderline value for the smallest change of SPR angle. This value is for the PBS solution on the immobilization of chitosan coating. As the immobilized chitosan only significantly attach the formalin molecules, the change of SPR angle greater than this marginal value directs the existence of formalin is that sample. In this account, equation (4.12) **[165]**, reveals the increase of the RI for the increases of concentration of formalin molecules in sample solution.

$$n_v = n_1 + c_v \, dn/dc \qquad (4.12)$$

Where, c_v is the concentration of formalin solution, n_1 represents the RI of immobilized chitosan and the rate of change of RI with the change of concentration of formalin solution is, $dn/dc = 0.182\ cm^3/gm$ [165]. As the RI of the sensing medium changes with the adsorption of formalin molecules, the SPR angle shifts rightward and make a change of propagation constant. Thus, this proposed improved-performance SPR-based sensor is employed to identify formalin in liquid sample using the angular investigation method.

A formalin solution for a range of concentration (from 10.00 nM to 1500 nM) and the solution were inserted into the contact of immobilized chitosan film on the graphene surface. The SPR curve for formalin concentrations in contact with the specific graphene/chitosan is shown in **Fig. 4.31.** The result shows that the SPR angle shifts insignificantly when the target formalin concentration was varied from 00.00 nM to 10.00 nM. It was perhaps because of less amount of formalin existence in these lower concentrated solutions to fix on coated chitosan.
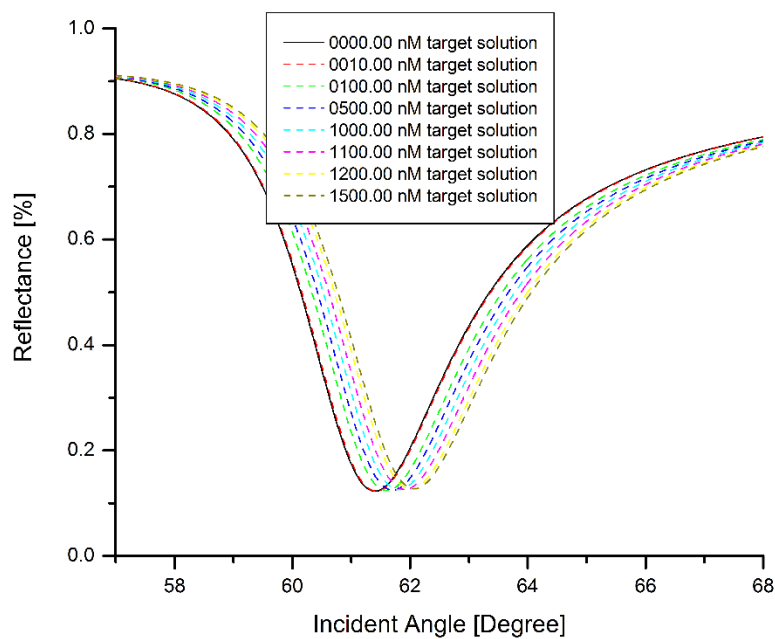
Fig. 4.31. SPR reflectivity curves for graphene/chitosan layer in contact with various formalin solution concentration ranged from 10 nM to 1500 nM

On the other hand, for high formalin concentration (100.00 nM and 1200 nM), the SPR angles were being changed to a significant amount. The change was due to the increment of formalin molecules that were being adsorbed by the chitosan surface. Thus, it accordingly enlarged the change of SPR angle. A similar type of finding was also reported in [160].

The change in SPR angle (θ_{SPR}) was calculated by subtracting between the SPR angle of target solution and the reference PBS solution (61.40°). The change in the SPR angle mostly

dependent on the bindings of chitosan and formalin. More specifically, more the attachment of formalin molecules on chitosan surface, greater the change of SPR angle can be witnessed. The variation of SPR angle was observed a range from 0.10° to 0.18° for the formalin concentration of 100.00 nM to 1200.00 nM. This outcome can be recognized to the additional number of immobilizing between target sample and the ligand and this led to a rise in the RI of the detecting layer. This outcome is in line with [166], who found that the rise of SPR angle is the consequence of the developing bond of target sample and probe reaction. However, for the concentration of 1500 nM, the SPR angle shift was decreased compared to the previous concentrations. Due to the high concentration of the formalin, the chitosan coated surface was entirely shielded and became congested and similar case has been reported for virus detection on an antibody coating [120].

Finally, the modification of RI due to the variation of different concentration of formalin solution was also checked and plotted in **Fig. 4.32**. This linear relationship (R^2=0.952) further justifies the goodness of the proposed sensor for formalin detection in a label free, fast and highly sensitive manner. A similar nature of relation was also found for a SPR aptasensor to detect AIV H5N1 [167].
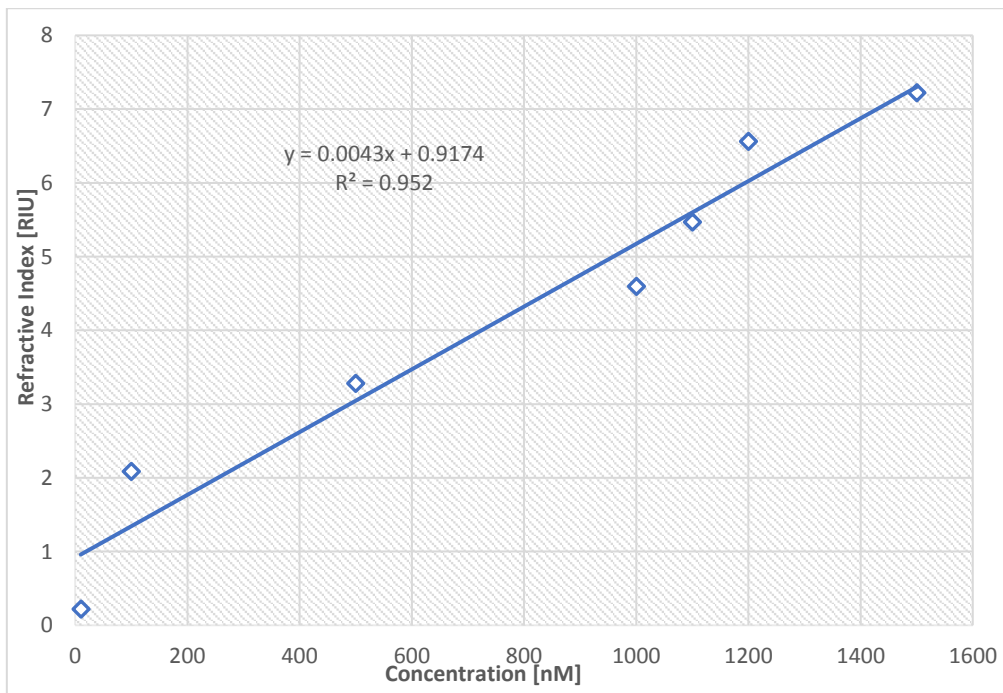
Fig. 4.32. Change of refractive index with respect to the change formalin solution's concentration for the proposed sensor

The concentration of formalin solution was varied between 0.0000 nM and 10 nM and related SPR angle shift is depicted in **Table 4.7**. Analysis shows that a linear relationship exists between the concentration and SPR angle changes, which is a desired characteristics for a sensor [157].

Table 4.7. The SPR angle and related SPR angle shift for various concentrations of formalin solution in contact with graphene/chitosan

Concentration of Formalin solution (nM)	SPR angle, θ_{SPR} (Degree)	SPR angle shift, $\Delta\theta_{SPR}$ (Degree)	Cumulative shift of resonance angle, $C\Delta\theta_{SPR}$ (Degree)
0000.00	61.40	0.00	0.00
0010.00	61.42	0.02	0.02
0100.00	61.60	0.18	0.20
0500.00	61.71	0.11	0.31
1000.00	61.81	0.10	0.41
1100.00	61.91	0.10	0.51
1200.00	62.01	0.10	0.61
1500.00	62.07	0.06	0.67

Similar linear trends were also found for the SPR angle shift and cumulative shift of resonance angle against formalin solution's concentration as listed in **Table 4.7**. This further ensure a good characteristic of the proposed sensor [168].

4.5 Performance Comparison between TiO2-SiO2 and ZnO based Sensor Structures

Table 4.8 lists the main performance parameters such as sensitivity, quality factor and detection accuracy of the TiO_2-SiO_2 and MoS_2-graphene composite structured SPR sensor. The sensitivity, quality factor, and detection accuracy of this proposed sensor structure are found $98°$. RIU^{-1}, 98.89 RIU^{-1} and 0.8889 respectively. In this observation the sensitivity and quality factor of the proposed TiO2-SiO2 based composite structure sensor are 18.07% and 10.66% greater than the conventional Ag only layered sensor respectively. But in the case of detection accuracy it is slightly less than the only silver layered sensor structure. Similarly, comparing with other composite the TiO2-SiO2-Ag-MoS2-graphene sensor structure outperform than the other single and multilayered structures. Therefore, TiO2-SiO2-Ag-MoS2-graphene multilayer structure was chosen for the proposed sensor.

Table 4.9 lists the main performance parameters such as sensitivity, quality factor and detection accuracy of the SPR sensor with different composite structure. It was revealed that the sensor with ZnO-Ag-PtSe$_2$-Graphene multilayers achieved the highest sensitivity.

Table 4.8. Performance Comparison of different layers of TiO_2-SiO_2 based Sensor Structures

Sensor Structure	Sensitivity ($°. RIU^{-1}$)	Quality Factor (RIU^{-1})	Detection Accuracy (Unitless)
Ag	83	89.36170	0.8936
Ag-Graphene	84	90.21739	0.9022
Ag-MoS_2	90	87.37864	0.8738
Ag- MoS_2-Graphene	92	87.61905	0.8762
TiO_2-Ag- MoS_2-Graphene	95	94.05941	0.9406
SiO_2-Ag- MoS_2-Graphene	91	80.53097	0.8053
TiO_2-SiO_2-Ag- MoS_2-Graphene	**98**	**98.88889**	**0.8889**

It was found that the proposed sensor's sensitivity (126.5^0/RIU), quality factor (8.140283 RIU^{-1}), and detection accuracy (0.814028) outperformed than other single and multi-layered structures. In this observation the sensitivity, quality factor and detection accuracy of the proposed ZnO based composite structure sensor are 16.26%, 12.98% and 12.98% greater than the conventional Ag only layered sensor respectively. Therefore, ZnO-Ag-PtSe$_2$-Graphene multilayer structure was chosen for the proposed sensor.

Table 4.9. Performance Comparison of Different ZnO based Sensor Structures

Sensor Structure	Sensitivity ($°. RIU^{-1}$)	Quality Factor (RIU^{-1})	Detection Accuracy (Unitless)
Ag	108.8	7.205298	0.72053
Ag-Graphene	111.0	7.083599	0.70836
Ag-PtSe$_2$	122.4	6.930917	0.693092
Ag-PtSe$_2$-Graphene	124.7	6.985994	0.698599
ZnO-Ag-PtSe$_2$-Graphene	**126.5**	**8.140283**	**0.814028**

These two different structures of SPR sensor with different materials are proposed for formalin detection in liquid solution. Both of them outperform in the case of formalin detection. But comparing performance between these two proposed sensors structures the sensitivity of ZnO-Ag-PtSe$_2$ sensor structure is 29.08% higher than the TiO_2-SiO_2-Ag-MoS_2-graphene composite sensor structure. Though the quality factor of the TiO_2-SiO_2-Ag-MoS_2-graphene composite sensor structure shows a greater value than the of ZnO-Ag-PtSe$_2$-graphene sensor structure and detection accuracy both the sensor structures show almost closer value. For a good sensor the value of sensitivity should be as high as possible with better quality factor and detection accuracy [153]. The ZnO-Ag-PtSe$_2$-graphene composite structure SPR sensor showed a higher sensitivity than the TiO_2-SiO_2-Ag-MoS_2-graphene composite sensor structure along with its reasonable values of quality factor and detection accuracy. From the above comparison, it is

clearly be emphasized in proposing the better one between these two proposed sensors the ZnO-Ag-PtSe₂-graphene composite structured sensor will be the better choice for detection formalin in liquid solution.

4.6 Performance Comparison with Existing Work

A comparison of performance study of these proposed SPR sensor structures with different metal coated graphene attached sensors has been listed in **Table 4.10**; it is observed that our proposed SPR sensor with Ag hybrid layer have better sensitivity than that of other existing sensors. The quality factor of the TiO_2-SiO_2-Ag-MoS_2-Graphene composite sensor structure has the highest value than that of other existing sensors. Also, the SNR value is on a reasonable state. The more significant performance parameter (sensitivity) has been found the highest value for the ZnO-Ag-$PtSe_2$-Graphene composite structured SPR sensor.

There are two recent works [99, 159], both are structurally same and also close to the one (TiO_2-SiO_2-Ag-MoS_2-Graphene) of these two proposed sensors. The main structural difference of this proposed sensor structure is that silver [proposed] has been used instead of gold [previous work]. Both of the above-mentioned recent works have been carried only for the sensitivity analysis.

Table. 4.10. Comparison of sensitivity, SNR and QF with for different design structure among proposed sensors with other existing works

Constructional Configuration	Sensitivity [Deg-RUI^{-1}]	Detection Accuracy	Quality factor	Wavelength [nm]	References
Graphene Coating	33.98	0.2987	2.78019	633	[145]
Au-Si-MoS₂	51.48	0.4688	3.90000	632.8	[124]
Graphene-Ag-Chromium substrate coating	68.03	0.6780	9.69100	633	[48]
Au/graphene/MoS2/PBS solution	87.8 0	1.2800	17.5600	633	[104]
Au/graphene/MoS2/PBS solution with TiO2-SiO2	82.83	--	--	633	[99]
TiO2-SiO2-Au- MoS2- Graphene	79.00	--	--	633	[159]
Ag with Graphene-MoS2-TiO2-SiO2	**98.00**	**0.8889**	**88.8889**	**633**	**Proposed**
ZnO-Ag-PtSe2-Graphene	126.5	0.8140288	8.140283	633	**Proposed**

From the **Table 4.10**, it is clearly evident that these two proposed sensors [this work] outperform than those two above mentioned recent work as well as than the other existing

works. This is because of sharper peak and large plasmonic effect of silver which provide higher sensitivity, quality factor, and detection accuracy of the proposed sensor.

After a comparative study, **Table 4.10** provides a transparent idea in selecting the better option of sensors to be used in formalin detection. The ZnO-Ag-PtSe$_2$-Graphene composite structured SPR sensor has higher sensitivity than another proposed work. Therefore, it can be clearly declared that the ZnO-Ag-PtSe$_2$-Graphene composite layer sensor will be he promising sensor for detecting the formalin in liquid solution.

4.7 Chapter Summary

This chapter presents the step by step performance of the two proposed composite structure SPR sensors in terms of SPR angular shifting, spectral width and RI using angular investigation approach. The performance is analyzed for different sensor structures of different material combinations. It is found that the TiO$_2$-SiO$_2$-Ag-MoS$_2$-Graphene composite structured proposed sensor's sensitivity is 15.31%, 14.29%, 8.16%, 6.12%, 3.06%, and 7.42% higher than the sensor structure with silver only, silver-graphene, silver-MoS$_2$, silver-MoS$_2$-graphene, TiO$_2$-Ag-MoS$_2$-graphene, and SiO$_2$-Ag-MoS$_2$-graphene respectively. In the same way, this proposed sensor's quality factor is also higher than the other partly composite sensor structures. Varying the silver layer thickness performance are also analyzed and an optimum thickness is determined considering the sensitivity, quality factor and detection accuracy as objectives. Electric field dispersal has been shown using FDTD solution technique with YEE algorithm.

Similarly, the proposed ZnO-Ag-PtSe$_2$-Graphene sensor's sensitivity was found to be 13.99%, 12.25%, and 3.24%, and 1.42% higher than the sensor structure with silver only, silver-graphene, silver-PtSe$_2$, and ZnO-Ag-PtSe$_2$-graphene respectively. In terms of quality factor, the new sensor achieved about 11.49%, 12.98%, 14.86%, and 14.18% higher quality factor compared to the silver only, silver-graphene, silver-PtSe$_2$, and ZnO-Ag-PtSe$_2$-graphene structures, respectively. Similarly, the detection accuracy was also found to be higher than the others. Varying the silver layer thickness performance are also analyzed and an optimum thickness is determined considering the sensitivity, quality factor, detection accuracy, and FWHM as objectives.

Finally, comparative study has been shown between these two proposed sensor structures with other existing works in literature and ZnO-Ag-PtSe$_2$-Graphene was found to be the best choice for formalin detection.

CHAPTER V

Conclusion and Future Works

5.1. Conclusions

The target of this dissertation is on the quantitative analysis of food preservatives detection employing the surface plasmon resonance technique which leads to the density changes in the adsorbing sheets of analyte in terms of the SPR angle. Firstly, a Graphene-MOS$_2$-Ag-TiO$_2$-SiO$_2$ structure has been designed and developed quantitatively using MATLAB. Angular interrogation method is principally utilized for the inspection of reflected light from the sensor. This sensor has been successfully used to detect the existence of food preservatives, especially formalin in liquid solution by using attenuated total reflection (ATR). It could be made a decision that the alteration in refractive index of analytes at the period of adsorbing process changes according to the incident light wavelength, metal film thickness, the concentration of the analytes and the buffer solution. Therefore, the proposed sensor releases a new space toward the food preservatives detection.

This work also gives attention on performance analysis of composite structured SPR sensor. Due to the outstanding and versatile properties of graphene and MoS$_2$, the 2D nanomaterials, such as high surface area, electrical conductivity, and biocompatibility, it has become remarkably potential sensor with high performance for food security applications. The sensitivity and quality factor found to be be 98 deg.RIU^{-1} and 98.89 RIU^{-1}, respectively as well as noteworthy measurements of detection accuracy. The reflectance vs SPR angle and transmittance vs SPR frequency attributes have been determined also by using the ATR method. The sensitivity value of 70°/RIU has figured out for conventional configuration of SPR sensor. On the other hand, the sensor based on graphene-MoS$_2$ composite configuration progresses this sensitivity to 76 °/RIU. Additionally, the sensitivity is newly improved to 98 deg/ RIU by inhaling TiO$_2$–SiO$_2$ composite layer.

In this dissertation, the effect of inserting graphene layer on electric field distribution is analyzed integrating the finite difference time domain (FDTD) method by applying the Lumerical FDTD solution Multiphysics software.

An alternative composite layer Graphene-PtSe$_2$-Ag-ZnO with BK7 glass prism sensor structure has been numerically designed and developed. A ZnO layer is deposited on BK7 prism, after that silver layer is deposited on ZnO layer and PtSe2 is deposited on the silver layer before

graphene. Quantitatively formalin has been detected utilizing this alternative and highly sensitive SPR sensor by the angular investigation using ATR method. Due to the outstanding and versatile properties of ZnO, graphene and PtSe2, it has become remarkably potential sensor with high performance for food security applications. For this structure the sensitivity and quality factor has found to be 126.5 deg.RIU^{-1} and 8140283 RIU^{-1}, respectively as well as significant value of detection accuracy. The proposed sensor's sensitivity has found to be 13.99%, 12.25%, and 3.24%, and 1.42% higher than the sensor structure with silver only, silver-graphene, silver-PtSe2, and ZnO-Ag-PtSe2-graphene respectively. In terms of quality factor, the new sensor achieved about 11.49%, 12.98%, 14.86%, and 14.18% higher quality factor compared to the silver only, silver-graphene, silver-PtSe2, and ZnO-Ag-PtSe2-graphene structures, respectively. This alternative sensor structure can successfully be used to detect formalin in liquid solution like the first proposed sensor with higher sensitivity.

Finally, the performance of these two proposed sensors for formalin detection has been compared with the existing sensors. As well, performance has also been studied individually for each composite structure. This analysis provides an in-depth quantitative elucidation that helps in understanding the role of the composition of materials in performance parameters. The performance comparison between these two proposed sensors gives a transparent indication that the ZnO-Ag-PtSe2-graphene structure is more promising structure for detecting formalin in liquid solution.

5.2. Future Works

The successful quantitative development of these proposed sensors has been accomplished through this dissertation. Further requirement is to implement for on-site detection of preservatives in the liquid food sample. The limitations of this scheme and the impending instructions to overwhelmed those limitations are reflected in the following discussions.

- ➤ Hardware implementation of the proposed hybrid SPR sensor will be the best way to verify the performance
- ➤ Optimization of thickness and composition of nano material in order to attain advanced wide-ranging of sensor surface and subsequently higher sensitivity by making more available capturing sites
- ➤ Optimization of layers for each material can be a potential attempt for further attaining of high sensor performance

REFERENCE

[1]   R. Winter, "A consumer's dictionary of food additives. Updated 4th ed., 4th rev," 1994.

[2]   S. K. Mirza, U. Asema, and S. S. Kasim, "To study the harmful effects of food preservatives on human health," *J. Med. Chem. Drug Discovery,* vol. 2, pp. 610-616, 2017.

[3]   S. Hideshima, M. Saito, K. Fujita, Y. Harada, M. Tsuna, S. Sekiguchi*, et al.*, "Label-free detection of allergens in food via surfactant-induced signal amplification using a field effect transistor-based biosensor," *Sensors and Actuators B: Chemical,* vol. 254, pp. 1011-1016, 2018.

[4]   G. Lack, "Epidemiologic risks for food allergy," *Journal of Allergy and Clinical Immunology,* vol. 121, pp. 1331-1336, 2008.

[5]   S. H. Sicherer, "Epidemiology of food allergy," *Journal of Allergy and Clinical Immunology,* vol. 127, pp. 594-602, 2011.

[6]   J. J. S. Chafen, S. J. Newberry, M. A. Riedl, D. M. Bravata, M. Maglione, M. J. Suttorp*, et al.*, "Diagnosing and managing common food allergies: a systematic review," *Jama,* vol. 303, pp. 1848-1856, 2010.

[7]   H. Fu, S. Zhang, H. Chen, and J. Weng, "Graphene enhances the sensitivity of fiber-optic surface plasmon resonance biosensor," *IEEE Sensors Journal,* vol. 15, pp. 5478-5482, 2015.

[8]   A. K. Mishra, S. K. Mishra, and R. K. Verma, "Graphene and beyond graphene MoS2: a new window in surface-plasmon-resonance-based fiber optic sensing," *The Journal of Physical Chemistry C,* vol. 120, pp. 2893-2900, 2016.

[9]   M. B. Hossain, "GRAPHENE COATED SURFACE PLASMON RESONANCE BIOSENSOR FOR BIOMEDICAL APPLICATIONS," RAJSHAHI UNIVERSITY OF ENGINEERING & TECHNOLOGY, 2016.

[10]   L. Wu, H. Chu, W. Koh, and E. Li, "Highly sensitive graphene biosensors based on surface plasmon resonance," *Optics express,* vol. 18, pp. 14395-14400, 2010.

[11]   C. Han, J. Canning, K. Cook, M. A. Hossain, and H. Ding, "Exciting surface plasmons on metal-coated multimode optical waveguides using skew rays," *Optics letters,* vol. 41, pp. 5353-5356, 2016.

[12]   B. Srinivasan and S. Tung, "Development and applications of portable biosensors," *Journal of laboratory automation,* vol. 20, pp. 365-389, 2015.

[13]   L. Wu, J. Guo, H. Xu, X. Dai, and Y. Xiang, "Ultrasensitive biosensors based on long-range surface plasmon polariton and dielectric waveguide modes," *Photonics Research,* vol. 4, pp. 262-266, 2016.

[14]   P. Pattnaik, "Surface plasmon resonance," *Applied biochemistry and biotechnology,* vol. 126, pp. 79-92, 2005.

[15]   J. Nico and M. J. Fischer, "Surface plasmon resonance: a general introduction," in *Surface Plasmon Resonance*, ed: Springer, 2010, pp. 1-14.

[16]   E. Fu, T. Chinowsky, K. Nelson, and P. Yager, "Handbook of surface plasmon resonance," 2008.

[17]   B. Liedberg, C. Nylander, and I. Lunström, "Surface plasmon resonance for gas detection and biosensing," *Sensors and actuators,* vol. 4, pp. 299-304, 1983.

[18]   F.-F. Ren, K.-W. Ang, J. Song, Q. Fang, M. Yu, G.-Q. Lo*, et al.*, "Surface plasmon enhanced responsivity in a waveguided germanium metal-semiconductor-metal photodetector," *Applied physics letters,* vol. 97, p. 091102, 2010.

[19]   S. K. Srivastava, V. Arora, S. Sapra, and B. D. Gupta, "Localized surface plasmon resonance-based fiber optic U-shaped biosensor for the detection of blood glucose," *Plasmonics,* vol. 7, pp. 261-268, 2012.

[20] J. Homola, "Surface plasmon resonance sensors for detection of chemical and biological species," *Chemical reviews,* vol. 108, pp. 462-493, 2008.

[21] Y. A. Akimov and W. Koh, "Resonant and nonresonant plasmonic nanoparticle enhancement for thin-film silicon solar cells," *Nanotechnology,* vol. 21, p. 235201, 2010.

[22] R. W. Wood, "On a remarkable case of uneven distribution of light in a diffraction grating spectrum," *Proceedings of the Physical Society of London,* vol. 18, p. 269, 1902.

[23] J. Pitarke, V. Silkin, E. Chulkov, and P. Echenique, "Theory of surface plasmons and surface-plasmon polaritons," *Reports on progress in physics,* vol. 70, p. 1, 2006.

[24] I. Venditti, "Gold nanoparticles in photonic crystals applications: A review," *Materials,* vol. 10, p. 97, 2017.

[25] E. Kretschmann and H. Raether, "Radiative decay of non radiative surface plasmons excited by light," *Zeitschrift für Naturforschung A,* vol. 23, pp. 2135-2136, 1968.

[26] A. De Leebeeck, L. S. Kumar, V. De Lange, D. Sinton, R. Gordon, and A. G. Brolo, "On-chip surface-based detection with nanohole arrays," *Analytical Chemistry,* vol. 79, pp. 4094-4100, 2007.

[27] Y. Zhao, Z.-q. Deng, and Q. Wang, "Fiber optic SPR sensor for liquid concentration measurement," *Sensors and Actuators B: Chemical,* vol. 192, pp. 229-233, 2014.

[28] J. Zhang, I. Khan, Q. Zhang, X. Liu, J. Dostalek, B. Liedberg*, et al.*, "Lipopolysaccharides detection on a grating-coupled surface plasmon resonance smartphone biosensor," *Biosensors and Bioelectronics,* vol. 99, pp. 312-317, 2018.

[29] C. Lertvachirapaiboon, A. Baba, K. Shinbo, and K. Kato, "A smartphone-based surface plasmon resonance platform," *Analytical methods,* vol. 10, pp. 4732-4740, 2018.

[30] J. Homola, J. Dostalek, S. Chen, A. Rasooly, S. Jiang, and S. S. Yee, "Spectral surface plasmon resonance biosensor for detection of staphylococcal enterotoxin B in milk," *International journal of food microbiology,* vol. 75, pp. 61-69, 2002.

[31] A. Rasooly, "Surface plasmon resonance analysis of staphylococcal enterotoxin B in food," *Journal of Food Protection,* vol. 64, pp. 37-43, 2001.

[32] J. Chung, S. Kim, R. Bernhardt, and J. C. Pyun, "Application of SPR biosensor for medical diagnostics of human hepatitis B virus (hHBV)," *Sensors and Actuators B: Chemical,* vol. 111, pp. 416-422, 2005.

[33] J. Ladd, A. D. Taylor, M. Piliarik, J. Homola, and S. Jiang, "Label-free detection of cancer biomarker candidates using surface plasmon resonance imaging," *Analytical and bioanalytical chemistry,* vol. 393, pp. 1157-1163, 2009.

[34] S. Filion-Côté, P. J. Roche, A. M. Foudeh, M. Tabrizian, and A. G. Kirk, "Design and analysis of a spectro-angular surface plasmon resonance biosensor operating in the visible spectrum," *Review of Scientific Instruments,* vol. 85, p. 093107, 2014.

[35] M. B. Hossain, I. M. Mehedi, M. Moznuzzaman, L. F. Abdulrazak, and M. A. Hossain, "High performance refractive index SPR sensor modeling employing graphene tri sheets," *Results in Physics,* vol. 15, p. 102719, 2019.

[36] M. B. Hossain, M. S. Hossain, M. Moznuzzaman, M. A. Hossain, M. Tariquzzaman, M. T. Hasan*, et al.*, "Numerical Analysis and Design of Photonic Crystal Fiber Based Surface Plasmon Resonance Biosensor," *Journal of Sensor Technology,* vol. 9, pp. 27-34, 2019.

[37] K. V. Sreekanth, S. Zeng, K.-T. Yong, and T. Yu, "Sensitivity enhanced biosensor using graphene-based one-dimensional photonic crystal," *Sensors and Actuators B: Chemical,* vol. 182, pp. 424-428, 2013.

[38] J. B. Khurgin and A. Boltasseva, "Reflecting upon the losses in plasmonics and metamaterials," *MRS bulletin,* vol. 37, pp. 768-779, 2012.

[39] X. Yu, Z. Yan, and D. Wang, "Simulation of surface plasmon resonance biosensor based on phase detection," *JOURNAL-TSINGHUA UNIVERSITY,* vol. 43, pp. 160-163, 2003.

[40] N. Atar, T. Eren, M. L. Yola, and S. Wang, "A sensitive molecular imprinted surface plasmon resonance nanosensor for selective determination of trace triclosan in wastewater," *Sensors and Actuators B: Chemical,* vol. 216, pp. 638-644, 2015.

[41] C. Onac, H. K. Alpoguz, M. L. Yola, and A. Kaya, "Transport of melamine by a new generation of nano-material membranes containing carbon nanotubes and determination with surface plasmon resonance," *Innovative Food Science & Emerging Technologies,* vol. 45, pp. 467-470, 2018.

[42] M. L. Yola, T. Eren, and N. Atar, "Molecular imprinted nanosensor based on surface plasmon resonance: application to the sensitive determination of amoxicillin," *Sensors and Actuators B: Chemical,* vol. 195, pp. 28-35, 2014.

[43] M. L. Yola, N. Atar, and A. Erdem, "Oxytocin imprinted polymer based surface plasmon resonance sensor and its application to milk sample," *Sensors and Actuators B: Chemical,* vol. 221, pp. 842-848, 2015.

[44] C. Situ, M. H. Mooney, C. T. Elliott, and J. Buijs, "Advances in surface plasmon resonance biosensor technology towards high-throughput, food-safety analysis," *TrAC Trends in Analytical Chemistry,* vol. 29, pp. 1305-1315, 2010.

[45] Y. Yanase, K. Yoshizaki, K. Kimura, T. Kawaguchi, M. Hide, and S. Uno, "Development of SPR Imaging-Impedance Sensor for Multi-Parametric Living Cell Analysis," *Sensors,* vol. 19, p. 2067, 2019.

[46] N.-H. Kim, M. Choi, T. W. Kim, W. Choi, S. Y. Park, and K. M. Byun, "Sensitivity and Stability Enhancement of Surface Plasmon Resonance Biosensors based on a Large-Area Ag/MoS2 Substrate," *Sensors,* vol. 19, p. 1894, 2019.

[47] M. Mitsushio, K. Miyashita, and M. Higo, "Sensor properties and surface characterization of the metal-deposited SPR optical fiber sensors with Au, Ag, Cu, and Al," *Sensors and Actuators A: Physical,* vol. 125, pp. 296-303, 2006.

[48] A. Verma, A. Prakash, and R. Tripathi, "Sensitivity enhancement of surface plasmon resonance biosensor using graphene and air gap," *Optics communications,* vol. 357, pp. 106-112, 2015.

[49] M. S. Rahman, M. Anower, M. K. Rahman, M. R. Hasan, M. B. Hossain, and M. I. Haque, "Modeling of a highly sensitive MoS2-Graphene hybrid based fiber optic SPR biosensor for sensing DNA hybridization," *Optik,* vol. 140, pp. 989-997, 2017.

[50] M. S. Rahman, S. S. Noor, M. Anower, L. F. Abdulrazak, M. M. Rahman, and K. Rikta, "Design and numerical analysis of a graphene-coated fiber-optic SPR biosensor using tungsten disulfide," *Photonics and Nanostructures-Fundamentals and Applications,* vol. 33, pp. 29-35, 2019.

[51] J. Homola, "Present and future of surface plasmon resonance biosensors," *Analytical and bioanalytical chemistry,* vol. 377, pp. 528-539, 2003.

[52] A. Hassan and I. Khan, "Surface plasmonic properties in graphene for the variation of chemical potential," in *2014 International Conference on Informatics, Electronics & Vision (ICIEV)*, 2014, pp. 1-4.

[53] H.-J. Li, L.-L. Wang, J.-Q. Liu, Z.-R. Huang, B. Sun, and X. Zhai, "Investigation of the graphene based planar plasmonic filters," *Applied Physics Letters,* vol. 103, p. 211104, 2013.

[54] Y. Feng, Y. Liu, X. Wang, D. Dong, Y. Shi, and L. Tang, "Tunable multichannel plasmonic filter based on a single graphene sheet on a Fibonacci quasiperiodic structure," *Plasmonics,* vol. 13, pp. 653-659, 2018.

[55] Y. Feng, Y. Liu, Y. Shi, X. Wang, and D. Dong, "An ultra-compact tunable intersection structure based on graphene nanoribbon," *Journal of Physics D: Applied Physics,* vol. 50, p. 185101, 2017.

[56] M. Liu, X. Yin, E. Ulin-Avila, B. Geng, T. Zentgraf, L. Ju, *et al.*, "A graphene-based broadband optical modulator," *Nature,* vol. 474, p. 64, 2011.

[57] B. Wang, X. Zhang, X. Yuan, and J. Teng, "Optical coupling of surface plasmons between graphene sheets," *Applied Physics Letters,* vol. 100, p. 131111, 2012.

[58] Y. Shao, J. Wang, H. Wu, J. Liu, I. Aksay, and Y. Lin, "Graphene based electrochemical sensors and biosensors: A review. Electroanal., 22, 1027–1036," ed, 2010.

[59] P. K. Maharana and R. Jha, "Chalcogenide prism and graphene multilayer based surface plasmon resonance affinity biosensor for high performance," *Sensors and Actuators B: Chemical,* vol. 169, pp. 161-166, 2012.

[60] Y. Jia, Z. Li, H. Wang, M. Saeed, and H. Cai, "Sensitivity Enhancement of a Surface Plasmon Resonance Sensor with Platinum Diselenide," *Sensors,* vol. 20, p. 131, 2020.

[61] W. Zhang, Z. Huang, W. Zhang, and Y. Li, "Two-dimensional semiconductors with possible high room temperature mobility," *Nano Research,* vol. 7, pp. 1731-1737, 2014.

[62] C. Yim, K. Lee, N. McEvoy, M. O'Brien, S. Riazimehr, N. C. Berner, *et al.*, "High-performance hybrid electronic devices from layered PtSe2 films grown at low temperature," *ACS nano,* vol. 10, pp. 9550-9558, 2016.

[63] M. Sajjad, E. Montes, N. Singh, and U. Schwingenschlögl, "Superior gas sensing properties of monolayer PtSe2," *Advanced Materials Interfaces,* vol. 4, p. 1600911, 2017.

[64] Z. Wang, Q. Li, F. Besenbacher, and M. Dong, "Facile synthesis of single crystal PtSe2 nanosheets for nanoscale electronics," *Advanced Materials,* vol. 28, pp. 10224-10229, 2016.

[65] X. Chia, A. Adriano, P. Lazar, Z. Sofer, J. Luxa, and M. Pumera, "Layered platinum dichalcogenides (PtS2, PtSe2, and PtTe2) electrocatalysis: monotonic dependence on the chalcogen size," *Advanced Functional Materials,* vol. 26, pp. 4306-4318, 2016.

[66] N.-F. Chiu, Y.-C. Tu, and T.-Y. Huang, "Enhanced sensitivity of anti-symmetrically structured surface plasmon resonance sensors with zinc oxide intermediate layers," *Sensors,* vol. 14, pp. 170-187, 2014.

[67] Ü. Özgür, Y. I. Alivov, C. Liu, A. Teke, M. Reshchikov, S. Doğan, *et al.*, "A comprehensive review of ZnO materials and devices," *Journal of applied physics,* vol. 98, p. 11, 2005.

[68] A. B. Djurišić and Y. H. Leung, "Optical properties of ZnO nanostructures," *small,* vol. 2, pp. 944-961, 2006.

[69] J. Wang, X. W. Sun, A. Wei, Y. Lei, X. Cai, C. M. Li, *et al.*, "Zinc oxide nanocomb biosensor for glucose detection," *Applied physics letters,* vol. 88, p. 233106, 2006.

[70] S. A. Kumar and S. M. Chen, "Nanostructured zinc oxide particles in chemically modified electrodes for biosensor applications," *Analytical Letters,* vol. 41, pp. 141-158, 2008.

[71] H. Liao, W. Wen, G. K. Wong, and G. Yang, "Optical nonlinearity of nanocrystalline Au/ZnO composite films," *Optics letters,* vol. 28, pp. 1790-1792, 2003.

[72] L. Wang, J. Wang, S. Zhang, Y. Sun, X. Zhu, Y. Cao, *et al.*, "Surface plasmon resonance biosensor based on water-soluble ZnO–Au nanocomposites," *Analytica chimica acta,* vol. 653, pp. 109-115, 2009.

[73] R. Kumar, A. S. Kushwaha, M. Srivastava, H. Mishra, and S. Srivastava, "Enhancement in sensitivity of graphene-based zinc oxide assisted bimetallic surface plasmon resonance (SPR) biosensor," *Applied Physics A,* vol. 124, p. 235, 2018.

[74] B. Liedberg, C. Nylander, and I. Lundström, "Biosensing with surface plasmon resonance—how it all started," *Biosensors and Bioelectronics,* vol. 10, pp. i-ix, 1995.

[75] F. S. Ligler, "Perspective on optical biosensors and integrated sensor systems," *Analytical chemistry,* vol. 81, pp. 519-526, 2008.

[76] E. Royuela, A. Negredo, and A. Sánchez-Fauquier, "Development of a one step real-time RT-PCR method for sensitive detection of human astrovirus," *Journal of virological methods,* vol. 133, pp. 14-19, 2006.

[77] R. Potyrailo, C. Surman, R. Chen, S. Go, K. Dovidenko, W. Morris, *et al.*, "Label-free biosensing using passive radio-frequency identification (RFID) sensors," in *TRANSDUCERS 2009-2009 International Solid-State Sensors, Actuators and Microsystems Conference*, 2009, pp. 2378-2380.

[78] P. Jolly, P. Damborsky, N. Madaboosi, R. R. Soares, V. Chu, J. P. Conde, *et al.*, "DNA aptamer-based sandwich microfluidic assays for dual quantification and multi-glycan profiling of cancer biomarkers," *Biosensors and Bioelectronics,* vol. 79, pp. 313-319, 2016.

[79] N. Formisano, P. Jolly, N. Bhalla, M. Cromhout, S. P. Flanagan, R. Fogel, *et al.*, "Optimisation of an electrochemical impedance spectroscopy aptasensor by exploiting quartz crystal microbalance with dissipation signals," *Sensors and Actuators B: Chemical,* vol. 220, pp. 369-375, 2015.

[80] J. Chung, R. Bernhardt, and J. C. Pyun, "Additive assay of cancer marker CA 19-9 by SPR biosensor," *Sensors and Actuators B: Chemical,* vol. 118, pp. 28-32, 2006.

[81] D.-P. Tang, R. Yuan, and Y.-Q. Chai, "Novel immunoassay for carcinoembryonic antigen based on protein A-conjugated immunosensor chip by surface plasmon resonance and cyclic voltammetry," *Bioprocess and biosystems engineering,* vol. 28, pp. 315-321, 2006.

[82] P. Norouzi, V. K. Gupta, F. Faridbod, M. Pirali-Hamedani, B. Larijani, and M. R. Ganjali, "Carcinoembryonic antigen admittance biosensor based on Au and ZnO nanoparticles using FFT admittance voltammetry," *Analytical chemistry,* vol. 83, pp. 1564-1570, 2011.

[83] X. Wang, Y. Li, H. Wang, Q. Fu, J. Peng, Y. Wang, *et al.*, "Gold nanorod-based localized surface plasmon resonance biosensor for sensitive detection of hepatitis B virus in buffer, blood serum and plasma," *Biosensors and Bioelectronics,* vol. 26, pp. 404-410, 2010.

[84] B. T. T. Nguyen, A. E. K. Peh, C. Y. L. Chee, K. Fink, V. T. Chow, M. M. Ng, *et al.*, "Electrochemical impedance spectroscopy characterization of nanoporous alumina dengue virus biosensor," *Bioelectrochemistry,* vol. 88, pp. 15-21, 2012.

[85] M. B. Hossain, T. Tasnim, L. F. Abdulrazak, M. M. Rana, and M. R. Islam, "A Numerical Approach to Design the Kretschmann Configuration Based Refractive Index Graphene-MoS 2 Hybrid Layers With TiO 2-SiO 2 Nano for Formalin Detection," *Photonic Sensors,* pp. 1-13, 2019.

[86] F. Prieto, B. Sepúlveda, A. Calle, A. Llobera, C. Domínguez, A. Abad, *et al.*, "An integrated optical interferometric nanodevice based on silicon technology for biosensor applications," *Nanotechnology,* vol. 14, p. 907, 2003.

[87] M. Pumera, S. Sanchez, I. Ichinose, and J. Tang, "Electrochemical nanobiosensors," *Sensors and Actuators B: Chemical,* vol. 123, pp. 1195-1205, 2007.

[88] D. Grieshaber, R. MacKenzie, J. Vörös, and E. Reimhult, "Electrochemical biosensors-sensor principles and architectures," *Sensors,* vol. 8, pp. 1400-1458, 2008.

[89] L. Anorga, A. Rebollo, J. Herran, S. Arana, E. Bandres, and J. Garcia-Foncillas, "Development of a DNA microelectrochemical biosensor for CEACAM5 detection," *IEEE Sensors Journal,* vol. 10, pp. 1368-1374, 2010.

[90]   M. Mujika, S. Arana, E. Castano, M. Tijero, R. Vilares, J. Ruano-Lopez*, et al.*, "Magnetoresistive immunosensor for the detection of Escherichia coli O157: H7 including a microfluidic network," *Biosensors and Bioelectronics,* vol. 24, pp. 1253-1258, 2009.

[91]   A. Otto, "A new method for exciting non-radioactive surface plasma oscillations," *phys. stat. sol,* vol. 26, pp. K99-K101, 1968.

[92]   P. N. Prasad, *Introduction to biophotonics*: John Wiley & Sons, 2004.

[93]   W. Lukosz and K. Tiefenthaler, "Embossing technique for fabricating integrated optical components in hard inorganic waveguiding materials," *Optics letters,* vol. 8, pp. 537-539, 1983.

[94]   P. V. Lambeck, "Integrated opto-chemical sensors," *Sensors and Actuators B: Chemical,* vol. 8, pp. 103-116, 1992.

[95]   F. S. Ligler and C. R. Taitt, "Fluorescence lifetime biosensing: entering the mainstream," *Optical Biosensors: Today and Tomorrow,* p. 287, 2008.

[96]   H. Raether, "Surface plasmons on smooth surfaces," in *Surface plasmons on smooth and rough surfaces and on gratings*, ed: Springer, 1988, pp. 4-39.

[97]   R. H. Ritchie, E. Arakawa, J. Cowan, and R. Hamm, "Surface-plasmon resonance effect in grating diffraction," *Physical Review Letters,* vol. 21, p. 1530, 1968.

[98]   P. E. Ciddor, "Refractive index of air: new equations for the visible and near infrared," *Applied optics,* vol. 35, pp. 1566-1573, 1996.

[99]   M. B. Hossain, M. M. Rana, L. F. Abdulrazak, S. Mitra, and M. Rahman, "Graphene-MoS2 with TiO2SiO2 layers based surface plasmon resonance biosensor: Numerical development for formalin detection," *Biochemistry and biophysics reports,* vol. 18, p. 100639, 2019.

[100]   M. O'Brien, K. Lee, R. Morrish, N. C. Berner, N. McEvoy, C. A. Wolden*, et al.*, "Plasma assisted synthesis of WS2 for gas sensing applications," *Chemical Physics Letters,* vol. 615, pp. 6-10, 2014.

[101]   Y. Luo, C. Chen, K. Xia, S. Peng, H. Guan, J. Tang*, et al.*, "Tungsten disulfide (WS 2) based all-fiber-optic humidity sensor," *Optics express,* vol. 24, pp. 8956-8966, 2016.

[102]   M. B. Hossain, M. M. Islam, L. F. Abdulrazak, M. M. Rana, T. B. A. Akib, and M. Hassan, "Graphene-Coated Optical Fiber SPR Biosensor for BRCA1 and BRCA2 Breast Cancer Biomarker Detection: a Numerical Design-Based Analysis," *Photonic Sensors,* pp. 1-13, 2019.

[103]   M. B. Hossain, T. B. A. Akib, L. F. Abdulrazak, and M. M. Rana, "Numerical modeling of graphene-coated fiber optic surface plasmon resonance biosensor for BRCA1 and BRCA2 genetic breast cancer detection," *Optical Engineering,* vol. 58, p. 037104, 2019.

[104]   M. S. Rahman, M. S. Anower, M. R. Hasan, M. B. Hossain, and M. I. Haque, "Design and numerical analysis of highly sensitive Au-MoS2-graphene based hybrid surface plasmon resonance biosensor," *Optics Communications,* vol. 396, pp. 36-43, 2017.

[105]   Q. Ouyang, S. Zeng, X.-Q. Dinh, P. Coquet, and K.-T. Yong, "Sensitivity enhancement of MoS2 nanosheet based surface plasmon resonance biosensor," *Procedia engineering,* vol. 140, pp. 134-139, 2016.

[106]   K. N. Shushama, M. M. Rana, R. Inum, and M. B. Hossain, "Graphene coated fiber optic surface plasmon resonance biosensor for the DNA hybridization detection: Simulation analysis," *Optics Communications,* vol. 383, pp. 186-190, 2017.

[107]   V. Ball and J. J. Ramsden, "Buffer dependence of refractive index increments of protein solutions," *Biopolymers: Original Research on Biomolecules,* vol. 46, pp. 489-492, 1998.

[108] D. A. Caporale and E. E. Swenson, "Two different BRCA2 mutations found in a multigenerational family with a history of breast, prostate, and lung cancers," *Advances in Genomics and Genetics,* vol. 4, p. 87, 2014.

[109] L. G. Carrascosa, A. Calle, and L. M. Lechuga, "Label-free detection of DNA mutations by SPR: application to the early detection of inherited breast cancer," *Analytical and bioanalytical chemistry,* vol. 393, p. 1173, 2009.

[110] S. D. Dufresne, D. R. Belloni, W. A. Wells, and G. J. Tsongalis, "BRCA1 and BRCA2 mutation screening using SmartCycler II high-resolution melt curve analysis," *Archives of pathology & laboratory medicine,* vol. 130, pp. 185-187, 2006.

[111] X. Zhao, X. Zhang, X.-S. Zhu, and Y.-W. Shi, "Long-range surface plasmon resonance sensor based on the GK570/Ag coated hollow fiber with an asymmetric layer structure," *Optics express,* vol. 27, pp. 9550-9560, 2019.

[112] L. Wu, Y. Jia, L. Jiang, J. Guo, X. Dai, Y. Xiang*, et al.*, "Sensitivity improved SPR biosensor based on the MoS2/graphene–aluminum hybrid structure," *Journal of Lightwave Technology,* vol. 35, pp. 82-87, 2016.

[113] K. Tamersit and F. Djeffal, "Double-gate graphene nanoribbon field-effect transistor for DNA and gas sensing applications: simulation study and sensitivity analysis," *IEEE Sensors Journal,* vol. 16, pp. 4180-4191, 2016.

[114] J. Maurya, Y. Prajapati, V. Singh, J. Saini, and R. Tripathi, "Improved performance of the surface plasmon resonance biosensor based on graphene or MoS2 using silicon," *Optics Communications,* vol. 359, pp. 426-434, 2016.

[115] P. Li, D. Zhang, Y. Zhang, W. Lu, W. Wang, and T. Chen, "Ultrafast and efficient detection of formaldehyde in aqueous solutions using chitosan-based fluorescent polymers," *ACS sensors,* vol. 3, pp. 2394-2401, 2018.

[116] A. K. Mishra and S. K. Mishra, "MgF2 prism/rhodium/graphene: efficient refractive index sensing structure in optical domain," *Journal of Physics: Condensed Matter,* vol. 29, p. 145001, 2017.

[117] E. Pokidysheva, Y. Zhang, A. J. Battisti, C. M. Bator-Kelly, P. R. Chipman, C. Xiao*, et al.*, "Cryo-EM reconstruction of dengue virus in complex with the carbohydrate recognition domain of DC-SIGN," *Cell,* vol. 124, pp. 485-493, 2006.

[118] T. C. Pierson, D. H. Fremont, R. J. Kuhn, and M. S. Diamond, "Structural insights into the mechanisms of antibody-mediated neutralization of flavivirus infection: implications for vaccine development," *Cell host & microbe,* vol. 4, pp. 229-238, 2008.

[119] H. H. Nguyen, J. Park, S. Kang, and M. Kim, "Surface plasmon resonance: a versatile technique for biosensor applications," *Sensors,* vol. 15, pp. 10481-10510, 2015.

[120] N. A. S. Omar, Y. W. Fen, J. Abdullah, C. E. N. C. E. Chik, and M. A. Mahdi, "Development of an optical sensor based on surface plasmon resonance phenomenon for diagnosis of dengue virus E-protein," *Sensing and bio-sensing research,* vol. 20, pp. 16-21, 2018.

[121] A. Mishra and S. Mishra, "Infrared SPR sensitivity enhancement using ITO/TiO2/silicon overlays," *EPL (Europhysics Letters),* vol. 112, p. 10001, 2015.

[122] J. Homola, S. S. Yee, and G. Gauglitz, "Surface plasmon resonance sensors," *Sensors and actuators B: Chemical,* vol. 54, pp. 3-15, 1999.

[123] J. Homola and M. Piliarik, "Surface plasmon resonance (SPR) sensors," in *Surface plasmon resonance based sensors*, ed: Springer, 2006, pp. 45-67.

[124] J. Maurya, Y. Prajapati, V. Singh, J. Saini, and R. Tripathi, "Performance of graphene–MoS 2 based surface plasmon resonance sensor using Silicon layer," *Optical and Quantum Electronics,* vol. 47, pp. 3599-3611, 2015.

[125] M. Hossain and M. Rana, "Graphene coated high sensitive surface plasmon resonance biosensor for sensing DNA hybridization," *Sensor Letters,* vol. 14, pp. 145-152, 2016.

[126] M. M. Habib, R. Roy, M. M. Islam, M. Hassan, M. M. Islam, and M. B. Hossain, "Study of graphene-MoS2 based SPR biosensor with graphene based SPR biosensor: comparative approach," *International Journal of Natural Sciences Research,* vol. 7, pp. 1-9, 2019.

[127] M. B. Hossain, M. R. Khan, M. S. Rahman, S. B. Badrudduza, M. Sabiha, and M. M. Rana, "Graphene-MoS2-Au-TiO2-SiO2 Hybrid SPR Biosensor: A New Window for Formalin Detection," *Journal of Materials and Applications,* vol. 8, pp. 51-58, 2019.

[128] J. Maurya, Y. Prajapati, V. Singh, and J. Saini, "Sensitivity enhancement of surface plasmon resonance sensor based on graphene–MoS 2 hybrid structure with TiO 2–SiO 2 composite layer," *Applied Physics A,* vol. 121, pp. 525-533, 2015.

[129] L. Wu, J. Guo, X. Dai, Y. Xiang, and D. Fan, "Sensitivity Enhanced by MoS 2–Graphene Hybrid Structure in Guided-Wave Surface Plasmon Resonance Biosensor," *Plasmonics,* vol. 13, pp. 281-285, 2018.

[130] L. Wu, J. Guo, Q. Wang, S. Lu, X. Dai, Y. Xiang, *et al.*, "Sensitivity enhancement by using few-layer black phosphorus-graphene/TMDCs heterostructure in surface plasmon resonance biochemical sensor," *Sensors and Actuators B: Chemical,* vol. 249, pp. 542-548, 2017.

[131] L. Diéguez, N. Darwish, M. Mir, E. Martínez, M. Moreno, and J. Samitier, "Effect of the refractive index of buffer solutions in evanescent optical biosensors," *Sensor Letters,* vol. 7, pp. 851-855, 2009.

[132] C.-W. Lin, K.-P. Chen, C.-N. Hsiao, S. Lin, and C.-K. Lee, "Design and fabrication of an alternating dielectric multi-layer device for surface plasmon resonance sensor," *Sensors and Actuators B: Chemical,* vol. 113, pp. 169-176, 2006.

[133] Y. Yuan and Y. Dai, "A revised LRSPR sensor with sharp reflection spectrum," *Sensors,* vol. 14, pp. 16664-16671, 2014.

[134] S. T. Kochuveedu, D.-P. Kim, and D. H. Kim, "Surface-plasmon-induced visible light photocatalytic activity of TiO2 nanospheres decorated by Au nanoparticles with controlled configuration," *The Journal of Physical Chemistry C,* vol. 116, pp. 2500-2506, 2012.

[135] J. Xu, X. Xiao, A. L. Stepanov, F. Ren, W. Wu, G. Cai, *et al.*, "Efficiency enhancements in Ag nanoparticles-SiO 2-TiO 2 sandwiched structure via plasmonic effect-enhanced light capturing," *Nanoscale research letters,* vol. 8, pp. 1-5, 2013.

[136] M. Singh, M. Holzinger, M. Tabrizian, S. a. Winters, N. C. Berner, S. Cosnier, *et al.*, "Noncovalently functionalized monolayer graphene for sensitivity enhancement of surface plasmon resonance immunosensors," *Journal of the American Chemical Society,* vol. 137, pp. 2800-2803, 2015.

[137] A. Shalabney and I. Abdulhalim, "Sensitivity-enhancement methods for surface plasmon sensors," *Laser & Photonics Reviews,* vol. 5, pp. 571-606, 2011.

[138] B. H. Ong, X. Yuan, S. C. Tjin, J. Zhang, and H. M. Ng, "Optimised film thickness for maximum evanescent field enhancement of a bimetallic film surface plasmon resonance biosensor," *Sensors and Actuators B: Chemical,* vol. 114, pp. 1028-1034, 2006.

[139] X.-M. Zhu, P.-H. Lin, P. Ao, and L. Sorensen, "Surface treatments for surface plasmon resonance biosensors," *Sensors and Actuators B: Chemical,* vol. 84, pp. 106-112, 2002.

[140] O. Lopez-Sanchez, D. Lembke, M. Kayci, A. Radenovic, and A. Kis, "Ultrasensitive photodetectors based on monolayer MoS 2," *Nature nanotechnology,* vol. 8, p. 497, 2013.

[141] K. F. Mak, C. Lee, J. Hone, J. Shan, and T. F. Heinz, "Atomically thin MoS 2: a new direct-gap semiconductor," *Physical review letters,* vol. 105, p. 136805, 2010.

[142] K. Rurack, "Flipping the light switch 'ON'–the design of sensor molecules that show cation-induced fluorescence enhancement with heavy and transition metal ions," *Spectrochimica Acta Part A: Molecular and Biomolecular Spectroscopy,* vol. 57, pp. 2161-2195, 2001.

[143] K. S. Novoselov, A. K. Geim, S. V. Morozov, D. Jiang, Y. Zhang, S. V. Dubonos, *et al.*, "Electric field effect in atomically thin carbon films," *science,* vol. 306, pp. 666-669, 2004.

[144] A. Hoggard, L.-Y. Wang, L. Ma, Y. Fang, G. You, J. Olson, *et al.*, "Using the plasmon linewidth to calculate the time and efficiency of electron transfer between gold nanorods and graphene," *Acs Nano,* vol. 7, pp. 11209-11217, 2013.

[145] A. Verma, A. Prakash, and R. Tripathi, "Performance analysis of graphene based surface plasmon resonance biosensors for detection of pseudomonas-like bacteria," *Optical and Quantum Electronics,* vol. 47, pp. 1197-1205, 2015.

[146] G. B. McGaughey, M. Gagné, and A. K. Rappé, "π-Stacking interactions alive and well in proteins," *Journal of Biological Chemistry,* vol. 273, pp. 15458-15463, 1998.

[147] K. N. Shushama, M. M. Rana, R. Inum, and M. B. Hossain, "Sensitivity enhancement of graphene coated surface plasmon resonance biosensor," *Optical and Quantum Electronics,* vol. 49, p. 381, 2017.

[148] M. Milanese, M. Knauer, G. Colangelo, D. Laforgia, and A. de Risi, "Numerical Optimization of SPR Sensors for Lube Oil Real-Time Optical Characterization in Large 2-Stroke Marine Diesel Engines," *Energy Procedia,* vol. 126, pp. 1075-1082, 2017.

[149] J. Xie, D. Zhang, X.-Q. Yan, M. Ren, X. Zhao, F. Liu, *et al.*, "Optical properties of chemical vapor deposition-grown PtSe2 characterized by spectroscopic ellipsometry," *2D Materials,* vol. 6, p. 035011, 2019.

[150] P. K. Maharana, R. Jha, and P. Padhy, "On the electric field enhancement and performance of SPR gas sensor based on graphene for visible and near infrared," *Sensors and Actuators B: Chemical,* vol. 207, pp. 117-122, 2015.

[151] M. Hossain and M. Rana, "DNA hybridization detection based on resonance frequency readout in graphene on Au SPR biosensor," *Journal of sensors,* vol. 2016, 2016.

[152] S. H. Choi, Y. L. Kim, and K. M. Byun, "Graphene-on-silver substrates for sensitive surface plasmon resonance imaging biosensors," *Optics express,* vol. 19, pp. 458-466, 2011.

[153] J. Maurya and Y. Prajapati, "A comparative study of different metal and prism in the surface plasmon resonance biosensor having MoS 2-graphene," *Optical and Quantum Electronics,* vol. 48, p. 280, 2016.

[154] V. Nayyeri, M. Soleimani, and O. M. Ramahi, "Modeling graphene in the finite-difference time-domain method using a surface boundary condition," *IEEE transactions on antennas and propagation,* vol. 61, pp. 4176-4182, 2013.

[155] W. M. Mukhtar, N. R. Ayob, R. M. Halim, N. Diyanah, N. F. M. Samsuri, A. R. A. Rashid, *et al.*, "Effect of noble metal thin film thicknesses on surface plasmon resonance (SPR) signal amplification," *J. Adv. Res. in Mater. Sci,* vol. 49, pp. 1-9, 2018.

[156] N. H. T. Tran, B. T. Phan, W. J. Yoon, S. Khym, and H. Ju, "Dielectric metal-based multilayers for surface plasmon resonance with enhanced quality factor of the plasmonic waves," *Journal of Electronic Materials,* vol. 46, pp. 3654-3659, 2017.

[157] S. C. Singh and C. Guo, "Design of extremely sensitive refractive index sensors in infrared for blood glucose detection," *IEEE Sensors Journal,* vol. 20, pp. 4628-4634, 2020.

[158] Q. Ouyang, S. Zeng, L. Jiang, L. Hong, G. Xu, X.-Q. Dinh, *et al.*, "Sensitivity enhancement of transition metal dichalcogenides/silicon nanostructure-based surface plasmon resonance biosensor," *Scientific reports,* vol. 6, p. 28190, 2016.

[159] M. B. Hossain, M. Hassan, L. F. Abdulrazak, M. M. Rana, M. M. Islam, and M. S. Rahman, "Graphene-MoS2-Au-TiO2-SiO2 hybrid SPR biosensor for formalin detection: numerical analysis and development," *Advanced Materials Letters,* vol. 10, pp. 656-662, 2019.

[160] Y. W. Fen, W. Yunus, and N. A. Yusof, "Optical properties of cross-linked chitosan thin film for copper ion detection using surface plasmon resonance technique," *Opt. Appl.,* vol. 41, pp. 999-1013, 2011.

[161] S. Nuasaen, P. Opaprakasit, and P. Tangboriboonrat, "Hollow latex particles functionalized with chitosan for the removal of formaldehyde from indoor air," *Carbohydrate polymers,* vol. 101, pp. 179-187, 2014.

[162] D. Kukkar, K. Vellingiri, R. Kaur, S. K. Bhardwaj, A. Deep, and K.-H. Kim, "Nanomaterials for sensing of formaldehyde in air: Principles, applications, and performance evaluation," *Nano Research,* vol. 12, pp. 225-246, 2019.

[163] C. Zhu, Z. Zeng, H. Li, F. Li, C. Fan, and H. Zhang, "Single-layer MoS2-based nanoprobes for homogeneous detection of biomolecules," *Journal of the American Chemical Society,* vol. 135, pp. 5998-6001, 2013.

[164] M. A. Habib, M. S. Reza, L. F. Abdulrazak, and M. S. Anower, "Extremely high birefringent and low loss microstructure optical waveguide: Design and analysis," *Optics Communications,* vol. 446, pp. 93-99, 2019.

[165] L. Diéguez, D. Caballero, J. Calderer, M. Moreno, E. Martínez, and J. Samitier, "Optical gratings coated with thin Si3N4 layer for efficient immunosensing by optical waveguide lightmode spectroscopy," *Biosensors,* vol. 2, pp. 114-126, 2012.

[166] D. R. Shankaran, K. V. Gobi, T. Sakai, K. Matsumoto, T. Imato, K. Toko*, et al.*, "A novel surface plasmon resonance immunosensor for 2, 4, 6-trinitrotoluene (TNT) based on indirect competitive immunoreaction: a promising approach for on-site landmine detection," *IEEE Sensors Journal,* vol. 5, pp. 616-621, 2005.

[167] H. Bai, R. Wang, B. Hargis, H. Lu, and Y. Li, "A SPR aptasensor for detection of avian influenza virus H5N1," *Sensors,* vol. 12, pp. 12506-12518, 2012.

[168] N. A. S. Omar, Y. W. Fen, J. Abdullah, A. R. Sadrolhosseini, Y. Mustapha Kamil, N. I. M. Fauzi*, et al.*, "Quantitative and selective surface plasmon resonance response based on a reduced graphene oxide–polyamidoamine nanocomposite for detection of dengue virus e-proteins," *Nanomaterials,* vol. 10, p. 569, 2020.

PUBLICATION LIST

Reviewed Journal

1. **Md. Moznuzzaman**, Md. Rafiqul Islam, Md. Biplob Hossain, Ibrahim Mustofa Mehedi, "Modeling of Highly Improved SPR Sensor for Formalin Detection", Results in Physics, vol. 16, 102874, 2020

2. Md. Biplob Hossain, Ibrahim Mustofa Mehedi, **Md. Moznuzzaman**, Lway Faisal Abdulrazak, Md. Amzad Hossain, "High Performance Refractive Index SPR Sensor Modeling Employing Graphene Tri Sheets", Results in Physics. Vol. 15, 102719, 2019

3. **Md. Moznuzzaman**, Imran Khan, Md. Rafiqul Islam, ''Nano-layered surface plasmon resonance-based highly sensitive biosensor for virus detection: An approach to detect SARS-CoV-2'', Nano- Micro Letters. (Submitted)

4. **Md. Moznuzzaman**, Md. Rafiqul Islam, Imran Khan, "Effect of layer thickness variation on sensitivity: An SPR based sensor for formalin detection". (Will be submitted soon)